Intelligent Microscopic Models for Traffic Flow Characterization

by

Faryal Ali

B.Sc., CECOS University of IT and Emerging Sciences, Peshawar, Pakistan, 2018

M.Sc., University of Engineering and Technology, Peshawar, Pakistan, 2021

A Dissertation Submitted in Partial Fulfillment of the Requirements for the Degree

of

DOCTOR OF PHILOSOPHY

in the Department of Electrical and Computer Engineering

© Faryal Ali, 2025
University of Victoria

All rights reserved. This dissertation may not be reproduced in
whole or in part, by photocopy or other means, without the permission of the author.

We acknowledge and respect the Lək̓ʷəŋən (Songhees and Xʷsepsəm/Esquimalt) Peoples on whose territory the university stands, and the Lək̓ʷəŋən and W̱SÁNEĆ Peoples whose historical relationships with the land continue to this day.

Intelligent Microscopic Models for Traffic Flow Characterization

by

Faryal Ali

B.Sc., CECOS University of IT and Emerging Sciences, Peshawar, Pakistan, 2018

M.Sc., University of Engineering and Technology, Peshawar, Pakistan, 2021

Supervisory Committee

Dr. Thomas Aaron Gulliver, Supervisor
(Department of Electrical and Computer Engineering)

Dr. Zawar Hussain Khan, Co-Supervisor
(Department of Electrical and Computer Engineering)

Dr. Phalguni Mukhopadhyaya, Outside Member
(Department of Civil Engineering)

Supervisory Committee

Dr. Thomas Aaron Gulliver, Supervisor
(Department of Electrical and Computer Engineering)

Dr. Zawar Hussain Khan, Co-Supervisor
(Department of Electrical and Computer Engineering)

Dr. Phalguni Mukhopadhyaya, Outside Member
(Department of Civil Engineering)

Abstract

In this dissertation, microscopic models for traffic flow characterization are studied. Based on the traffic flow evolution characteristics and aiming to characterize the traffic behavior accurately and realistically, this research focuses on developing realistic traffic flow models to improve traffic safety, efficiency, and pollution control. A traffic model based on driver response is introduced considering both driver reaction and sensitivity. Driver sensitivity includes typical, sluggish, or aggressive drivers. Then the pavement condition is investigated using the pavement condition index (PCI). The impact of fog on visibility is a major factor affecting traffic congestion and safety. Thus, the traffic behavior based on visibility during foggy weather is also investigated. In addition, the recent introduction of connected autonomous vehicles (CAVs) has had a significant impact on road networks. Therefore, a spring-mass based traffic model to evaluate human-driven vehicle (HV), autonomous vehicle (AV), and CAV behavior on a horizontal curve is proposed. Further, CAV behavior at bottlenecks considering cyberattacks is investigated. This dissertation also provides an energy consumption model considering driver energy-saving awareness. The performance of traffic models is presented and compared with the intelligent driver (ID) model, and traffic stability is analyzed. The results demonstrate the advantages of the proposed approach.

Contents

List of Figures

List of Tables

Acknowledgements

First and foremost, praises and thanks to Allah Almighty for showering countless blessings and for giving me strength, courage, patience, and wisdom to bring this work to completion.

I would like to express my deepest gratitude to my supervisor Dr. T. A. Gulliver for giving me the opportunity to be part of his research group and work towards my PhD, and for his support, feedback, and expertise. It is truly an honor to have worked under a researcher of such high standing.

My heartfelt appreciation and gratitude to my mentor and co-supervisor Dr. Z. H. Khan for his persistent help, unwavering support, guidance, patience, and for always being available. His continuous encouragement, advice, and inspiration gave me the confidence to complete my PhD productively and enthusiastically. I am indeed grateful to him for believing in me, motivating me during my challenging moments, sharing his in-depth knowledge and experience, and helping me evolve as a researcher and a person.

I am also thankful to Dr. Gulliver and Dr. Khan for giving me independence in my research which has certainly led to new opportunities.

I would like to extend my sincere thanks to Dr. P. Mukhopadhyaya from the Civil Engineering Department for serving as my supervisory committee member. I am also thankful to Dr. Eric J. Miller from the University of Toronto for serving as External Examiner.

I would also express my gratitude to Dr. Khurram Shehzad Khattak from the University of Engineering and Technology, Peshawar, Pakistan for his initial help and valuable insights.

I owe sincere and earnest thanks to my parents for their love, care, and continuous support, and for giving me the wings to fly and achieve my dreams. Many thanks to my sister (Shahilal) who has always been there for me and heard me out. A wholehearted thanks to my uncle (Khan Alam) for all his support, love, and inspiration, and for regularly reaching out to me while I was in Canada.

Who truly deserves it, I set the brightest of honors.
And to those who seek, a new world waits for them.
(Dr. Allama Muhammad Iqbal)

Dedication

To

My Parents (Muhammad Ali and Shehla Ali)

List of Acronyms

Acronym	Definition
ACC	Adaptive cruise control
ADAS	Advanced driver assistant system
ADS	Automated driving system
AV	Autonomous vehicle
AWS	Amazon web service
BRT	Bus rapid transit
CAV	Connected autonomous vehicle
DOS	Denial-of-service
DT	Detection latency
ES	Exposed surface
FHWA	Federal highway administration
GHG	Greenhouse gas
HV	Human-driven vehicle
ID	Intelligent driver
IEA	International energy agency
IS	Impact scope
PCI	Pavement condition index
PR	Propagation rate
RT	Recovery time
SI	Severity impact
VSL	Variable speed limit
V2V	Vehicle-to-vehicle communication
V2X	Vehicle to other systems communication

List of Symbols

dv/dt	Driver response
a_{max}	Maximum acceleration
b	Minimum acceleration (Deceleration)
a	Acceleration
v	Speed (Velocity)
v_{max}	Maximum speed (Desired speed)
s	Distance headway
D	Desired distance headway
s_j	Jam spacing
τ	Time headway
τ_s	Safe time headway
τ/τ_s	Driver sensitivity
Δv	Speed difference
δ	Acceleration exponent
L	Vehicle length
Δt	Time step size
s_e	Equilibrium distance headway
ρ	Traffic density
Q	Traffic flow
f_s	Partial derivative with respect to distance headway
f_v	Partial derivative with respect to speed (velocity)
$f_{\Delta v}$	Partial derivative with respect to the change in speed
J	Jacobian matrix
λ	Eigen values
k	Phase shift
ρ_m	Maximum density

$h = s/D$	Ratio of distance headway to desired distance headway
T_r	Reaction time
V_d	Visibility distance
$V_{d_{max}}$	Maximum visibility distance
m	Vehicle mass
s'	Safe distance headway
S	Distance
R	Radius of curvature
g	Gravitational acceleration
f	Friction coefficient
e	Superelevation
ξ	Reaction time of HVs, AVs, and CAVs
c	Cyberattack intensity
E	Total energy consumption
ρ_{air}	Air density
A_d	Air drag coefficient
A	Vehicle front area
I	Vehicle internal energy consumption intensity coefficient
B	Vehicle braking energy consumption intensity coefficient
γ	Driver energy conservation awareness

Chapter 1
Introduction

1.1 Motivation and Background

In recent years, substantial consideration has been given to traffic modeling. This modeling involves the characterization and analysis of traffic behavior and has gained considerable importance due to the prevalence of traffic congestion. Congestion occurs when the volume of traffic is high relative to the capacity of the road, leading to traffic jams. It is anticipated that employing an accurate traffic model can improve the efficiency of traffic flow. The development of high traffic density along a road occurs due to accidents, slow-moving vehicles, and traffic control elements, leading to long traffic queues, delayed dissipation, and significant emissions. To mitigate these traffic problems, it is important to develop effective traffic forecasting and management strategies, utilizing realistic traffic flow predictions obtained from traffic flow models [1]–[3]. These models provide an accurate representation of traffic behavior, leading to improved utilization of road infrastructure, congestion alleviation, and reduction of traffic queues. In addition, these models help in the reduction of traffic delays, excessive fuel consumption, pollution, and safety problems [4]–[7].

Autonomous vehicles (AVs) and connected autonomous vehicles (CAVs) have recently been introduced on highway networks. These vehicles are equipped with varying driver assistance systems ranging from basic cruise control to communication with other vehicles (V2V) or other systems (V2X) without human intervention [8], [9]. These vehicles have been engineered to improve safety, comfort, mobility, and environmental sustainability [10]. AVs navigate autonomously using sensors and communications without human involvement. They perform driving tasks based on sensor data and internal systems [11]. AVs respond in real time to received data and use intelligent software to ensure passenger safety, comfort, and operational efficiency [12]. Automated driving systems encompass both hardware, such as sensors, and software, such as trajectory planning systems. They assist drivers in dynamic driving tasks including monitoring the driving environment and controlling lateral and longitudinal motion [13].

CAVs are a promising technology to reduce traffic accidents and emissions, and improve traffic efficiency [14]. They navigate through the road network using sensors to observe the surrounding environment, control systems to make decisions, and actuators for operations such as steering and braking [11]. Advanced sensors such as LiDAR, millimeter-wave radar, and cameras allow CAVs to perceive their surroundings and identify objects such as pedestrians and traffic signals in real time [15]. Wireless communications technology such as 5G and Wi-Fi provide connectivity with nearby vehicles to improve safety and road capacity by adjusting the distance headway between vehicles [14], [16]. According to the Virginia Department of Transportation, highway capacity increases by approximately 28% and 92% for AVs and CAVs, respectively, compared to human-driven vehicles (HVs) [11]. It is anticipated that CAVs will define the future of transportation systems and 24 % to 87% of vehicles in the U.S. will be Level 4 (L4) autonomous by 2045 [17]. The adoption of CAVs will affect traffic behavior, thus, it is important to model these dynamics. This study proposes new traffic models that aim to accurately and realistically characterize the behavior of traffic to improve traffic conditions.

Three types of models are employed for traffic flow characterization: microscopic, macroscopic, and mesoscopic. Microscopic models consider individual vehicle behavior and employ parameters such as vehicle position, velocity (speed), and time and distance headways [18]. They are used to predict vehicle dynamics and are often based on driver physical and psychological responses [19]. Macroscopic models, on the other hand, consider aggregate traffic behavior and are used to determine average density, velocity (speed), and flow [20]. Mesoscopic models take into account both individual and aggregate behavior [21] and typically employ probability distributions [19]. Hence, small groups of vehicles and their interactions are considered.

Pipes [22] and Reuschel [23] were the first to introduce microscopic traffic models. Velocity (speed) was determined using the distance between following and leading vehicles. However, their models are simplistic and cannot adequately characterize traffic behavior [24]. Newell [25] proposed a model for vehicle behavior in dense traffic. Velocity (speed) is based on the distance headway, so a larger distance headway results in a lower density and, hence, a greater velocity (speed). However, this relationship results in high acceleration, which is not realistic [26]. Moreover, this model neglects variations in driver behavior as a constant time headway is employed [27]. Bando et al. [28] improved the Newell model, but this results in unrealistic

characterization as the velocity (speed) differences are ignored, leading to unstable dynamics. Moreover, the acceleration can be very high when the velocity (speed) is far from the equilibrium distribution, and the density is not considered. It has been shown that this model leads to traffic accidents because of the small distances between vehicles.

Helbing and Tilch [29] developed a model that considers the reaction to velocity (speed) differences and, thus, accurately characterizes the time headway and velocity (speed) during congestion. However, acceleration occurs over a short time, which is typical of an aggressive driver, so slow and average driver behavior is neglected. Gipps [30] proposed a model based on driver response to forward traffic with realistic acceleration. However, this model is only suitable for a small range of parameters.

Treiber, Henneck, and Helbing [26] developed the intelligent driver (ID) model to overcome the drawbacks of previous models. It can provide realistic acceleration and deceleration and collision free behavior. With this model, driver behavior is based on the velocity (speed) and distance headway of forward vehicles, and typical traffic parameters are employed [31]–[33]. However, the acceleration exponent δ in the ID model is a constant and so cannot characterize driver behavior under different traffic conditions. This leads to unrealistic behavior as it is not based on traffic physics. The ID model was modified in [34] for traffic at signalized intersections. However, a value of $\delta = 4$ was employed, so real traffic conditions were neglected [35]. This constant was chosen as the best fit for general traffic environments. A similar approach was employed in [36] for deceleration at intersections. In this case, the distances between vehicles are very small even with a high velocity (speed), which is unrealistic.

The ID model is employed for CAVs to improve traffic safety and passenger comfort [12], [37]. Li et al. [38] employed this model to characterize the car-following behavior of CAVs while Schakel et al. [39] proposed an improved ID model to explore CAV traffic stability. In this case, there is an abrupt decrease in velocity (speed) when the density reaches half its maximum (critical density), which is unrealistic as the velocity (speed) should be smooth. A modified ID model was proposed in [40] to better characterize real traffic conditions. However, CAV behavior with this model is not realistic because under actual traffic conditions drivers take longer to achieve smooth car-following behavior and the variations in headway are greater [41]. The ID model has also been integrated into cooperative and Adaptive Cruise Control (ACC) systems [42], [43]. Unfortunately,

the safe distance with this model is too small when the velocity (speed) is high which can result in accidents when employed in ACC and related systems.

Following a comprehensive examination of the subject area it was determined that model improvements are still needed. The most important is adjusting the traffic flow based on the predicted traffic conditions. In this study, traffic is examined to characterize the behavior accurately and realistically. In addition, CAV behavior is investigated to promote safe, efficient, and environmentally sustainable transportation systems. In particular, the effect of weather and pavement conditions, AVs, CAVs, and HVs on highways, CAVs at bottlenecks, cyberattacks, driver awareness of energy consumption, and driver reaction and sensitivity will be assessed.

To evaluate the performance, the Euler technique is used to discretize the traffic models. This technique is presented in Section 1.2. Further, to better understand the traffic congestion mechanism, a stability analysis of traffic models is performed. A brief introduction to traffic stability is given in Section 1.3.

1.2 The Euler Technique

The Euler technique is used to evaluate traffic models. It is a simple but effective method to solve systems of differential equations and is widely used in traffic simulators. This technique divides time into discrete steps and the vehicle position, speed, and acceleration are approximated using the model at each time step. The change in distance with respect to time results in a change in speed given by

$$\frac{dS}{dt} = v, \tag{1.1}$$

and the temporal change in speed leads to changes in acceleration given by

$$\frac{dv}{dt} = a. \tag{1.2}$$

For the Euler technique, the position and speed for the traffic models is

$$S_F^{x+1} = S_F^x + \Delta t \times v_F^x \tag{1.3}$$

$$v_F^{x+1} = v_F^x + \Delta t \times a_F^x \tag{1.4}$$

where x is the current time step and $x + 1$ is the next time step. S_F^x, v_F^x, and a_F^x are the position, speed, and acceleration, respectively, of the following vehicle in the xth time interval where

$$t = x\Delta t \tag{1.5}$$

and Δt is the duration of a time step.

1.3 Traffic Stability

A traffic model is unstable if the traffic flow amplifies disturbances, whereas it is stable if these disturbances dissipate and the flow becomes smooth [44], [45]. For traffic flows, two types of stability are of particular interest, local stability and string stability. In local stability, perturbations grow both in amplitude and number of affected vehicles and become permanent. This means if local instability occurs, the traffic flow will not return to its original, unperturbed state, and this form of instability is undesirable [46].

String stability refers to disturbances that might grow but all vehicles eventually return to their original undisturbed state. This type of stability is related to stop-and-go waves. That is, if a model is string unstable, disturbances will grow and after it has passed several cars, a nonlinear effect will take over resulting in stop-and-go waves [46].

Stop-and-go traffic refers to repeated acceleration and deceleration causing traffic to come to a stop and then start again, resulting in congestion [46]. This is because when a driver accelerates, they increase the density of upstream vehicles, leading to slower speeds downstream. Similarly, when a driver brakes or decelerates suddenly, they cause a disturbance that propagates upstream, leading to stop-and-go waves [46]. In this dissertation, the string stability of traffic models is assessed.

1.4 Dissertation Organization

This chapter introduced intelligent microscopic models for traffic flow characterization**.** The remaining chapters of the dissertation are structured as follows.

Chapter 2

In this chapter, a new microscopic traffic model is proposed that characterizes driver response according to reaction and sensitivity. Driver response in the ID model is based on a fixed acceleration exponent and so does not follow traffic physics. This inadequate characterization results in unrealistic traffic behavior. With the proposed model, drivers can be aggressive, sluggish, or typical. It is shown that the proposed model has better stability and characterizes traffic more realistically than the ID model.

Chapter 3

In this chapter, a traffic flow model is developed that incorporates vehicle vibrations due to pavement condition. The ID model employs a fixed exponent, so traffic behavior is the same regardless of the road condition. Thus, it ignores the underlying physics. To address this limitation, the proposed model employs the pavement condition index (PCI) in describing traffic behavior. The results show that the performance of the proposed model varies with the PCI, as expected, and aligns more closely with reality. Thus, the traffic behavior is more accurate than with the ID model.

Chapter 4

The impact of fog on visibility is a major factor affecting traffic congestion and safety. This chapter proposes a microscopic traffic model that captures the features of traffic in foggy weather and characterizes it based on visibility. The proposed model is evaluated on a circular road and compared to the ID model. It is shown that the proposed model characterizes traffic realistically with lower acceleration and deceleration. A stability analysis is performed showing that the proposed model does not create stop-and-go waves and is stable even during foggy weather.

Chapter 5

Highway geometry plays a crucial role in maintaining traffic safety and operational efficiency. In this chapter, a traffic model is developed from a spring-mass system theory perspective to investigate traffic dynamics on horizontal highway curves. By utilizing a spring-mass system analogy, the proposed model provides a more accurate and realistic representation of traffic. This model is used to evaluate the behavior of HVs, AVs, and CAVs over a circular road. It is shown that CAVs perform better than HVs and AVs on horizontal curves, leading to a better understanding of safety and efficiency in horizontal road segments. Further, it is shown that the proposed model outperforms the ID model.

Chapter 6

Bottlenecks reduce both traffic safety and efficiency, resulting in congestion and collisions. The introduction of CAVs has had a significant impact on road networks and can improve traffic efficiency at bottlenecks. This chapter proposes a microscopic traffic model to investigate CAV behavior at bottlenecks and examine the effect of cyberattacks. The proposed model is evaluated on a circular road and compared to the ID model. The results indicate that the proposed model improves traffic capacity and efficiency. Further, it can realistically characterize CAV behavior under cyberattacks and can effectively manage the corresponding disruptions.

Chapter 7

Road traffic significantly impacts global energy consumption and emissions, both of which contribute to climate change. Thus, energy conservation and emission reduction in road transportation are critical concerns, and traffic flow modeling is key to evaluating and improving these metrics. Therefore, this chapter provides a microscopic traffic model to characterize energy consumption reflecting driver energy-saving awareness. The results demonstrate that energy consumption with the proposed model decreases as driver energy-saving awareness increases. Furthermore, the proposed model performs well when compared to the ID model.

Chapter 8

This chapter concludes the dissertation, providing a brief description of the contributions and possible future extensions.

Chapter 2

A Traffic Model Considering Driver Reaction and Sensitivity

This chapter considers driver reaction and sensitivity to characterize traffic behavior. During congestion, stop-and-go waves cause drivers to vary their speed which creates poor traffic dynamics [47], [48]. The distance between vehicles and time headway affects driver response and can result in significant variations in traffic flow. Time headway τ is the time required to align to forward traffic conditions, and the distance headway is traversed during this time [49]. Traffic alignment is the adjustment in velocity when a forward change in traffic occurs. A driver responds slowly with a large distance headway and quickly with a small distance headway [20]. Further, driver response is affected by sensitivity which is proportional to the change in velocity (speed) [20]. Since driver response is not the same for all traffic conditions, it should be considered in a model for accurate and realistic traffic characterization.

A microscopic traffic model is proposed here which models the acceleration exponent in the ID model [26] using driver reaction and sensitivity. Driver sensitivity is the reaction to changes in velocity (speed) and can be typical, sluggish, or aggressive. This variable exponent provides better stability and is more realistic than the fixed exponent in the ID model. This is because it is based on real traffic parameters. The performance of the proposed and ID models is evaluated on a single-lane circular road of length 1200 m. A platoon of 21 vehicles is considered for 150 s.

The remainder of this chapter is organized as follows. The proposed and ID models are discussed in Section 2.1. Section 2.2 presents the traffic stability. The performance of these models is investigated in Section 2.3. Finally, Section 2.4 gives some concluding remarks.

2.1 Traffic Models

The ID model characterizes vehicle movement and is given by [26]

$$\frac{dv}{dt} = a_{max}\left(1 - \left(\frac{v}{v_{max}}\right)^{\delta} - \left(\frac{D}{s}\right)^{2}\right), \tag{2.1}$$

where a_{max} is the maximum acceleration, v is the vehicle velocity (speed), v_{max} is the maximum velocity (desired speed) on the road, s is the distance headway between vehicles, and δ is the acceleration exponent. This exponent is a constant chosen to fit traffic behavior and is not based on traffic dynamics. According to (2.1), acceleration is a function of driver response, the distance between vehicles, and the time needed to adapt to traffic conditions. Driver response is affected by the ratio of velocity (speed) to maximum velocity (desired speed). For a smooth flow with little acceleration, this ratio approaches 1 so the velocity (speed) is near maximum. The term D represents the desired distance headway during traffic alignment and can be expressed as [26]

$$D = s_j + \tau v + \frac{v\Delta v}{2\sqrt{a_{max}b}} \tag{2.2}$$

where b is the minimum acceleration (deceleration), s_j is the jam spacing as shown in Figure 2.1, which is the smallest possible distance between vehicles at maximum density, τ is the time headway, and Δv is the difference in velocity (speed). In this model, driver response to changes in traffic conditions is described by the fixed exponent δ, so vehicle behavior is the same for all scenarios, which is unrealistic. Therefore, a model is proposed that characterizes driver response using a variable exponent that is based on traffic physics.

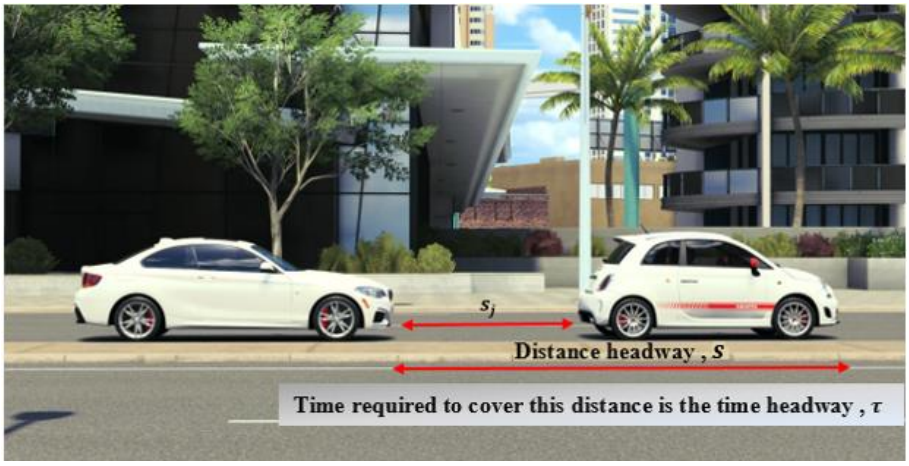

Figure 2.1 The distance and time headways between leading and following vehicles.

A driver reacts based on the acceleration required to align to forward vehicles. This depends on the time headway between vehicles, so a large time headway results in a slow reaction. Conversely, the driver reaction is quick for a small time headway and the acceleration is large. Thus, driver reaction during alignment can be characterized as

$$V_t = a\tau, \tag{2.3}$$

However, the ratio of distance headway s to desired distance headway D influences this reaction, so (2.3) is modified to

$$V_r = a\tau\left(\frac{S}{D}\right) \tag{2.4}$$

The value of $\frac{S}{D}$ varies between 0 and 1. When $\frac{S}{D} = 0$, the driver response is 0 so there is no change in velocity (speed). In this case, the density is maximum, i.e., during congestion when there is no vehicle movement. When $\frac{S}{D} = 1$, the change in velocity (speed) is large so the traffic flow is smooth, and the maximum speed is achieved.

Driver sensitivity plays a significant role in the driver response. The safe time headway is defined as

$$\tau_s = \tau_p + \tau_r + \tau \tag{2.5}$$

where τ_p is the time required to perceive changes in traffic, τ_r is the time required to react and τ is the time required to cover the distance headway. The safe time headway is required to cover the distance headway safely and avoid accidents. Driver response is fast when the time headway is smaller than the safe time headway. In heterogeneous traffic, vehicles frequently change lanes to occupy any forward distance, so vehicles align quickly to avoid lane changes by other vehicles. This reduces the distance headway and time headway, and is a major cause of stop-and-go traffic. When the time headway is greater than the safe time headway, traffic flow is smooth, and the distance headway can increase. In this case, lane changes do not reduce the time headway and driver response is slow.

Driver sensitivity can be expressed as $\frac{\tau}{\tau_s}$. A driver is aggressive when $\frac{\tau}{\tau_s} < 1$ and cautious when $\frac{\tau}{\tau_s} > 1$. For a typical driver, $\frac{\tau}{\tau_s} = 1$. Therefore, the driver response from (2.4) can be expressed as

$$a\tau\left(\frac{S}{D}\right)\left(\frac{\tau}{\tau_s}\right) \tag{2.6}$$

The proposed model is obtained by replacing δ in (2.1) with (2.6) giving

$$\frac{dv}{dt} = a_{max}\left(1 - \left(\frac{v}{v_{max}}\right)^{a\tau\left(\frac{s}{D}\right)\left(\frac{\tau}{\tau_s}\right)} - \left(\frac{D}{s}\right)^2\right). \tag{2.7}$$

The traffic density is given by $\rho = \frac{1}{s_e}$ [47] where s_e is the equilibrium distance headway. At equilibrium, changes in velocity (speed) are negligible, that is, $\Delta v = 0$. Incorporating this equilibrium condition in (2.2) and substituting (2.1) gives s_e for the ID model [26] as

$$s_e = (s_j + \tau v)\left(1 - \left(\frac{v}{v_{max}}\right)^{\delta}\right)^{-\frac{1}{2}} \tag{2.8}$$

For the proposed model, substituting δ with (2.6) in (2.8) gives

$$s_e = (s_j + \tau v)\left(1 - \left(\frac{v}{v_{max}}\right)^{a\tau\left(\frac{s}{D}\right)\left(\frac{\tau}{\tau_s}\right)}\right)^{-\frac{1}{2}} \tag{2.9}$$

According to (2.8), the equilibrium distance headway between vehicles with the ID model is the same for all the traffic conditions because δ is a constant chosen as a compromise to fit all scenarios. Conversely, (2.9) is based on the distance and time headways and so is not a constant. Thus, changes in equilibrium distance headway are affected by driver sensitivity and reaction.

The traffic flow is the product of velocity (speed) and density $Q = \frac{v}{s_e}$ [31] so the ID model flow is

$$Q = \frac{1}{(s_j + \tau v)\left(1 - \left(\frac{v}{v_{max}}\right)^{\delta}\right)^{-\frac{1}{2}}} v, \tag{2.10}$$

while the proposed model flow is

$$Q = \frac{1}{(s_j + \tau v)\left(1 - \left(\frac{v}{v_{max}}\right)^{a\tau\left(\frac{s}{D}\right)\left(\frac{\tau}{\tau_s}\right)}\right)^{-\frac{1}{2}}} v, \tag{2.11}$$

This indicates that the traffic flow with the proposed model is based on driver reaction and sensitivity. A smaller distance headway results in faster driver response as there are significant interactions between the vehicles, i.e., during congestion [20], so the flow is low. Conversely, with a large distance headway driver response is slow and there are few interactions between the

vehicles so the flow is high [20]. Further, a higher sensitivity results in larger changes in traffic flow.

2.2 Traffic Stability

In this section, the theoretical and numerical stability of the ID and proposed models are evaluated.

2.2.1 Theoretical Traffic Stability

The stability of both the ID and proposed models is analyzed over an infinite road. The driver response and vehicles are assumed identical and the equilibrium distance headway s_e is maintained between all vehicles [50]. Thus, drivers align to forward conditions with little acceleration and only small changes in equilibrium velocity (speed) $v_e(s_e)$ occur. The changes in distance headway x are therefore small as are the changes in velocity (speed) y. The distance headway during a change in velocity (speed) is then

$$s = s_e + x, \tag{2.12}$$

and the corresponding velocity (speed) is

$$v = v_e(s_e) + y. \tag{2.13}$$

During traffic alignment over the distance headway, the temporal change in velocity (speed) [51] is

$$x(t) = \frac{dx}{dt} = y_l - y_F \tag{2.14}$$

where the subscripts l and F denote the leading and following vehicles, respectively. The changes in headway are small as the changes in $v_e(s_e)$ are small, so $y(t)$ during alignment can be expressed as [50]

$$y(t) = \frac{dy}{dt} = f_s x_F + (f_v + f_{\Delta v})y_F - f_{\Delta v} y_l, \tag{2.15}$$

where $f_{\Delta v}$ is the partial derivative with respect to the change in velocity (speed), f_v is the partial derivative with respect to velocity (speed), and f_s is the partial derivative with respect to distance headway, and are given by

$$f_s = \frac{\partial f}{\partial s}, f_v = \frac{\partial f}{\partial v}, \text{ and } f_{\Delta v} = \frac{\partial f}{\partial_{\Delta v}}.$$

Equations (2.14) and (2.15) are solved using Fourier-Ansatz as

$$x(t) = \hat{x} e^{\gamma t + ik}, \tag{2.16}$$

$$y(t) = \hat{y}e^{\gamma t + ik}, \tag{2.17}$$

so (2.16) and (2.17) take the form

$$\begin{pmatrix} x(t) \\ y(t) \end{pmatrix} = \begin{pmatrix} \hat{x} \\ \hat{y} \end{pmatrix} e^{\gamma t + ik}, \tag{2.18}$$

where $\gamma = \alpha + i\omega$ is the change in traffic oscillations during alignment and $i = \sqrt{-1}$. The real part α denotes the change in amplitude, $\omega = \frac{2\pi}{T}$ is the oscillation frequency, T is the oscillation period, k is the phase shift that corresponds to the delay experienced by a driver [50], and $\hat{y}$ and $\hat{x}$ are the changes in velocity (speed) and distance headway, respectively.

Substituting (2.18) in (2.14) and (2.15) gives

$$x(t) = y - ye^{ik}, \tag{2.19}$$

$$y(t) = f_s x e^{ik} + (f_v + f_{\Delta v})ye^{ik} - f_{\Delta v}y. \tag{2.20}$$

The model is stable if the real parts of the eigenvalues are negative. The eigenvalues are obtained from

$$\left| J - \begin{pmatrix} \lambda & 0 \\ 0 & \lambda \end{pmatrix} \right| = 0, \tag{2.21}$$

where J is the Jacobian matrix given by

$$J = \begin{pmatrix} j_{11} & j_{12} \\ j_{21} & j_{22} \end{pmatrix}$$

and j_{11} and j_{21} are the partial differentials of (2.19) and (2.20) w.r.t. x and j_{12} and j_{22} the partial differentials of (2.19) and (2.20) w.r.t y so that

$$J = e^{ik}\begin{pmatrix} 0 & e^{-ik} - 1 \\ f_s & (f_v + f_{\Delta v}) - f_{\Delta v}e^{-ik} \end{pmatrix} \tag{2.22}$$

Then substituting (2.22) in (2.21) we have

$$\begin{vmatrix} \lambda & 1 - e^{-ik} \\ -f_s & \lambda - f_v - f_{\Delta v} + f_{\Delta v}e^{-ik} \end{vmatrix} = 0, \tag{2.23}$$

which gives

$$\lambda^2 + \left(-f_v - f_{\Delta v} + f_{\Delta v}e^{-ik}\right)\lambda + f_s\left(1 - e^{-ik}\right) = 0. \tag{2.24}$$

Let $X(k) = -f_v - f_{\Delta v} + f_{\Delta v}e^{-ik}$ and $Y(k) = f_s\left(1 - e^{-ik}\right)$ in (4.24) so that

$$\lambda^2 + X(k)\lambda + Y(k) = 0. \tag{2.25}$$

The eigenvalues from (2.25) are

$$\lambda_{1,2} = -\frac{X(k)}{2}\left(1 \pm \sqrt{1 - \frac{4Y(k)}{X^2(k)}}\right), \tag{2.26}$$

The model is string stable [50] if the real parts of the eigenvalues are negative. In this case, vehicles maintain the distance headway and changes in the equilibrium velocity (speed) are small [52]. Then the oscillations in flow decay over time so it is stable (smooth). A model is unstable if the flow increases over time. An example is stop-and-go traffic which occurs during congestion. In this case, acceleration is high whereas in string stable traffic acceleration is low [47]. In unstable traffic, $k \to 0$ so there is a negligible delay between changes in flow (traffic waves) [50]. Using Taylor series, $Y(k)$ and $X(k)$ can be approximated for a small delay, i.e., $k \to 0$, as

$$X(k) = -f_v - if_{\Delta v}k, \tag{2.27}$$

$$Y(k) = if_s k + \frac{f_s}{2}k^2. \tag{2.28}$$

At equilibrium [50]

$$f_s = -v_e'(s_e)f_v. \tag{2.29}$$

where $v_e'(s_e)$ is the gradient of the equilibrium velocity (speed) with respect to the equilibrium distance headway. Substituting (2.29) in (2.28) gives

$$Y(k) = -iv_e'(s_e)f_v - \frac{v_e'(s_e)}{2}f_v \tag{2.30}$$

Let

$$\begin{aligned} X(k) &= a_1 + a_2 k, \\ Y(k) &= b_1 k + b_2 k^2, \end{aligned} \tag{2.31}$$

where

$$\begin{aligned} a_1 &= -f_v, \\ a_2 &= -if_{\Delta v}, \\ b_1 &= -iv_e'(s_e)f_v = iv_e'(s_e)a_1, \\ b_2 &= -\frac{v_e'(s_e)}{2}f_v = \frac{v_e'(s_e)}{2}a_1. \end{aligned} \tag{2.32}$$

Employing a Taylor series approximation, the square root in (2.26) becomes

$$\sqrt{1-\frac{4Y(k)}{X^2(k)}} = 1-\frac{2Y(k)}{X^2(k)}-\frac{2Y^2(k)}{X^4(k)}. \tag{2.33}$$

which results in

$$\lambda_2 = \frac{-Y(k)X^2(k)-Y^2(k)}{X^3(k)}. \tag{2.34}$$

and from (2.31)

$$\lambda_2 = -\frac{b_1}{a_1}k+\left(\frac{b_1a_2}{a_1^2}-\frac{b_2}{a_1}-\frac{b_1^2}{a_1^3}\right)k^2. \tag{2.35}$$

Now using (2.32) we obtain

$$\lambda_2 = -iv_e'(s_e)k+\frac{v_e'(s_e)}{f_v}\left[\frac{-2f_{\Delta v}-f_v}{2}-v_e'(s_e)\right]k^2. \tag{2.36}$$

The real part of (2.36) denotes the change in amplitude of the traffic oscillations (growth rate). The traffic flow is string stable if this is negative. Since

$$v_e'(s_e) \geq 0 \text{ and } f_v < 0, \tag{2.37}$$

$\left[\frac{-2f_{\Delta v}-f_v}{2}-v_e'(s_e)\right]$ is the string stability criterion [53], i.e.

$$v_e'(s_e) \leq -\frac{f_v}{2}-f_{\Delta v}. \tag{2.38}$$

From (2.37) and (2.38), the product of $\left[-\frac{2f_{\Delta v}-f_v}{2}-v_e'(s_e)\right]$ and $\frac{v_e'(s_e)}{f_v}$ indicates that λ_2 has a negative real part.

At equilibrium, f_v and $f_{\Delta v}$ for the ID model (2.1) are

$$f_v = a_{max}\left(-\frac{\delta v_e(s_e)^{\delta-1}}{v_{max}^{\delta}}-\frac{2\tau\left(s_j+v_e(s_e)\tau\right)}{s_e^2}\right), \tag{2.39}$$

$$f_{\Delta v} = -\frac{v_e(s_e)}{s_e}\sqrt{\frac{a_{max}}{b}}\left(\frac{s_j+v_e(s_e)\tau}{s_e}\right) \tag{2.40}$$

Using (2.39) and (2.40), the string stability criteria from (2.38) is

$$\begin{aligned} v_e'(s_e) \leq{}& \frac{a_{max}\left(\delta(s_e)^2v_e(s_e)^{\delta-1}+2\tau s_jv_{max}^{\delta}+2v_e(s_e)\tau^2v_{max}^{\delta}\right)}{2(s_e)^2v_{max}^{\delta}} \\ &+\frac{v_e(s_e)\sqrt{a_{max}b}\left(s_e+\tau v_e(s_e)\right)}{(s_e)^2b} \end{aligned} \tag{2.41}$$

This shows that changes in velocity (speed) with the ID model are characterized with the constant δ. A traffic string is more stable with a larger value of δ, but in this case congestion ends quickly. Thus, making δ larger to ensure stability ignores traffic physics and results in unrealistic traffic behavior. The velocity (speed) changes during traffic alignment are affected by driver sensitivity and reaction. Thus, to ensure appropriate behavior δ in (2.41) is replaced with (2.6) which gives the proposed model stability criteria as

$$v_e'(s_e) \leq \frac{a_{max}\left(a\tau\left(\frac{s}{D}\right)\left(\frac{\tau}{\tau_s}\right)(s_e)^2 v_e(s_e)^{a\tau\left(\frac{s}{D}\right)\left(\frac{\tau}{\tau_s}\right)-1} + 2\tau s_j v_{max}^{a\tau\left(\frac{s}{D}\right)\left(\frac{\tau}{\tau_s}\right)} + 2v_e(s_e)\tau^2 v_{max}^{a\tau\left(\frac{s}{D}\right)\left(\frac{\tau}{\tau_s}\right)}\right)}{2(s_e)^2 v_{max}^{a\tau\left(\frac{s}{D}\right)\left(\frac{\tau}{\tau_s}\right)}} + \frac{v_e(s_e)\sqrt{a_{max}b}\left(s_e+\tau v_e(s_e)\right)}{(s_e)^2 b}. \quad (2.42)$$

With the proposed model, changes in velocity (speed) are based on driver sensitivity and reaction. Drivers are more sensitive to large changes in velocity (speed) which results in a traffic flow that is string stable [20]. Further, a smaller distance headway than at equilibrium means vehicles move slowly so congestion takes longer to dissipate [19]. Conversely, a larger distance headway than at equilibrium means congestion dissipates quickly resulting in a stable traffic flow.

2.2.2 Numerical Traffic Stability

Both models are evaluated over a 1000 m single-lane circular road for 180 s with a platoon of 21 vehicles. The time headway with the ID model is 2 s. For the proposed model, $\tau = 1$ s which corresponds to an aggressive driver, $\tau = 2.5$ s which corresponds to a sluggish driver, and $\tau = 2$ s which corresponds to a typical driver, are considered. The value of $h = \frac{s}{D}$ ranges between 0 and 1, so here $0.3, 0.5$, and 1 are used. The value of δ varies between 1 and ∞, and is usually 4 [26]. Hence, the values of δ considered are $1,\ 4$ and 20. The initial equilibrium velocity (speed) is 4 m/s and the number of vehicles is 21. A perturbation is induced at 30 s based on the minimum acceleration. The stability analysis parameters for the ID and proposed models are given in Table 2.1.

Table 2.1 Stability analysis parameters.

Parameter	**Value**
Proposed model acceleration, a	1.5 m/s^2
Time headway for the ID model, τ	2 s
Time headway for the aggressive driver, τ	1 s
Time headway for the sluggish driver, τ	2.5 s
Time headway for the typical driver, τ	2 s
Ratio of distance headway to desired distance headway, $h = \frac{s}{D}$	0.3, 0.5, and 1
Jam spacing, s_j	5 m
Maximum acceleration, a_{max}	0.73 m/s^2
Minimum acceleration (deceleration), b	1.67 m/s^2
Vehicle length, L	5 m
Time step size, Δt	0.5 s
Initial equilibrium velocity (speed)	4 m/s
Acceleration exponent	1, 4, and 20
Safe time headway, τ_s	2 s

Figure 2.2 presents the velocity (speed) trajectories for the ID and proposed models. The trajectory of the 1st vehicle is represented by the red line while the black lines indicate the trajectories of the following 20 vehicles. For the ID model, when $\delta = 1$ the velocity (speed) of the 1st vehicle decreases to 3.1 m/s and then increases to 4.3 m/s at 38.0 s. At 47.5 s, the velocity (speed) oscillates between 3.8 and 4.2 m/s and increases over time. At 179.5 s, the velocity (speed) fluctuates between 2.5 and 5.1 m/s as shown in Figure 2.2a. When $\delta = 4$, the velocity (speed) of the 1st vehicle decreases to 3.1 m/s and then increases to 4.3 m/s at 37.0 s. At 47.5 s, the velocity (speed) oscillates between 3.7 and 4.3 m/s, and at 179.5 s it fluctuates between 0.03 and 7.4 m/s as shown in Figure 2.2b. When $\delta = 20$, the velocity (speed) of the 1st vehicle decreases to 3.1 m/s and then increases to 4.3 m/s at 37.0 s. At 45.5 s, the velocity (speed) oscillates between 3.7 and 4.3 m/s, and at 179.5 s it fluctuates between 0.03 and 7.4 m/s as shown in Figure 2.2c.

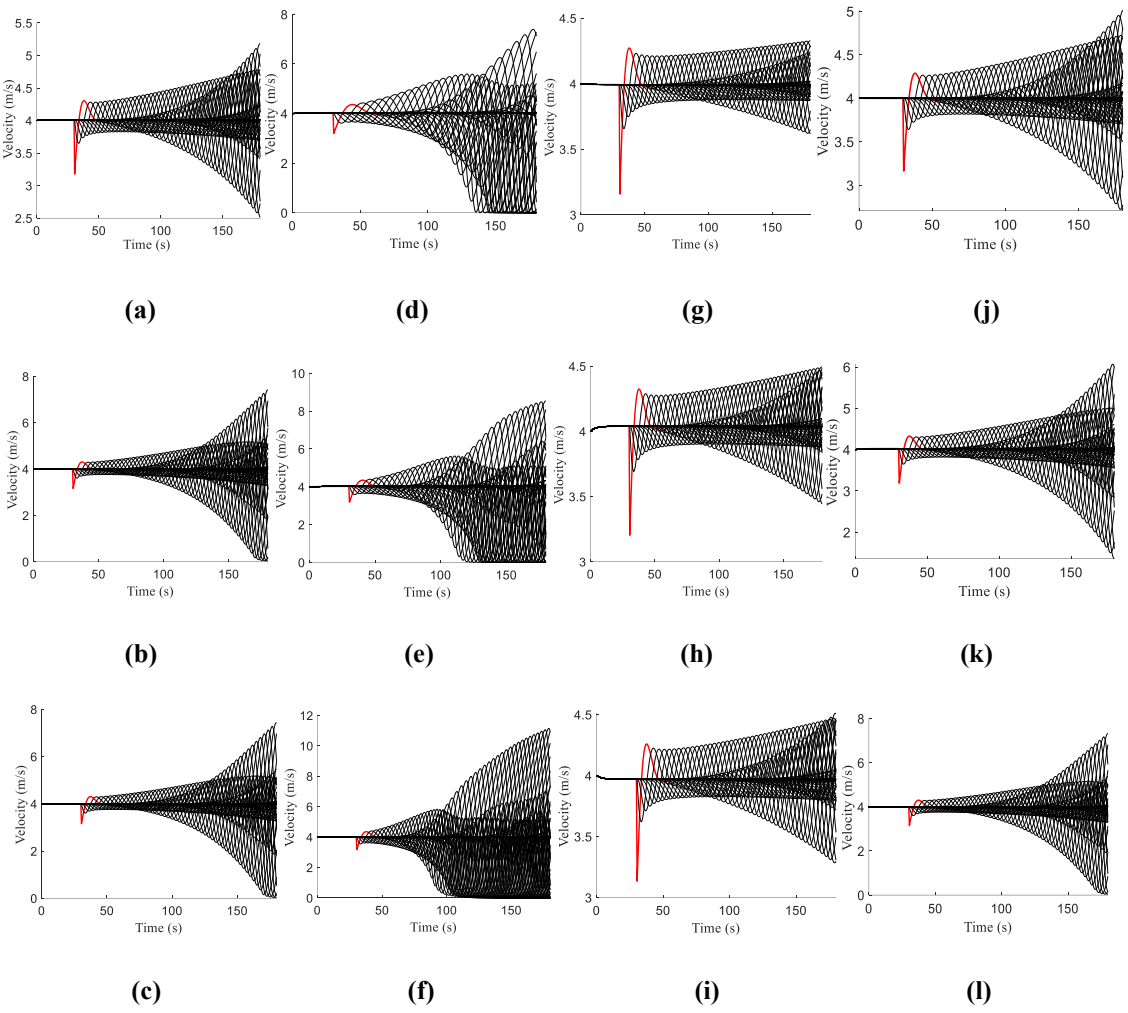

Figure 2.2 Velocity (speed) on a 1000 m circular road for the ID model with **(a)** $\delta = 1$, **(b)** $\delta = 4$, **(c)** and $\delta = 20$, and the proposed model when $\frac{\tau}{\tau_s} < 1$ with **(d)** $h = 0.3$, **(e)** $h = 0.5$, and **(f)** $h = 1.0$, $\frac{\tau}{\tau_s} > 1$ with **(g)** $h = 0.3$, **(h)** $h = 0.5$, and **(i)** $h = 1.0$, and $\frac{\tau}{\tau_s} = 1$ with **(j)** $h = 0.3$, **(k)** $h = 0.5$, and **(l)** $h = 1.0$.

For the proposed model with $\frac{\tau}{\tau_s} < 1$ (aggressive driver), when $h = 0.3$ the velocity (speed) of the first vehicle decreases to 3.2 m/s and then increases to 4.3 m/s at 43.5 s. At 63.0 s, it oscillates between 3.5 m/s and 4.5 m/s. These oscillations increase over time and at 178.0 s, the velocity (speed) fluctuates between 0.03 and 7.3 m/s as shown in Figure 2.2d. When $h = 0.5$, the velocity (speed) of the first vehicle decreases to 3.1 m/s and then increases to 4.3 m/s at 40.0 s. At 50.5 s, the velocity (speed) oscillates between 3.6 and 4.4 m/s, and at 179.5 s it fluctuates between 0.07 and 8.5 m/s as shown in Figure 2.2e. When $h = 1.0$, the velocity (speed) of the 1st vehicle

decreases to 3.1 m/s and then increases to 4.3 m/s at 37.5 s. At 69.5 s, the velocity (speed) oscillates between 3.1 and 5.1 m/s, and at 179.0 s it fluctuates between 0.16 and 11.1 m/s as shown in Figure 2.2f.

With $\frac{\tau}{\tau_s} > 1$ (sluggish driver), at $h = 0.3$ the velocity (speed) of the 1st vehicle decreases to 3.1 m/s and then increases to 4.2 m/s at 38.0 s. At 52.0 s, the velocity (speed) oscillates between 3.8 and 4.2 m/s, and at 179.5 s it fluctuates between 3.6 and 4.3 m/s as shown in Figure 2.2g. When $h = 0.5$, the velocity (speed) of the 1st vehicle decreases to 3.2 m/s and then increases to 4.3 m/s at 37.5 s. At 47.5 s, the velocity (speed) oscillates between 3.8 and 4.2 m/s, and at 179.5 s it fluctuates between 3.4 and 4.4 m/s as shown in Figure 2.2h. When $h = 1.0$, the velocity (speed) of the 1st vehicle decreases to 3.1 m/s and then increases to 4.2 m/s at 38.0 s. At 55.0 s, the velocity (speed) oscillates between 3.8 and 4.2 m/s, and at 179.0 s it fluctuates between 3.2 and 4.5 m/s as shown in Figure 2.2i.

When $\frac{\tau}{\tau_s} = 1$ (typical driver), at $h = 0.3$ the velocity (speed) of the 1st vehicle decreases to 3.1 m/s and then increases to 4.2 m/s at 38.0 s. At 47.5 s, the velocity (speed) oscillates between 3.7 and 4.2 m/s, and at 179.5 s it fluctuates between 2.7 and 4.9 m/s as shown in Figure 2.2j. When $h = 0.5$, the velocity (speed) of the 1st vehicle decreases to 3.2 m/s and then increases to 4.3 m/s at 37.0 s. At 53.5 s, the velocity (speed) fluctuates between 3.8 and 4.3 m/s and at 179.0 s it oscillates between 1.4 and 6.0 m/s as shown in Figure 2.2k. When $h = 1.0$, the velocity (speed) of the 1st vehicle decreases to 3.1 m/s and then increases to 4.3 m/s at 37.0 s. At 52.0 s, the velocity (speed) fluctuates between 3.7 and 4.3 m/s and at 179.5 s it oscillates between 0.04 and 7.3 m/s as shown in Figure 2.2l.

Figure 2.3 presents the time and space evolution of the vehicles over a circular road of length 1000 m for the ID and proposed models. This shows the instability that results with both models is in the form of stop-and-go waves. For the ID model, as δ increases the stop-and-go waves propagate over time and space as shown in Figures 2.3a to 2.3c. For the proposed model, with $\frac{\tau}{\tau_s} < 1$ (aggressive driver) the stop-and-go waves are larger, and with $\frac{\tau}{\tau_s} > 1$ (sluggish driver) they are smaller, than with $\frac{\tau}{\tau_s} = 1$ (typical driver) as shown in Figures 2.3d to 2.3l.

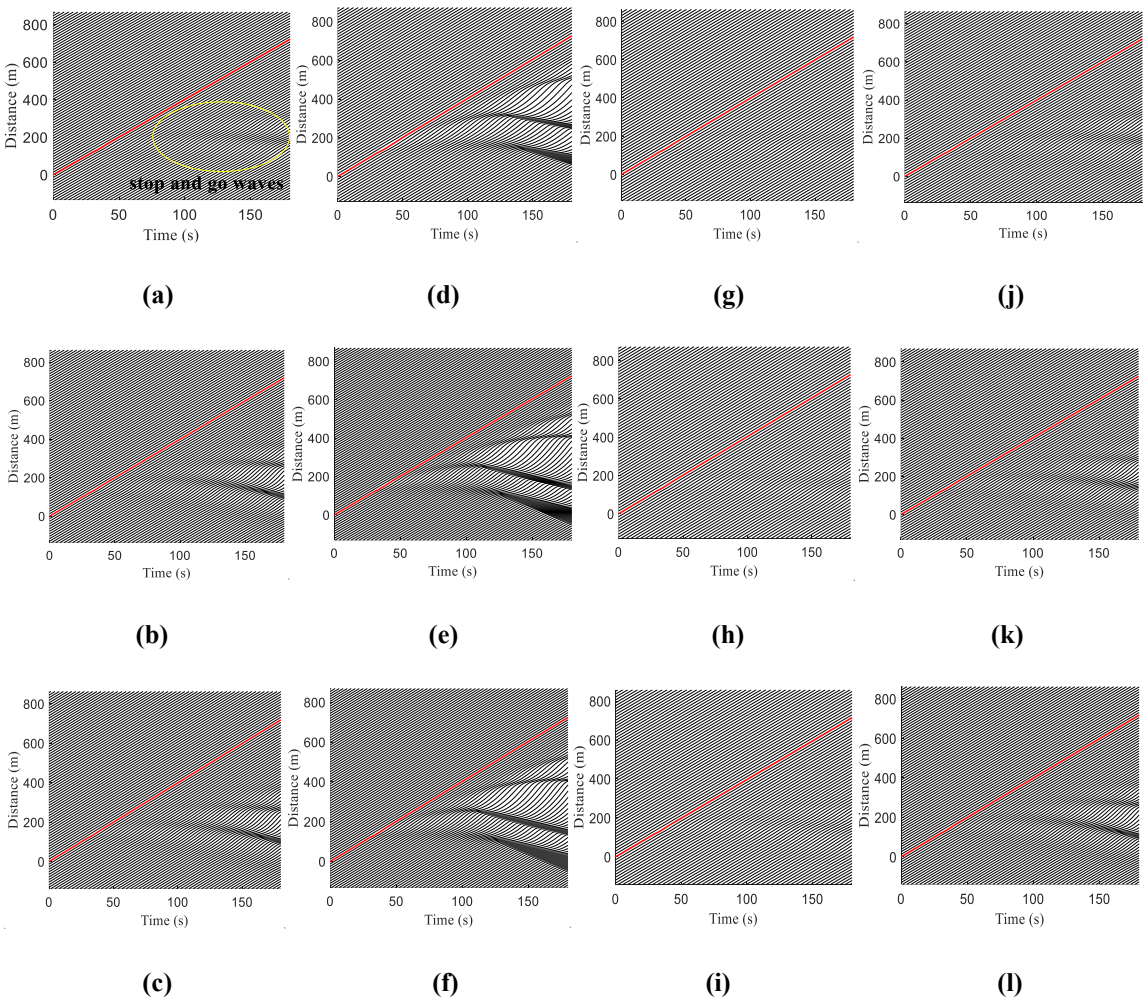

Figure 2.3 Spatial and temporal vehicle evolution with the ID model for **(a)** $\delta = 1$, **(b)** $\delta = 4$, and **(c)** $\delta = 20$, and the proposed model for $\frac{\tau}{\tau_s} < 1$ and **(d)** $h = 0.3$, **(e)** $h = 0.5$, and **(f)** $h = 1.0$, for $\frac{\tau}{\tau_s} > 1$ and **(g)** $h = 0.3$, **(h)** $h = 0.5$, and **(i)** $h = 1.0$, and for $\frac{\tau}{\tau_s} = 1$ and **(j)** $h = 0.3$, **(k)** $h = 0.5$, and **(l)** $h = 1.0$.

The results in Figures 2.2 and 2.3 show that with the proposed model the velocity (speed) oscillations are larger for an aggressive driver and hence more stop-and-go waves are produced. This is expected since there are significant interactions between the vehicles which cause congestion [20]. With a sluggish driver, the oscillations are smaller and hence fewer stop-and-go waves are produced. This is because there are fewer interactions between vehicles so the traffic is smooth [20]. The ID model [26] employs a constant exponent δ which is not based on driver response but rather is a compromise used to characterize all situations. Hence, with the ID model

the velocity (speed) oscillations and stop-and-go waves produced are based on this value which is inadequate and unrealistic.

2.3 Traffic Models Performance

The performance of the proposed and ID models is evaluated over a single-lane circular road of length 1200 m for 150 s using the explicit Euler method [47] with a time step of 0.5 s. There are no vehicles exits or entrances on the road. The ID model is evaluated with time headway 2 s. The proposed model is evaluated with $\tau = 1$ s (sensitivity $\frac{\tau}{\tau_s} < 1$) which corresponds to an aggressive driver, $\tau = 2.5$ s (sensitivity $\frac{\tau}{\tau_s} > 1$) which corresponds to a sluggish driver, and $\tau = 2$ s (sensitivity $\frac{\tau}{\tau_s} = 1$) which corresponds to a typical driver. The value of $h = \frac{s}{D}$ ranges between 0 and 1, so here $0.3, 0.5$ and 1.0 are used. The value of the acceleration exponent δ varies between 1 and ∞ and is usually 4 [26], so $\delta = 1, 4,$ and 20 are employed. The maximum normalized density is $\frac{1}{s_j} = 0.2$ and a platoon of 21 vehicles is considered. The simulation parameters are given in Table 2.2.

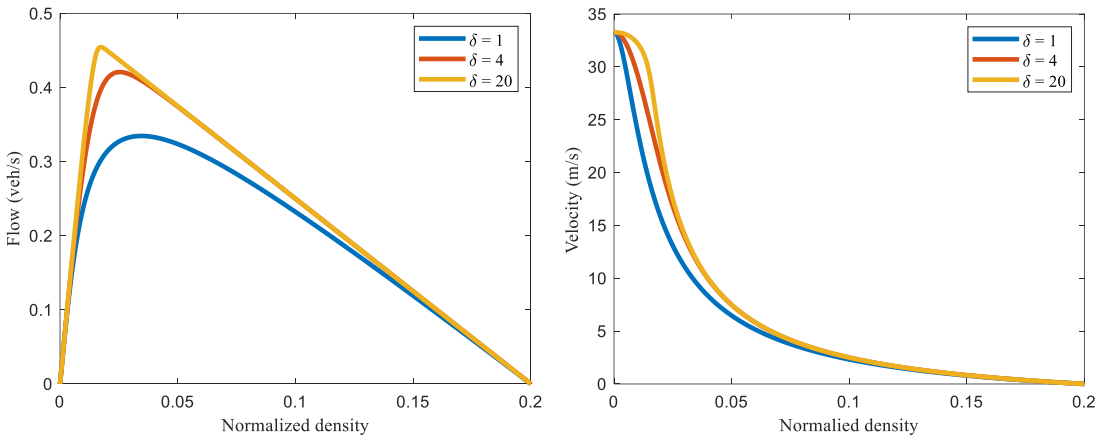

Figure 2.4 Vehicle behavior with the ID model for $\delta = 1,\ 4,$ and 20, **(a)** flow and **(b)** velocity (speed).

Table 2.2 Simulation parameters.

Parameter	**Value**
Maximum velocity (desired speed), v_{max}	33.3 m/s
Maximum acceleration, a_{max}	0.73 m/s^2
Minimum acceleration (deceleration), b	1.67 m/s^2
Jam spacing, s_j	5 m
Time headway for the ID model, τ	2 s
Time headway for the aggressive driver, τ	1 s
Time headway for the sluggish driver, τ	2.5 s
Time headway for the typical driver, τ	2 s
Safe time headway, τ_s	2 s
Ratio of distance headway to desired distance headways, $h = \frac{s}{D}$	0.3, 0.5 and 1.0
Proposed model acceleration, a	1.5 m/s^2
Time step size, Δt	0.5 s
Acceleration exponent, δ	1, 4, and 20
Maximum normalized density, $\rho_m = \frac{1}{s_j}$ at $v = 0$ m/s	0.2
Vehicle length, L	5 m

Figure 2.4 presents the flow and velocity (speed) with the ID model and the results are summarized in Table 2.3. When $\delta = 1$, the maximum flow is 0.33 veh/s at a density of 0.03, and the corresponding velocity (speed) is 9.9 m/s. When $\delta = 4$, the maximum flow is 0.42 veh/s at a density of 0.02, and the corresponding velocity (speed) is 16.9 m/s. When $\delta = 20$, the maximum flow is 0.45 veh/s at a density of 0.02, and the corresponding velocity (speed) is 27.3 m/s. Table 2.3 shows that a smaller value of δ results in a lower maximum flow and velocity (speed), but a larger density. As δ increases, the maximum flow increases while the density decreases, whereas the corresponding velocity (speed) increases.

Table 2.3 Maximum flow, density, and critical velocity (speed) for the ID model.

Acceleration exponent δ	**Maximum flow (veh/s)**	**Maximum density**	**Critical velocity (speed) (m/s)**
1	0.33	0.03	9.9
4	0.42	0.02	16.9
20	0.45	0.02	27.3

Figure 2.5 presents the flow and velocity (speed) with the proposed model for $h = 0.3,\ 0.5,$ and 1.0 and the results are summarized in Table 2.4. With $h = 0.3$ (aggressive driver), the maximum flow is 0.32 veh/s at a density of 0.03 and the corresponding velocity (speed) is 9.4 m/s. For $h = 0.5$, the maximum flow is 0.40 veh/s at a density of 0.04, and the corresponding velocity (speed) is 10.2 m/s. For $h = 1.0$, the maximum flow is 0.52 veh/s at a density of 0.05, and the corresponding velocity (speed) is 11.3 m/s. With $\frac{\tau}{\tau_s} > 1$ (sluggish driver), the maximum flow at $h = 0.3$ is 0.30 veh/s at a density of 0.03, and the corresponding velocity (speed) is 10.3 m/s. For $h = 0.5$, the maximum flow is 0.33 veh/s at a density of 0.02, and the corresponding velocity (speed) is 13.2 m/s. For $h = 1.0$, the maximum flow is 0.35 veh/s at a density of 0.02, and the corresponding velocity (speed) is 17.2 m/s. With $\frac{\tau}{\tau_s} = 1$ (typical driver), at $h = 0.3$ the maximum flow is 0.33 veh/s at a density of 0.04 and the corresponding velocity (speed) is 9.2 m/s. For $h = 0.5$, the maximum flow is 0.37 veh/s at a density of 0.03, and the corresponding velocity (speed) is 11.3 m/s. For $h = 1.0$, the maximum flow is 0.41 veh/s at a density of 0.03, and the corresponding velocity (speed) is 12.1 m/s. Table 2.4 indicates that with an aggressive driver, an increase in h increases the maximum flow, density, and velocity (speed). However, with sluggish and typical drivers, an increase in h increases the maximum flow and velocity (speed) but decreases the density. Moreover, with an aggressive driver an increase in h results in a faster increase in the maximum flow compared to a sluggish driver. As expected, with a typical driver the flow and velocity (speed) behavior are between the results for aggressive and sluggish drivers.

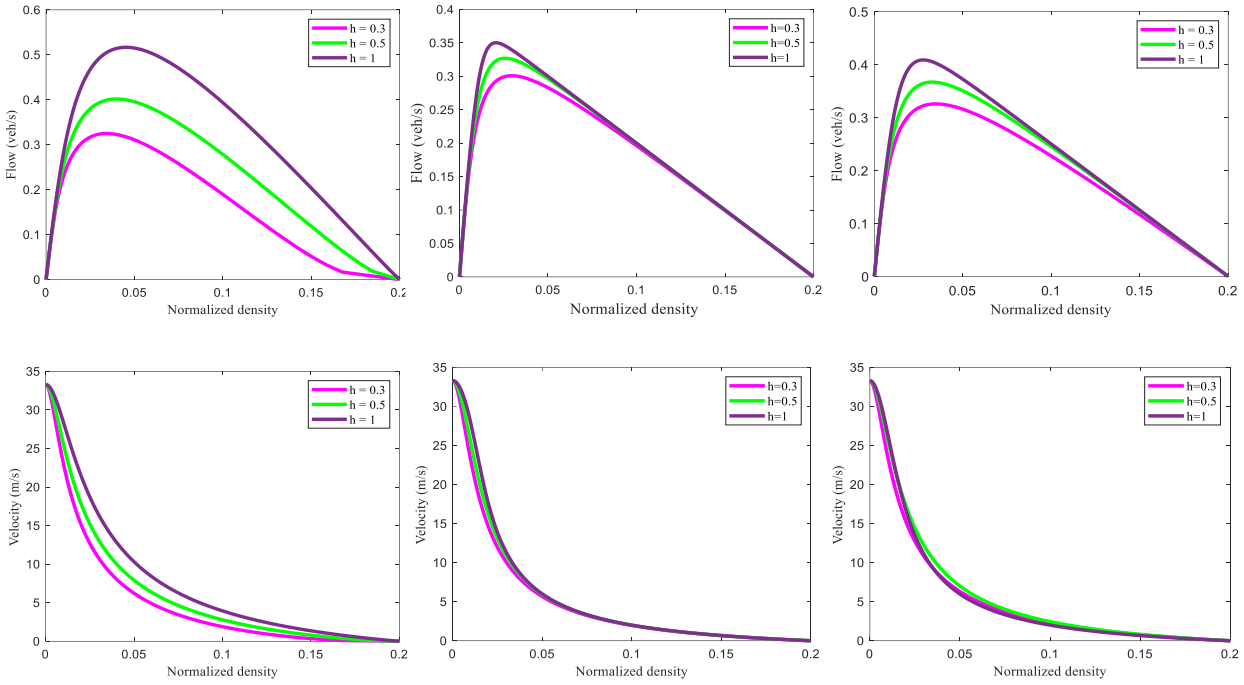

Figure 2.5 Flow and velocity (speed) with the proposed model versus density with $\frac{\tau}{\tau_s} < 1$, $\frac{\tau}{\tau_s} > 1$, and $\frac{\tau}{\tau_s} = 1$ for $h = 0.3,\ 0.5$ and 1.

Table 2.4 Maximum flow, density, and critical velocity (speed) with the proposed model.

Driver sensitivity	$\boldsymbol{h = \frac{s}{D}}$	**Maximum flow (veh/s)**	**Maximum density**	**Critical velocity (speed) (m/s)**
$\frac{\tau}{\tau_s} < 1$ (aggressive driver)	0.3	0.32	0.03	9.4
	0.5	0.40	0.04	10.2
	1.0	0.52	0.05	11.3
$\frac{\tau}{\tau_s} > 1$ (sluggish driver)	0.3	0.30	0.03	10.3
	0.5	0.33	0.02	13.2
	1.0	0.35	0.02	17.2
$\frac{\tau}{\tau_s} = 1$ (typical driver)	0.3	0.33	0.04	9.2
	0.5	0.37	0.03	11.3
	1.0	0.41	0.03	12.1

Figure 2.6 presents the temporal and spatial evolution of a queue for the ID model and the congestion results are summarized in Table 2.5. This shows that the velocity (speed) within the queue is zero. When $\delta = 1$, the queue dissipates at 57.5 s as shown in Figure 2.6a, and the corresponding velocity (speed) is 1.3 m/s. When $\delta = 4$, the queue dissipates at 56.0 s as shown in Figure 2.6b, and the corresponding velocity (speed) is 1.2 m/s. When $\delta = 20$, the queue exists from 0 to 55.5 s, and the velocity (speed) after the queue dissipates varies between 1.1 and 5.2 m/s. However, a new queue forms at 84.5 s and remains until 150.0 s, spanning 40.0 to 53.3 m as shown in Figure 2.6c. With $\delta = 1$, the maximum velocity (speed) is 20.0 m/s, whereas with $\delta = 4$ and 20 it is 25.0 and 30.0 m/s, respectively. These results indicate that the traffic queue with the ID model dissipates based on the constant δ rather than driver response, which is unrealistic.

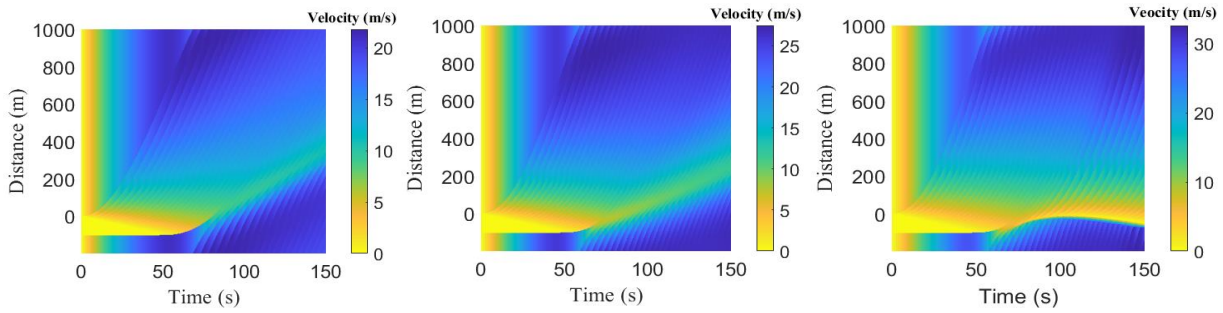

(a) **(b)** **(c)**

Figure 2.6 Velocity (speed) versus time and space with the ID model over a 1200 m circular road for **(a)** $\delta = 1$, **(b)** $\delta = 4$, and **(c)** $\delta = 20$.

Table 2.5 Velocity (speed) and time for the ID model during and after congestion.

Acceleration exponent $\boldsymbol{\delta}$	**Time during which congestion occurs (s)**	**Velocity (speed) after congestion dissipates (m/s)**	**Time after congestion dissipates (s)**
1	$0 - 57.5$	1.3	57.5
4	$0 - 56.0$	1.2	56.0
20	$0 - 55.5$ and $84.5 - 150.0$	$1.1 - 5.2$	$84.5 - 150.0$

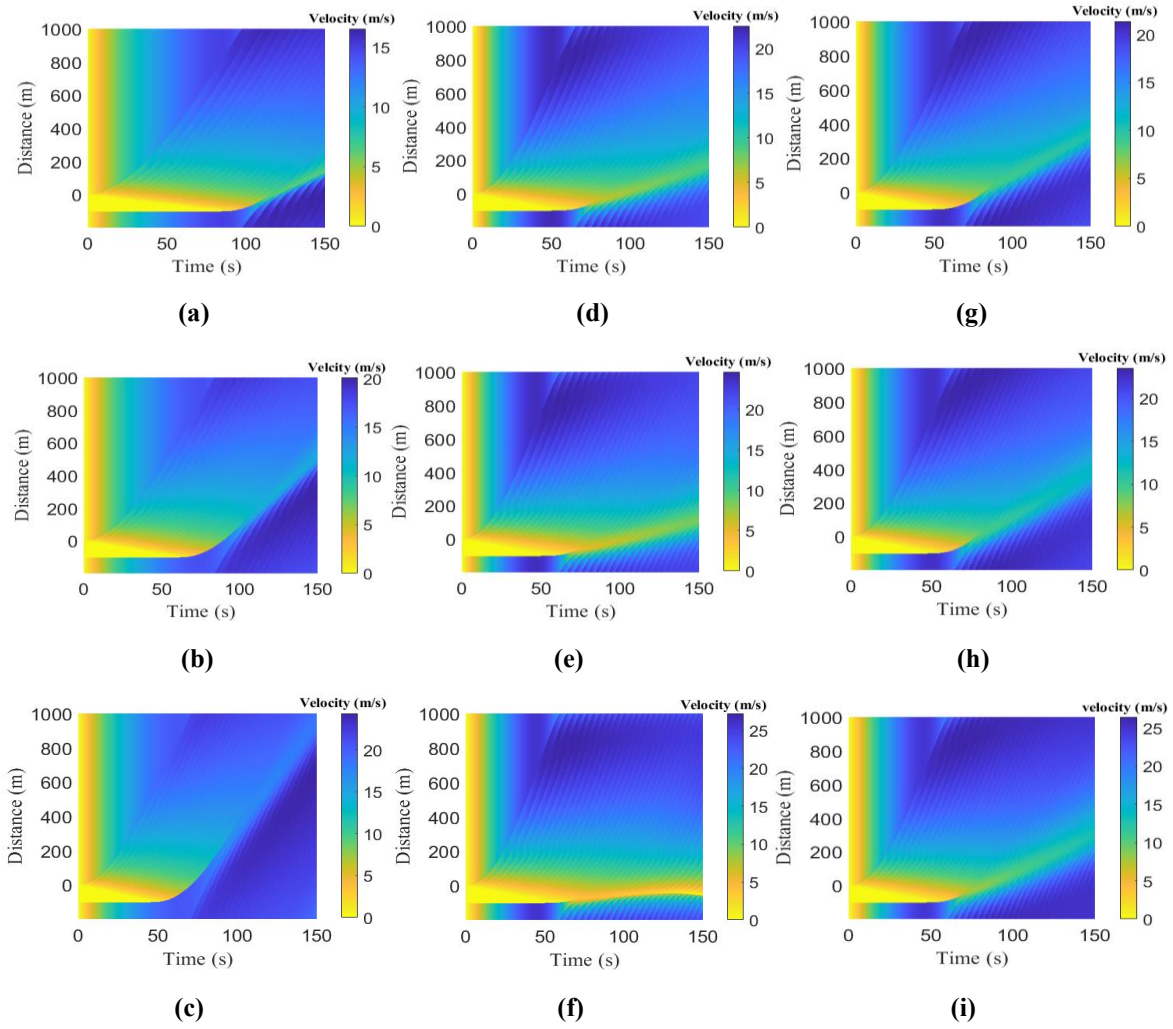

Figure 2.7 Velocity (speed) versus time and space for the proposed model over a 1200 m circular road for $\frac{\tau}{\tau_s} < 1$ with **(a)** $h = 0.3$, **(b)** $h = 0.5$, and **(c)** $h = 1.0$, $\frac{\tau}{\tau_s} > 1$ with **(d)** $h = 0.3$, **(e)** $h = 0.5$, and **(f)** $h = 1.0$, and $\frac{\tau}{\tau_s} = 1$ with **(g)** $h = 0.3$, **(h)** $h = 0.5$, and **(i)** $h = 1.0$.

Figure 2.7 presents the temporal and spatial evolution of a queue with the proposed model and the congestion results are summarized in Table 2.6. This shows that the velocity (speed) within the queue is zero. For $\frac{\tau}{\tau_s} < 1$ (aggressive driver), with $h = 0.3$ the queue dissipates at 91.5 s as shown in Figure 2.7a, and the corresponding velocity (speed) is 1.3 m/s. With $h = 0.5$ and 1.0 the queue dissipates at 68.0 and 54.5 s, respectively, as shown in Figures 2.7b and 2.7c. With $h = 0.5$, the velocity (speed) after the queue dissipates is 1.6 m/s, while with $h = 1.0$ it is 2.5 m/s. For $\frac{\tau}{\tau_s} > 1$ (sluggish driver), with $h = 0.3$ and 0.5 the queue dissipates at 62.5 and 61.0 s, respectively, as

shown in Figures 2.7d and 2.7e. With $h = 0.3$ the velocity (speed) after the queue dissipates is 1.4 m/s while with $h = 0.5$ it is 1.2 m/s. With $h = 1.0$ the initial queue dissipates at 60.0 s and the corresponding velocity (speed) is between 1.0 and 1.9 m/s as shown in Table 2.6. A queue again develops at 125.0 s and lasts until 150.0 s between -43.3 and -56.6 m as shown in Figure 2.7f. For $\frac{\tau}{\tau_s} = 1$ (typical driver), with $h = 0.3$ the queue dissipates at 60.0 s as shown in Figure 2.7g, and the corresponding velocity (speed) is 1.7 m/s. With $h = 0.5$ and 1.0, the queue dissipates at 58.5 and 59.0 s, respectively, as shown in Figures 2.7h and 2.7i. With $h = 0.5$ the velocity (speed) after the queue is 1.8 m/s while with $h = 1.0$ the velocity (speed) is 2.1 m/s. The largest velocity (speed) after the queue dissipates is 2.5 m/s. These results indicate that queue dissipation is quick with an aggressive driver compared to a sluggish driver. Further, the dissipation with a typical driver is between that with aggressive and sluggish drivers, as expected.

Table 2.6 Velocity (speed) and time for the proposed model during the queue and after the queue dissipates.

Driver Sensitivity	$\boldsymbol{h = \frac{s}{D}}$	**Time during which congestion occurs (s)**	**Velocity (speed) after congestion dissipates (m/s)**	**Time after congestion dissipates (s)**
$\frac{\tau}{\tau_s} < 1$ (aggressive driver)	0.3	$0 - 91.5$	1.3	91.5
	0.5	$0 - 68.0$	1.6	68.0
	1.0	$0 - 54.5$	2.5	54.5
$\frac{\tau}{\tau_s} > 1$ (sluggish driver)	0.3	$0 - 62.5$	1.4	62.5
	0.5	$0 - 61.0$	1.2	61.0
	1.0	$0 - 60.0$ and $125.0 - 150.0$	1.0 and 1.9	60.0 and 125.0
$\frac{\tau}{\tau_s} = 1$ (typical driver)	0.3	$0 - 60.0$	1.7	60.0
	0.5	$0 - 58.5$	1.8	58.5
	1.0	$0 - 59.0$	2.1	59.0

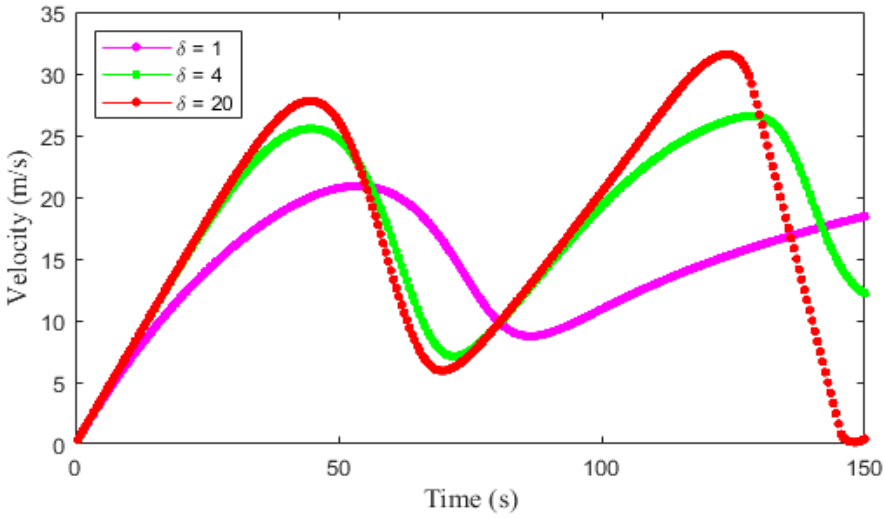

Figure 2.8 Velocity (speed) with the ID model for $\delta = 1,\ 4$, and 20 over a 1200 m circular road.

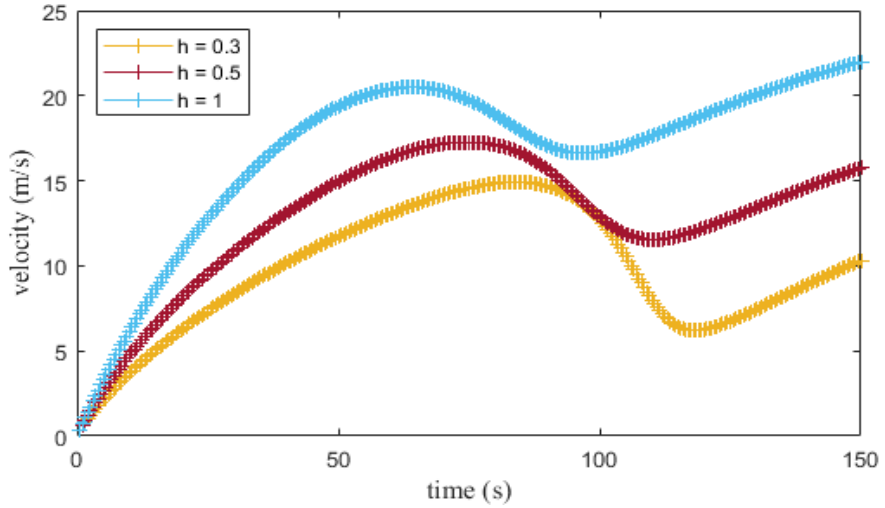

Figure 2.9 Velocity (speed) with the proposed model for $h = 0.3, 0.5$, and 1.0 with $\frac{\tau}{\tau_s} < 1$ over a 1200 m circular road.

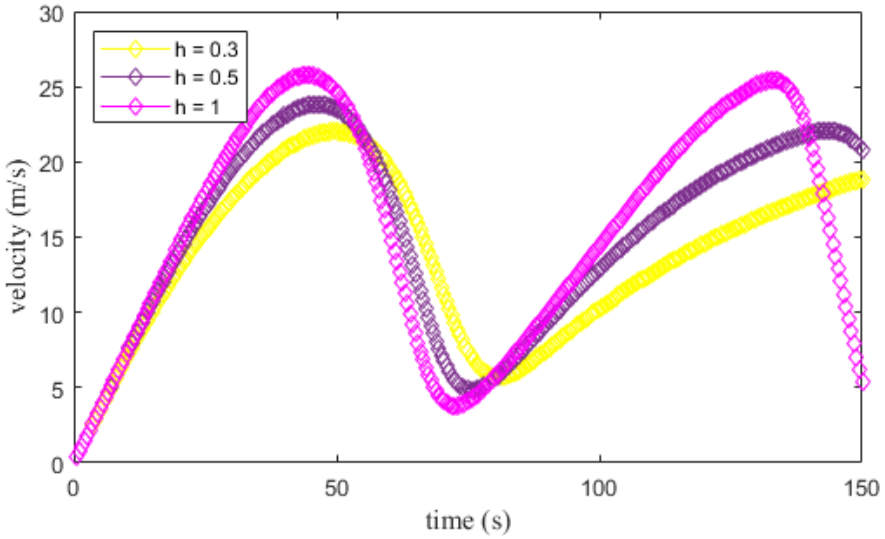

Figure 2.10 Velocity (speed) with the proposed model for $h = 0.3, 0.5$, and 1.0 with $\frac{\tau}{\tau_s} > 1$ over a 1200 m circular road.

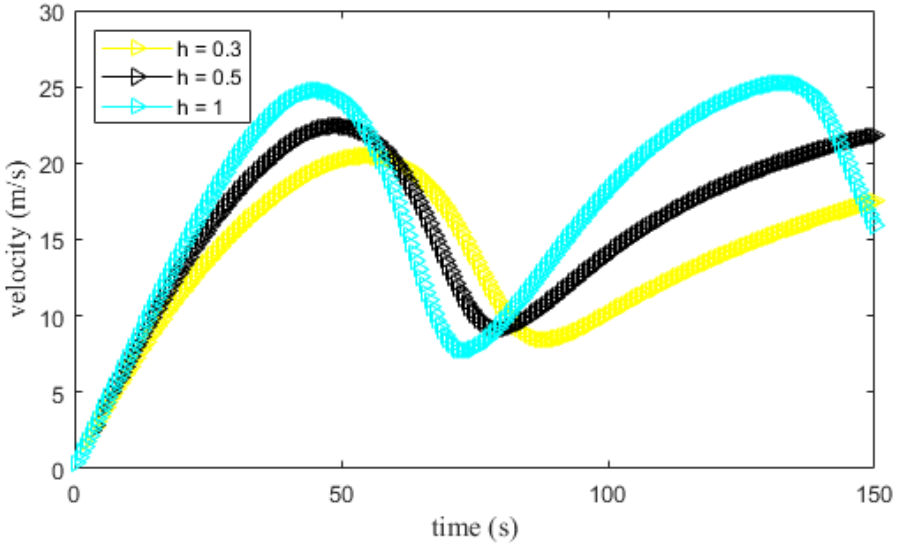

Figure 2.11 Velocity (speed) with the proposed model for $h = 0.3, 0.5$, and 1.0 with $\frac{\tau}{\tau_s} = 1$ over a 1200 m circular road.

Figure 2.8 presents the velocity (speed) with the ID model over a 1200 m road for $\delta = 1,\ 4,$ and 20. This shows that an increase in δ increases the variations in velocity (speed). The corresponding velocity (speed) with the proposed model for $\frac{\tau}{\tau_s} < 1$ (aggressive driver), is given in Figure 2.9. This indicates that the variations in velocity (speed) are smaller with a larger value of h. The velocity (speed) with the proposed model for $\frac{\tau}{\tau_s} > 1$ (sluggish driver) and $\frac{\tau}{\tau_s} = 1$ (typical driver), is presented in Figures 2.10 and 2.11, respectively. These show that the variations in velocity (speed) increase with h.

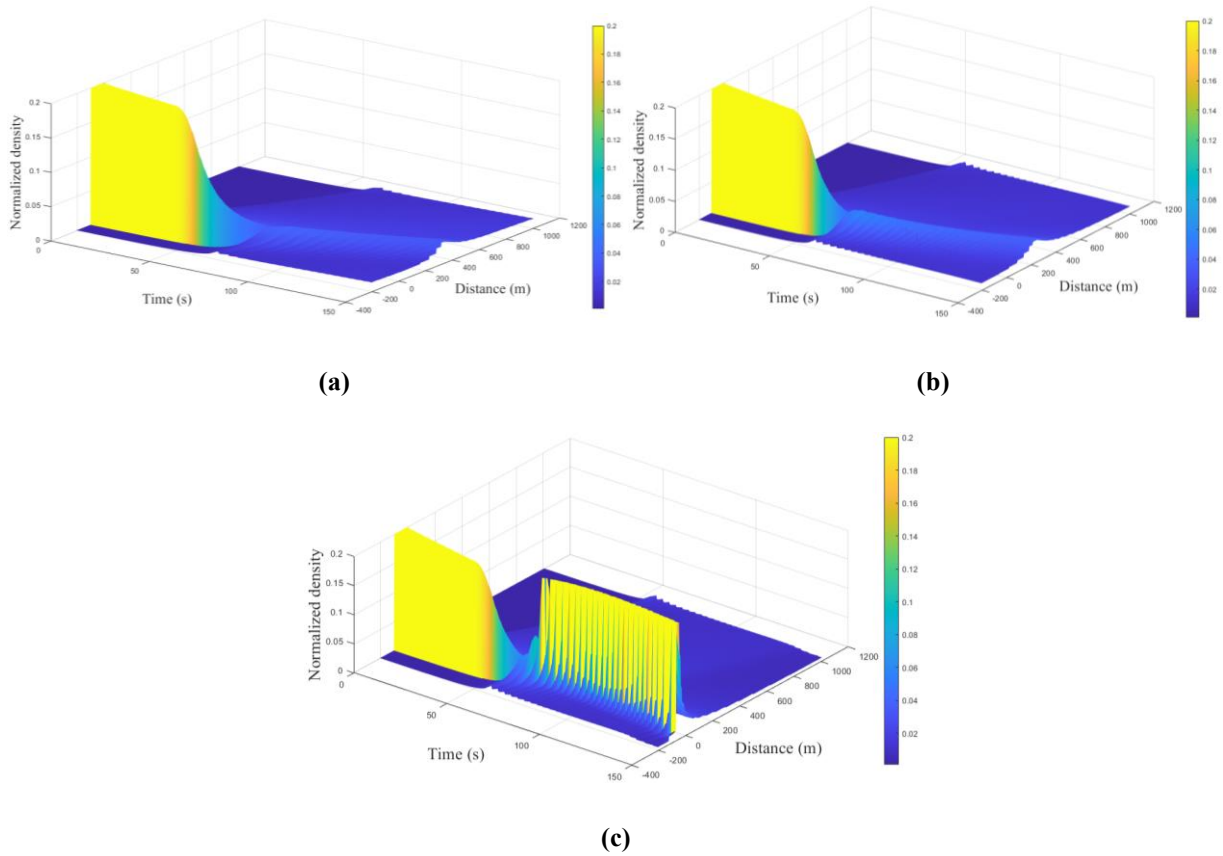

Figure 2.12 Traffic density with the ID model over a 1200 m circular road for **(a)** $\delta = 1$, **(b)** $\delta = 4$, and **(c)** $\delta = 20$.

Figure 2.12 presents the density evolution over time and distance with the ID model. When $\delta = 1$, the density is 0.012 from 0 to 136.5 m at 149.5 s. At 336.3 m, it is 0.03 and then decreases to 0.016 at 709.2 m as shown in Figure 2.12a. From 0 to 47.0 s there is a traffic queue as the density is 0.20. At 80.5 s, the density at 148.0 s decreases to 0.032 after the congestion ends.

When $\delta = 4$, at 147.0 s the density is 0.014 from 0 to 23.3 m. It increases to 0.036 at 219.8 m and then decreases to 0.014 at 619.4 m as shown in Figure 2.12b. From 0 to 45.0 s the density is 0.20 which indicates a traffic queue. At 149.00 s, the density decreases to 0.036. When $\delta = 20$, at 147.0 s the density between -66.6 m and -50.0 m is 0.20 which indicates a traffic queue. At 509.9 m, it decreases to 0.008 as shown in Figure 2.12c. It is 0.20 from 0 to 46.5 s so there is a traffic queue. The density then decreases to 0.05 at 66.0 s. A queue again develops at 77.0 s as the density is 0.20 and remains until 150.0 s between -66.6 and -50.0 m. Figure 2.12 shows that as δ increases the change in density over time increases which indicates the model is unstable.

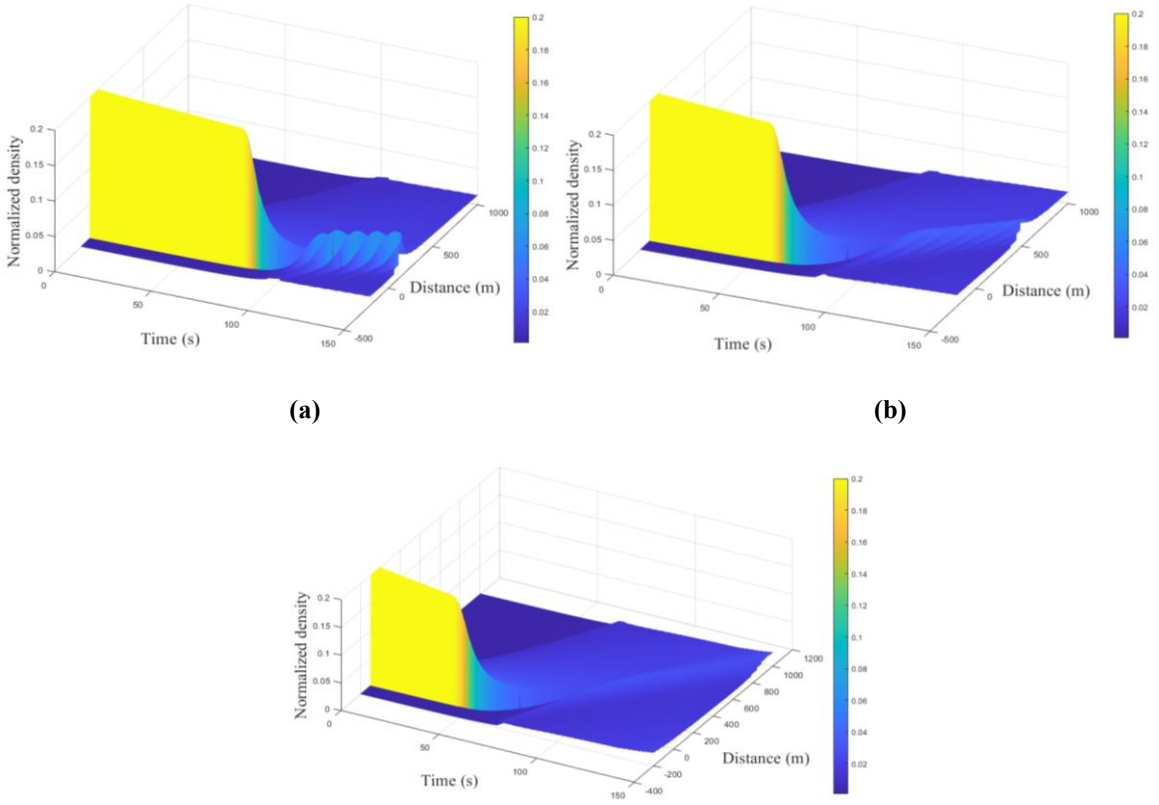

Figure 2.13 Traffic density with the proposed model over a 1200 m circular road for $\frac{\tau}{\tau_s} < 1$ and **(a)** $h = 0.3$, **(b)** $h = 0.5$, and **(c)** $h = 1.0$.

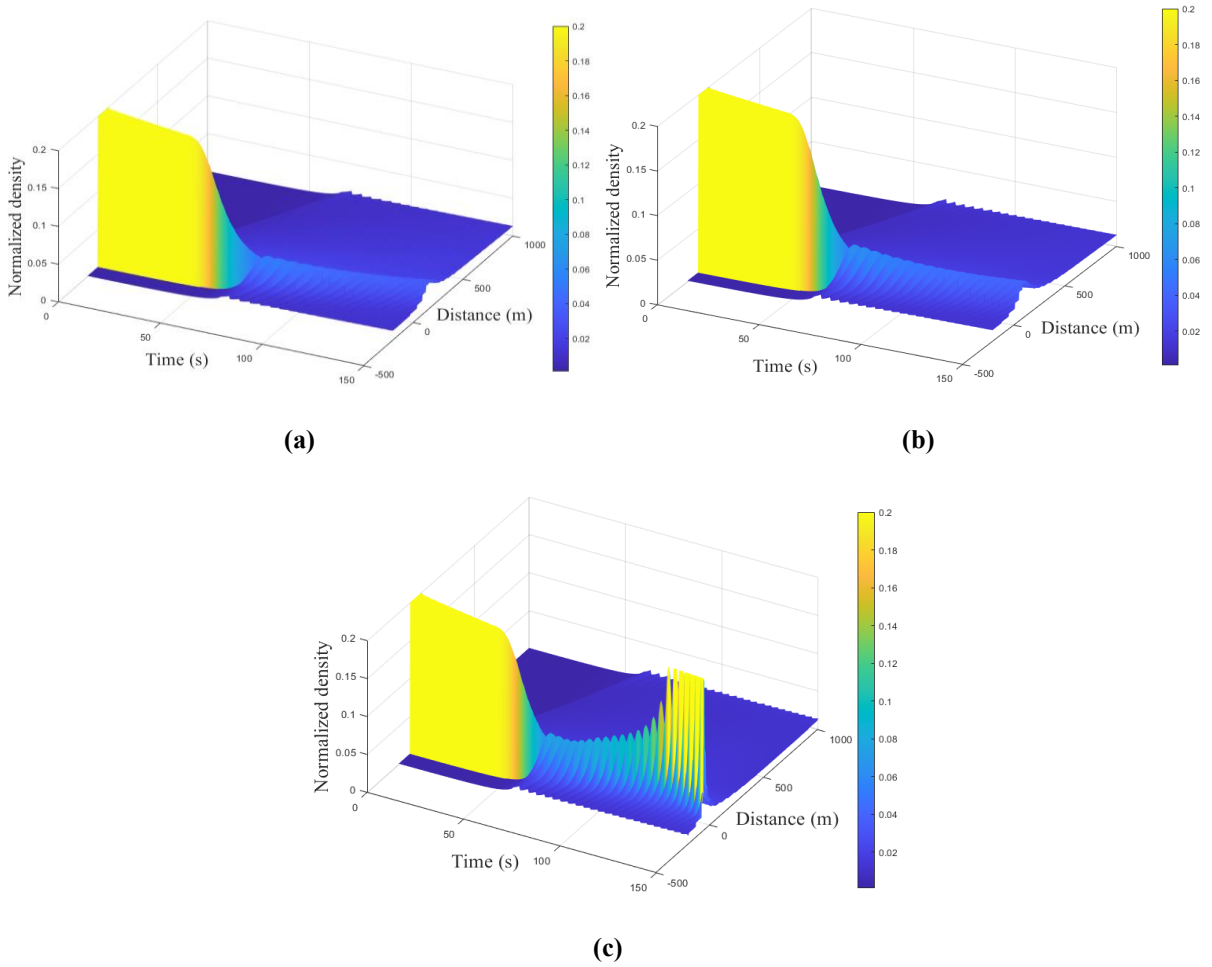

Figure 2.14 Traffic density with the proposed model over a 1200 m circular road for $\frac{\tau}{\tau_s} > 1$ and **(a)** $h = 0.3$, **(b)** $h = 0.5$, and **(c)** $h = 1.0$.

Figure 2.13 presents the density evolution over time and distance with the proposed model for $\frac{\tau}{\tau_s} < 1$ (aggressive driver). With $h = 0.3$, from 0 to 53.3 m at 149.0 s the density is 0.01. It increases to 0.06 at 129.8 m and then decreases to 0.016 at 456.2 m as shown in Figure 2.13a. From 0 to 79.0 s the density is 0.20 which indicates a traffic queue. At 114.5 s the queue dissipates and the density decreases to 0.05 and then increases to 0.06 at 149.0 s. With $h = 0.5$, from 0 to 336.3 m at 148.5 s the density is 0.012. It increases to 0.03 at 492.8 m and then decreases to 0.016 at 885.7 m as shown in Figure 2.13b. From 0 to 49.50 s, it is 0.20 which indicates a queue, and at 149.0 s it decreases to 0.035. With $h = 1.0$, from 0 to 732.6 m at 149.5 s the density is 0.014. At 985.6 m it increases to 0.020 as shown in Figure 2.13c. From 0 to 43.0 s the density is

0.20 which indicates a queue. At 146.0 s, the queue dissipates and the density decreases to 0.015 at 169.8 m.

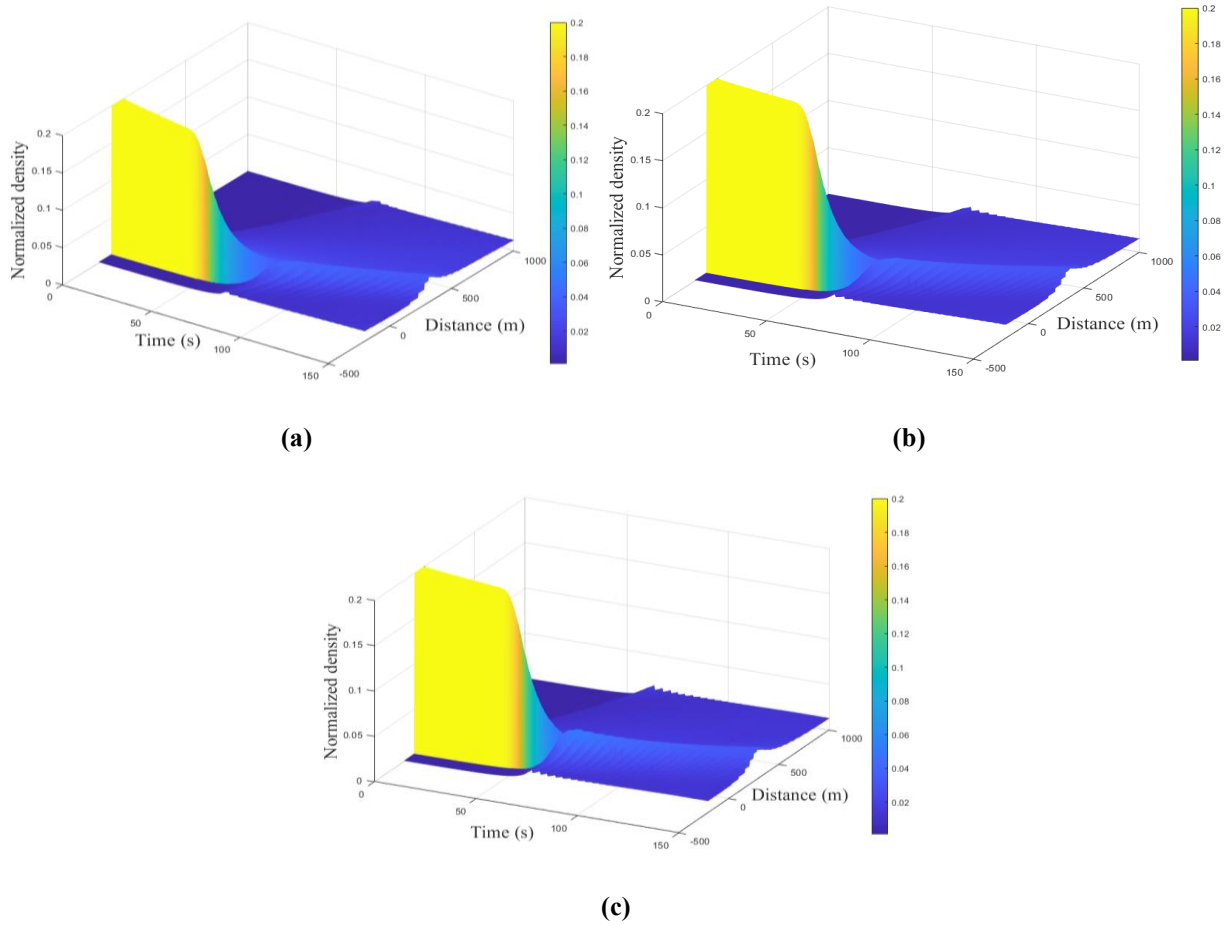

Figure 2.15 Traffic density with the proposed model over a 1200 m circular road for $\frac{\tau}{\tau_s} = 1$ and **(a)** $h = 0.3$, **(b)** $h = 0.5$, and **(c)** $h = 1.0$.

Figure 2.14 presents the density evolution over time and distance with the proposed model for $\frac{\tau}{\tau_s} > 1$ (sluggish driver). With $h = 0.3$, from 0 to 26.6 m the density is 0.014 at 149.5 s. From 0.02 to 329.6 m it decreases to 0.015 at 586.0 m as shown in Figure 2.14a. From 0 to 48.5 s, it is 0.20 which indicates a traffic queue, and at 149.0 s it decreases to 0.03. With $h = 0.5$, from 0 to 9.99 m at 150.0 s the density is 0.017. At 99.9 m, it increases to 0.038 and then decreases to 0.014 at 479.5 m as shown in Figure 2.14b. From 0 to 48.5 s it is 0.20, which indicates a queue, and at 149.0 s it decreases to 0.03. With $h = 1.0$, from -56.6 to -43.2 m at 150.0 s the density is 0.20 which indicates a queue. It then decreases to 0.012 at 316.3 m as shown in Figure 2.14c.

From 0 to 49.5 s the density is 0.20 which indicates a queue, and at 70.0 s it decreases to 0.07. A queue with density 0.20 again forms at 131.0 s and remains until 150.0 s between -56.6 and -43.2 m.

Figure 2.15 presents the density evolution over time and distance with the proposed model for $\frac{\tau}{\tau_s} = 1$ (typical driver). With $h = 0.3$, from 0 to 153.2 m at 150.0 s the density is 0.012. It then decreases to 0.01 at 526.1 m as shown in Figure 2.15a. From 0 to 43.5 s, the density is 0.20 which indicates a queue, and at 147.5 s it decreases to 0.032. With $h = 0.5$, from 0 to 149.8 m at 150.0 s the density is 0.013. It then increases to 0.029 at 362.9 m and decreases to 0.016 at 729.2 m as shown in Figure 2.15b. From 0 to 46.0 s, the density is 0.20 which indicates a queue, and at 148.5 s it decreases to 0.03. With $h = 1.0$, from 0 to 79.9 m at 149.0 s the density is 0.015 and decreases to 0.013 at 785.8 m as shown in Figure 2.15c. From 0 to 45.0 s, the density is 0.20 which indicates a queue and it decreases to 0.032 at 148.0 s.

The results presented in this section indicate that with the proposed model and an aggressive driver, the changes in velocity (speed) and density are small, whereas with a sluggish driver these changes are large. As expected, the response with a typical driver is between that of an aggressive driver and a sluggish driver. However, the ID model employs a fixed exponent regardless of the density and velocity (speed) and so the results are unrealistic. Thus, the proposed model achieves a smooth flow considering driver reaction and sensitivity, which is more realistic than with the ID model.

2.4 Conclusion

A new microscopic traffic model was introduced which is based on driver response considering both driver reaction and sensitivity. The performance of the proposed model was compared with the well-known ID model over a circular road that can be considered a worst-case scenario. The results obtained show that the density and velocity (speed) evolution with the proposed model are realistic as they are based on real traffic parameters. Conversely, the constant exponent used in the ID model produces less realistic results. Moreover, the variations in velocity (speed) are greater with a sluggish driver compared to an aggressive driver, as expected.

The stability results demonstrate that with the proposed model, a large driver sensitivity means congestion dissipates quickly. Further, the large sensitivity with such a driver creates larger oscillations in velocity (speed) and greater stop-and-go waves than with a sluggish driver (small

sensitivity), as expected. Hence, the traffic behavior with the proposed model is more stable than the ID model. This is because the ID model employs a constant exponent δ to characterize traffic behavior which is not based on real traffic dynamics.

Chapter 3

A Traffic Model Incorporating Vehicle Vibrations Due to Pavement Condition

Pavement condition significantly impacts traffic behavior. Pavement deterioration causes traffic accidents, congestion, pollution, and time delays. Moreover, poor roads impact the smooth flow of traffic resulting in rider discomfort and increased vehicle operating costs [54]. Congestion lowers vehicle speeds so emissions are increased. Further, vehicle speed is reduced by an average of 55% when the road condition is poor compared to when it is excellent, and average emissions increase by 2.49%. Road safety is a primary concern worldwide as road accidents cause approximately 1.35 million fatalities each year [55]. It is also dangerous as uneven pavement and potholes, damaged concrete, cracks, and exposed rebar can cause drivers to lose control resulting in severe accidents [56]. Efficient traffic forecasting and control are essential to alleviate traffic problems such as congestion and improve road infrastructure. This requires a practical model for traffic prediction.

This chapter introduces a microscopic traffic model that incorporates the pavement condition to accurately represent traffic behavior. The pavement condition is evaluated using the pavement condition index (PCI), which is an indicator of pavement condition and quality, and thus affects driver behavior and traffic flow. It ranges between 0 to 100 [54]. Incorporating the PCI results in a model that provides a more comprehensive and accurate representation of traffic behavior. First, field experiments to determine the impact of vehicle vibrations on the PCI were conducted on the Grand Trunk highway in Peshawar, located in the Khyber Pakhtunkhwa province of Pakistan. This road section spans 7 km (7000 m) and consists of two lanes. It extends from the Chamkani Bus Rapid Transit (BRT) station to Pabbi. Then, the proposed and ID models are implemented using the Euler technique in MATLAB.

The rest of the chapter is organized as follows. In Section 3.1, traffic models are presented. Section 3.2 evaluates the performance of models. Finally, Section 3.3 gives some concluding remarks.

3.1 Traffic Models

The ID model is used for microscopic traffic characterization and is expressed as [26]

$$\frac{dv}{dt} = a_{max}\left(1 - \left(\frac{v}{v_{max}}\right)^{\delta} - \left(\frac{D}{s}\right)^{2}\right), \tag{3.1}$$

where a_{max} is the maximum acceleration, v is the speed, v_{max} is the maximum speed (desired speed), and δ is a fixed acceleration exponent. s is the distance headway and D is the desired distance headway, given by [26]

$$D = s_j + \tau v + \frac{v\Delta v}{2\sqrt{a_{max}b}} \tag{3.2}$$

where b is the minimum acceleration (deceleration), s_j is the jam spacing as illustrated in Figure 3.1, Δv is the speed difference, and τ is the time required by a vehicle to adjust its speed to the speed of the leading vehicle.

The ID model characterizes driver response to traffic conditions based on a fixed value δ. Thus, driver behavior does not vary based on these conditions, so it is unrelated to traffic physics and results in inadequate and unrealistic traffic characterization.

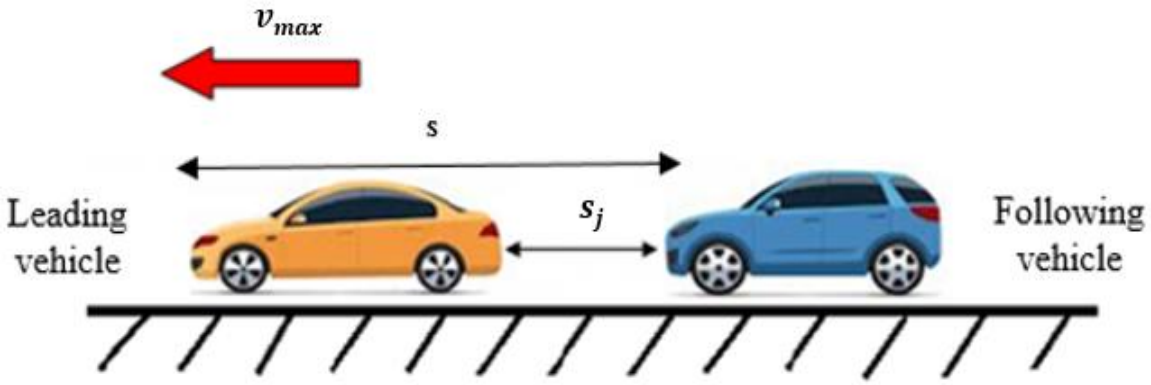

Figure 3.1 Intelligent driver (ID) model parameters.

Field experiments were conducted by driving a test vehicle over the road segment in Peshawar, Pakistan, between 12 AM and 2 AM. One lane in each direction was traversed 12 times with speeds of 35 km/h (9.72 m/s), 45 km/h (12.50 m/s), and 55 km/h (15.27 m/s). Thus, for a given speed, a lane was traversed four times. These speeds were selected to represent typical traffic observed on the road segment. Data were collected using an On-Board Diagnostic-II scanner connected to a smartphone with the BotlnckDectr [57] mobile app. This allowed for the recording of various

parameters including GPS location, in-vehicle noise, vibration, and time. During the experiments, the smartphone was positioned on the vehicle dashboard. The data were transmitted to the Amazon Web Services (AWS) cloud. It was then analyzed to obtain the PCI of the road segment. The relationships between PCI and vehicle vibrations obtained are

$$\delta = -0.0169PCI + 4.068 \tag{3.3}$$

$$\delta = -0.0265PCI + 5.037 \tag{3.4}$$

$$\delta = -0.0251PCI + 5.209 \tag{3.5}$$

for speeds of approximately 9.72 m/s, 12.50 m/s, and 15.27 m/s, respectively. The PCI ranges from 0 to 100 where 0 corresponds to a poor road condition and 100 to an excellent road condition. Thus, δ and PCI are linearly related. As the pavement condition degrades, the oscillations increase, which reduces passenger comfort, i.e., a higher PCI corresponds to lower vibrations. Substituting (3.3), (3.4) and (3.5) in (3.1) gives the proposed model for speeds of 9.72 m/s, 12.50 m/s, and 15.27 m/s, respectively.

$$\frac{dv}{dt} = a_{max}\left(1 - \left(\frac{v}{v_{max}}\right)^{(-0.0169PCI + 4.068)} - \left(\frac{D}{s}\right)^2\right) \qquad (v_{max} = 9.72 \text{ m/s}) \tag{3.6}$$

$$\frac{dv}{dt} = a_{max}\left(1 - \left(\frac{v}{v_{max}}\right)^{(-0.0265PCI + 5.037)} - \left(\frac{D}{s}\right)^2\right) \qquad (v_{max} = 12.50 \text{ m/s}) \tag{3.7}$$

$$\frac{dv}{dt} = a_{max}\left(1 - \left(\frac{v}{v_{max}}\right)^{(-0.0251PCI + 5.209)} - \left(\frac{D}{s}\right)^2\right) \qquad (v_{max} = 15.27 \text{ m/s}) \tag{3.8}$$

An excellent road condition is required to avoid traffic congestion and accidents and efficiently align to forward vehicles. In this case, there is free flow traffic which corresponds to $PCI = 100$. A poor road condition can result in congestion due to the reduction in vehicle speed. In this case, $PCI = 0$ and vehicle acceleration and deceleration are large so the emissions are high. With the proposed model, alignment is according to the PCI and is more realistic compared with fixed δ.

The traffic density can be expressed as $\rho = 1/s_e$ [47] where s_e is the distance headway at equilibrium. In this case, $\Delta v = 0$ so substituting (3.2) in (3.1) gives for the ID model

$$a_{max}\left(1 - \left(\frac{v}{v_{max}}\right)^{\delta} - \left(\frac{s_j + \tau v}{s_e}\right)^2\right) = 0 \tag{3.9}$$

and rearranging gives

$$s_e = (s_j + \tau v)\left(1 - \left(\frac{v}{v_{max}}\right)^{\delta}\right)^{-\frac{1}{2}} \tag{3.10}$$

Thus, the fixed δ in the ID model results in a constant distance headway between vehicles at equilibrium regardless of the traffic conditions. In contrast, in the proposed model the distance headway is based on the PCI. The distance headway at equilibrium is obtained by substituting (3.3), (3.4), and (3.5) in (3.10) which gives

$$s_e = (s_j + \tau v)\left(1 - \left(\frac{v}{v_{max}}\right)^{(-0.0169PCI + 4.068)}\right)^{-\frac{1}{2}} \quad (v_{max} = 9.72 \text{ m/s}) \tag{3.11}$$

$$s_e = (s_j + \tau v)\left(1 - \left(\frac{v}{v_{max}}\right)^{(-0.0265PCI + 5.037)}\right)^{-\frac{1}{2}} \quad (v_{max} = 12.50 \text{ m/s}) \tag{3.12}$$

$$s_e = (s_j + \tau v)\left(1 - \left(\frac{v}{v_{max}}\right)^{(-0.0251PCI + 5.209)}\right)^{-\frac{1}{2}} \quad (v_{max} = 15.27 \text{ m/s}) \tag{3.13}$$

The product of density and speed is traffic flow [31] so that

$$Q = \frac{v}{s_e} \tag{3.14}$$

and substituting (3.10) in (3.14) gives the flow for the ID model as

$$Q = \frac{v}{(s_j + \tau v)\left(1 - \left(\frac{v}{v_{max}}\right)^{\delta}\right)^{-\frac{1}{2}}} \tag{3.15}$$

This is unrealistic as it relies on a fixed exponent. The proposed model considers the PCI to determine traffic flow and so is more realistic. The traffic flow can be expressed as

$$Q = \frac{v}{(s_j + \tau v)\left(1 - \left(\frac{v}{v_{max}}\right)^{(-0.0169PCI + 4.068)}\right)^{-\frac{1}{2}}} \quad (v_{max} = 9.72 \text{ m/s}) \tag{3.16}$$

$$Q = \frac{v}{(s_j + \tau v)\left(1 - \left(\frac{v}{v_{max}}\right)^{(-0.0265PCI + 5.037)}\right)^{-\frac{1}{2}}} \quad (v_{max} = 12.50 \text{ m/s}) \tag{3.17}$$

$$Q = \frac{v}{(s_j + \tau v)\left(1 - \left(\frac{v}{v_{max}}\right)^{(-0.0251PCI + 5.209)}\right)^{-\frac{1}{2}}} \quad (v_{max} = 15.27 \text{ m/s}) \tag{3.18}$$

The proposed model indicates that when the road condition is poor, the vehicle vibrations are large and the flow is small. Whereas, when the road condition is excellent, the vehicle vibrations are small and the flow is large.

3.2 Traffic Models Performance Evaluation

In this section, the performance of the proposed model and ID models is evaluated on a circular road of length 3000 m. The Euler scheme is employed with time step size 0.50 s. The proposed model is simulated for 400 s and the ID model for 150 s. Based on (3.3), (3.4), and (3.5) the maximum speed (desired speed) v_{max} for the proposed model is set to 9.72 m/s, 12.50 m/s, and 15.27 m/s. The v_{max} for the ID model is 20 m/s [32]. The jam spacing is set to 2.0 m [50], the maximum acceleration is 0.73 m/s², and the minimum acceleration (deceleration) is 1.67 m/s² [26]. The acceleration exponent δ is typically 1 or greater and is often set to 4 [26]. Thus, here $\delta = 1, 4,$ and 20. The PCI values considered are $PCI = 0, 50,$ and 100. The maximum normalized density is set to $1/s_j = 0.50$ and the critical density is 0.25 [58]. The maximum flow is obtained at the critical density with speed v_{max}. Thus, the speed is normalized by v_{max} and the flow is normalized by $0.25 \times v_{max}$. The simulation parameters are summarized in Table 3.1.

Table 3.1 Simulation parameters.

Parameter	**Value**
Maximum speed (desired speed) for the proposed model, v_{max}	9.72 m/s, 12.50 m/s and 15.27 m/s
Maximum speed (desired speed) for the ID model, v_{max}	20 m/s
Time headway for ID and proposed model, τ	2.0 s
Jam spacing, s_j	2.0 m
Maximum acceleration, a_{max}	0.73 m/s^2
Vehicle length, L	5.0 m
Acceleration exponent for the ID model, δ	1, 4, and 20
Pavement condition index, PCI	0, 50 and 100
Minimum acceleration (deceleration), b	1.67 m/s^2
Time step size, Δt	0.50 s

Figure 3.2 gives the normalized flow for the proposed model with $v_{max} = 9.72$ m/s and $PCI = 0, 50,$ and 100. When $PCI = 0,$ the flow at 19.0 s is 0.0010. It is 0.0021 at 106.5 s,

increasing to 0.0032 at 293.0 s and 0.0035 at 400 s. When $PCI = 50$, the flow at 19.5 s is 0.0010. It is 0.0020 at 162.5 s, increasing to 0.0031 at 288.0 s and 0.0038 at 400 s. When $PCI = 100$, the flow at 21.5 s is 0.0010. It is 0.0025 at 172.0 s, increasing to 0.0033 at 285.5 s and 0.0044 at 400 s.

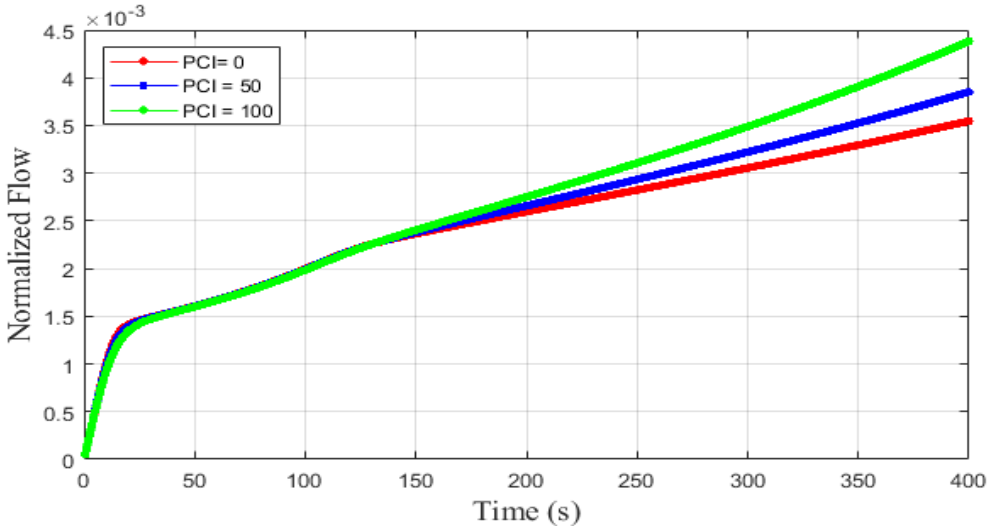

Figure 3.2 Normalized flow for the proposed model with $v_{max} = 9.72$ m/s over a 3000 m circular road.

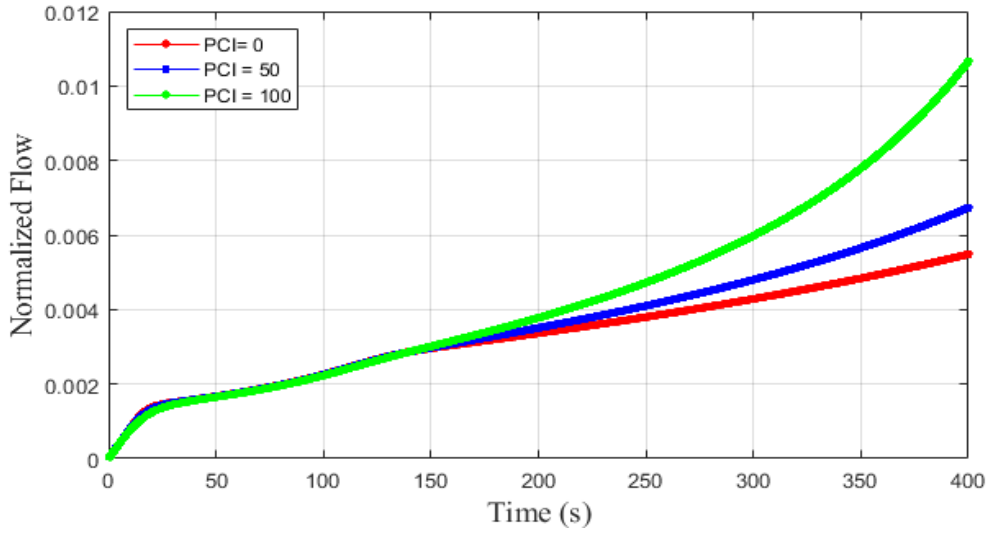

Figure 3.3 Normalized flow for the proposed model with $v_{max} = 12.50$ m/s over a 3000 m circular road.

Figure 3.3 gives the normalized flow for the proposed model with $v_{max} = 12.50$ m/s and $PCI = 0,\ 50$, and 100. When $PCI = 0$, the flow at 20.0 s is 0.0012. It is 0.0029 at 156.0 s, increasing to 0.0042 at 268.5 s and 0.0054 at 400 s. When $PCI = 50$, the flow at 22.5 s is 0.0013. It is 0.0033 at 167.0 s, increasing to 0.0045 at 276.0 s and 0.0063 at 400 s. When $PCI = 100$, the flow at 23.5 s is 0.0010. It is 0.0037 at 179.0 s, increasing to 0.0062 at 313.5 s and 0.0110 at 400 s.

Figure 3.4 gives the normalized flow for the proposed model with $v_{max} = 15.27$ m/s and $PCI = 0,\ 50$, and 100. When $PCI = 0$, the flow at 22.0 s is 0.0013. It is 0.0050 at 217.5 s, increasing to 0.0079 at 307.5 s and 0.0140 at 400 s. When $PCI = 50$, the flow at 25.0 s is 0.0013. It is 0.0052 at 220.5 s, increasing to 0.0110 at 324.0 s and 0.0270 at 400 s. When $PCI = 100$, the flow at 27.5 s is 0.0010, increasing to 0.0070 at 234.5 s and 0.0770 at 400 s.

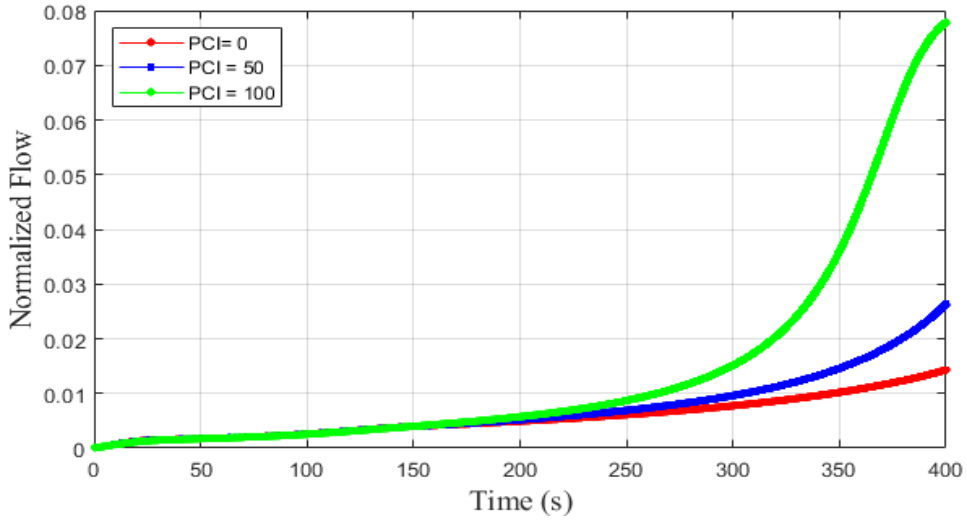

Figure 3.4 Normalized flow for the proposed model with $v_{max} = 15.27$ m/s over a 3000 m circular road.

Figure 3.5 gives the normalized flow for the ID model with $\delta = 1, 4$, and 20 and $v_{max} = 20$ m/s. When $\delta = 1$, the flow at 31.5 s is 0.0013, increasing to 0.0024 at 94.0 s and 0.0063 at 150 s. When $\delta = 4$, the flow at 33.0 s is 0.0017. It is 0.0020 at 80.0 s, increasing to 0.0039 at 116.0 s and 0.0088 at 150 s. When $\delta = 20$, at 28.0 s the flow is 0.0012. It is 0.0032 at 100.5 s, increasing to 0.0060 at 130.0 s and 0.0095 at 150 s.

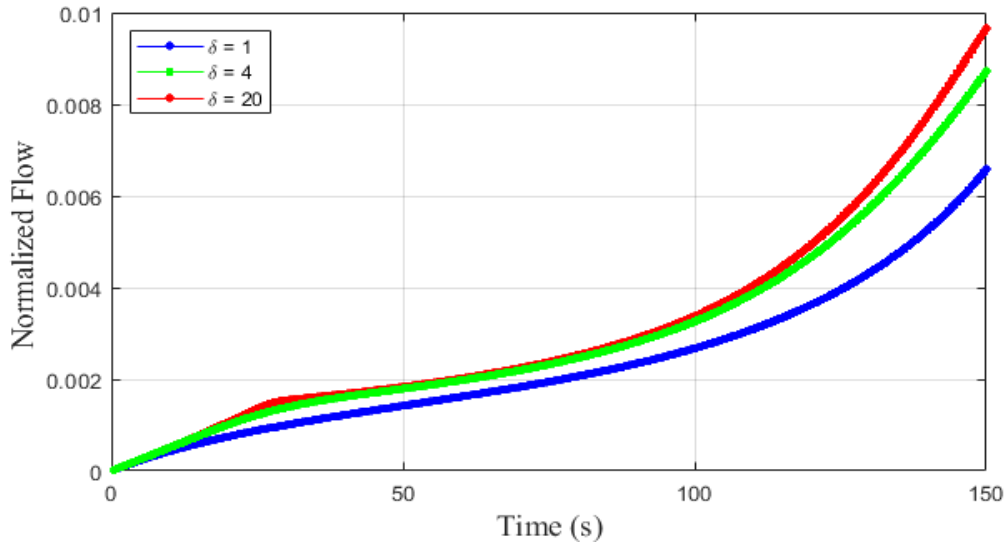

Figure 3.5 Normalized flow for the ID model with $\delta = 1, 4,$ and 20 over a 3000 m circular road.

Figure 3.6 gives the normalized speed with $v_{max} = 9.72$ m/s and $PCI = 0, 50,$ and 100 for the proposed model. When $PCI = 0$, the speed is 0.39 from 0.5 s to 15.0 s, decreasing to 0.23 at 15.5 s, and then increasing to 0.46 at 20.0 s. The speed oscillates between 0.16 and 0.64 from 236.5 s to 399.0 s as indicated in Figure 3.6a. The speed when $PCI = 50$ is similar to that when $PCI = 0$. It is 0.39 from 0.5 s to 15.0 s, decreasing to 0.23 at 15.5 s, and then increasing to 0.46 at 21.0 s. The speed oscillates between 0.21 and 0.58 from 263.0 s to 399.5 s as indicated in Figure 3.6b. When $PCI = 100$, the speed is 0.40 from 0.5 s to 15.0 s, decreasing to 0.23 at 15.5 s, and then increasing to 0.46 at 19.5 s. The speed oscillates between 0.32 and 0.48 from 315.0 s to 399.0 s as indicated in Figure 3.6c. For all PCI values, there are road segments where the speed is constant such as between -1947.8 m and -426.7 m at 397.5 s when $PCI = 0$, between -1932.3 m and -228.4 m at 392.0 s when $PCI = 50$, and between -1962.4 m and -428.1 m at 393.5 s when $PCI = 100$.

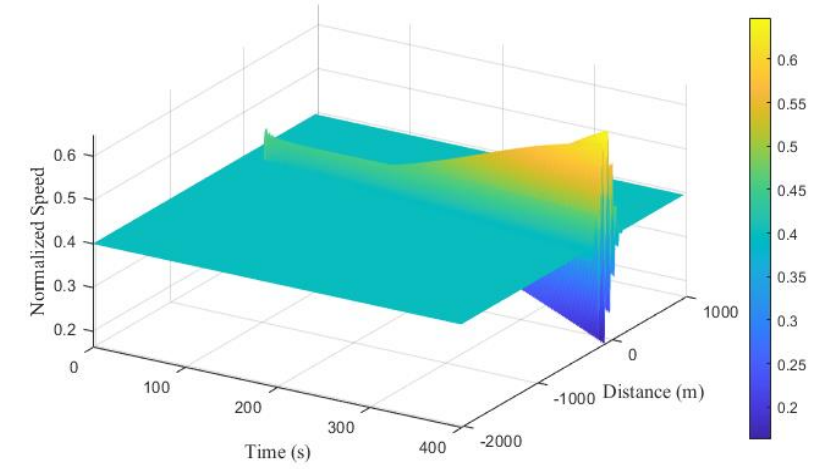

(a)

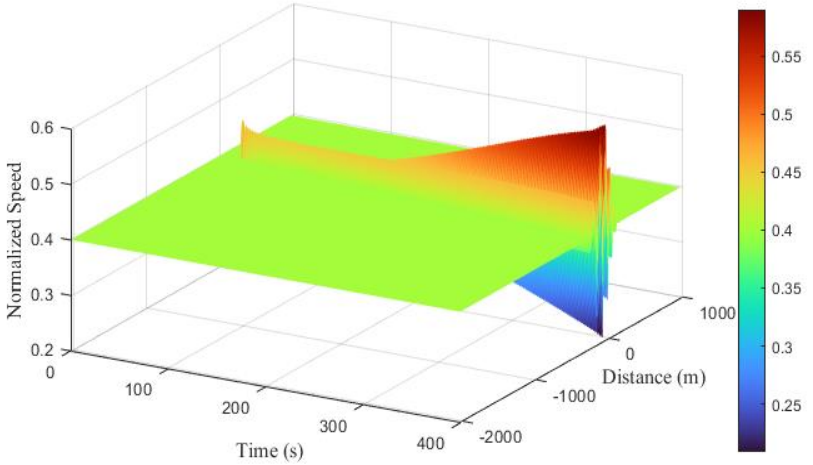

(b)

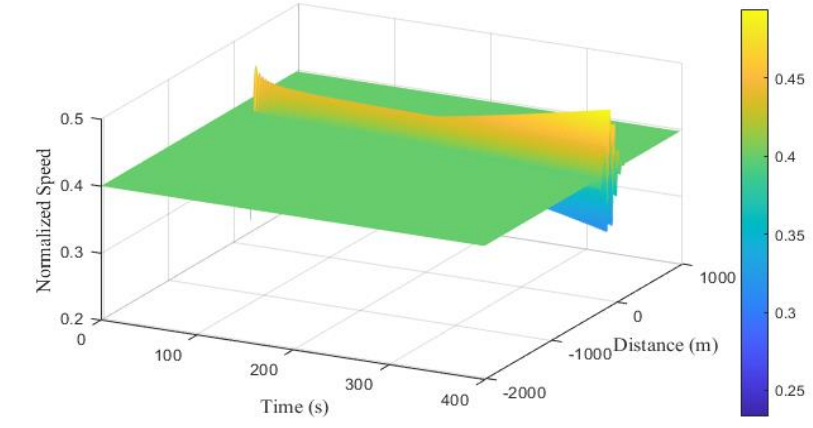

(c)

Figure 3.6 Normalized speed for the proposed model with $v_{max} = 9.72$ m/s over a 3000 m circular road, **(a)** $PCI = 0$, **(b)** $PCI = 50$, **(c)** $PCI = 100$.

Figure 3.7 gives the normalized speed with $v_{max} = 12.50$ m/s and $PCI = 0, 50,$ and 100 for the proposed model. When $PCI = 0$, the speed from 0.5 s to 15.0 s is 0.15, decreasing to 0.09 at 15.5 s, and then increasing to 0.18 at 19.5 s. The speed oscillates between 0.06 and 0.27 from 255.0 s to 399.0 s as indicated in Figure 3.7a. Similarly, when $PCI = 50$ the speed is 0.15 from 0.5 s to 15.0 s, decreasing to 0.09 at 15.5 s, and then increasing to 0.18 at 20.5 s. The speed oscillates between 0.06 and 0.26 from 258.0 s to 399.0 s as indicated in Figure 3.7b. The speed is also similar when $PCI = 100$. It is 0.15 from 0.5 s to 15.0 s, decreasing to 0.09 at 15.5 s and then increasing to 0.18 at 19.5 s. The speed oscillates between 0.09 and 0.22 from 294.5 s to 399.5 s as indicated in Figure 3.7c. For all PCI values, there are road segments where the speed is constant such as between -2022.5 m and -237.5 m at 397.0 s when $PCI = 0$, between -1922.7 m and -245.5 m at 395.0 s when $PCI = 50$, and between -1953.75 m and -230.0 m at 390.0 s when $PCI = 100$.

Figure 3.8 gives the normalized speed with $v_{max} = 15.27$ m/s and $PCI = 0,\ 50,$ and 100 for the proposed model. When $PCI = 0$, the speed from 0.5 s to 15.0 s is 0.11, decreasing to 0.06 at 15.5 s, and then increasing to 0.13 at 19.5 s. The speed oscillates between 0.04 and 0.20 from 241.0 s to 399.0 s as indicated in Figure 3.8a. The speed behavior is similar when $PCI = 50$. It is 0.11 from 0.5 s to 15.0 s, decreasing to 0.06 at 15.5 s, and then increasing to 0.14 at 20.5 s. The speed oscillates between 0.04 and 0.20 from 267.5 s to 399.0 s as indicated in Figure 3.8b. Similar speed behavior also occurs when $PCI = 100$. It is 0.11 from 0.5 s to 15.0 s, decreasing to 0.06 at 15.5 s, and then increasing to 0.13 at 20.5 s. The speed oscillates between 0.05 and 0.18 from 278.5 s to 399.5 as indicated in Figure 3.8c. For all PCI values, there are road segments where the speed is constant such as between -1945.4 m and -244.3 m at 391.0 s when $PCI = 0$, between -1911.8 m and -239.7 m at 388.5 s when $PCI = 50$, and between -1817.1 m and -371.4 m at 384.0 s when $PCI = 100$.

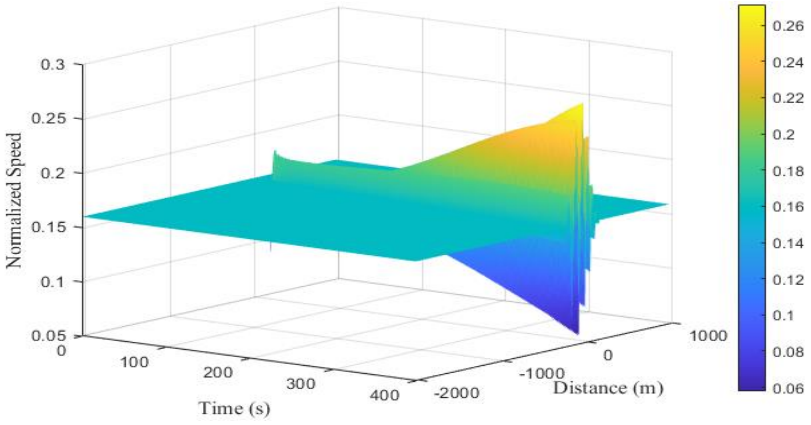

(a)

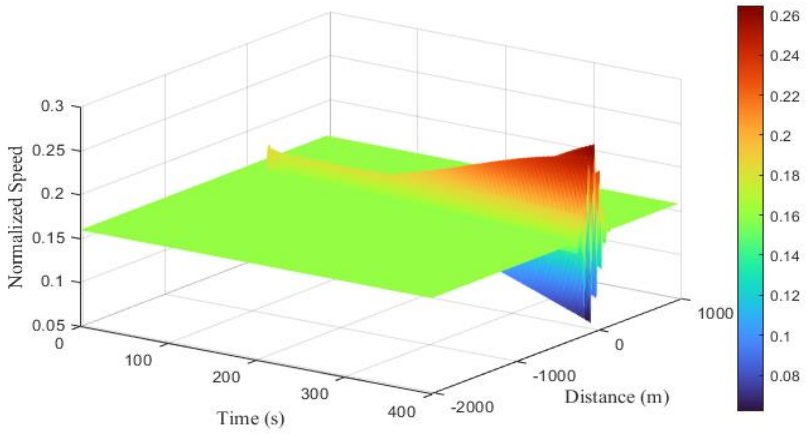

(b)

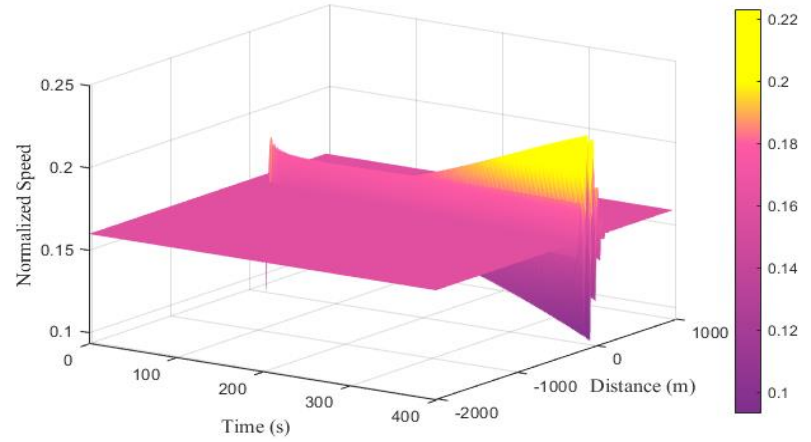

(c)

Figure 3.7 Normalized speed for the proposed model with $v_{max} = 12.50$ m/s over a 3000 m circular road, **(a)** $PCI = 0$, **(b)** $PCI = 50$, **(c)** $PCI = 100$.

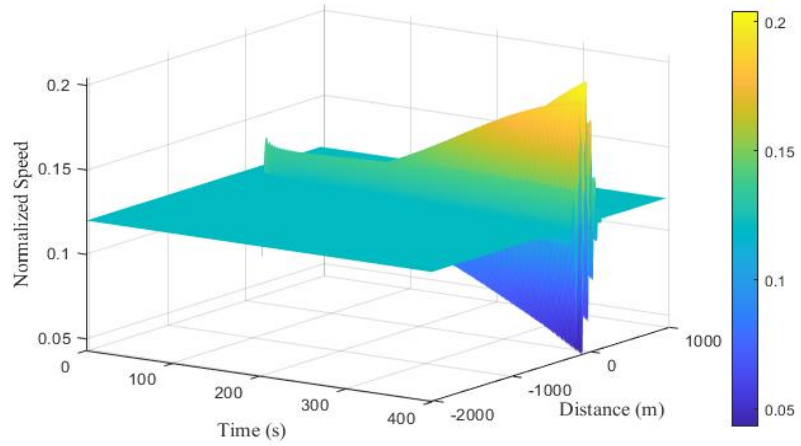

(a)

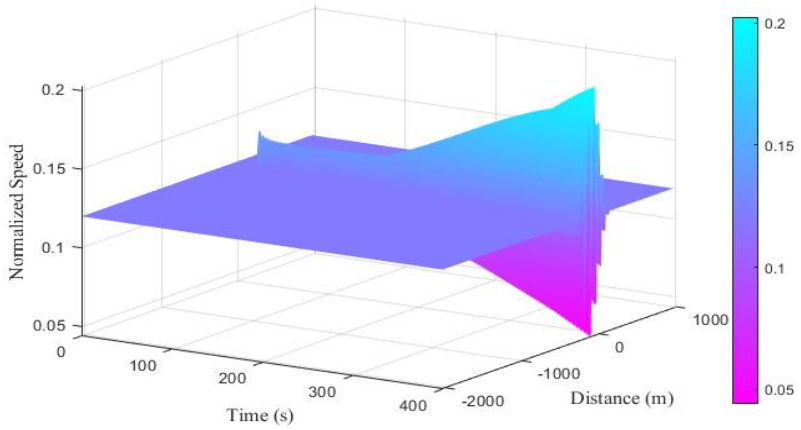

(b)

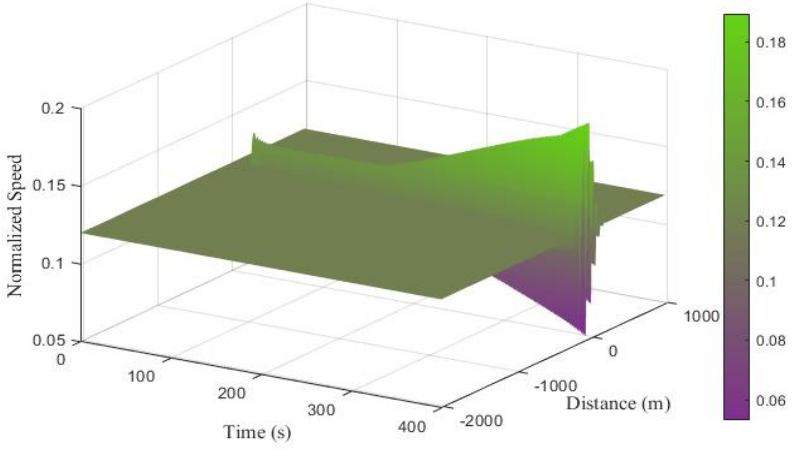

(c)

Figure 3.8 Normalized speed for the proposed model with $v_{max} = 15.27$ m/s over a 3000 m circular road, **(a)** $PCI = 0$, **(b)** $PCI = 50$, **(c)** $PCI = 100$.

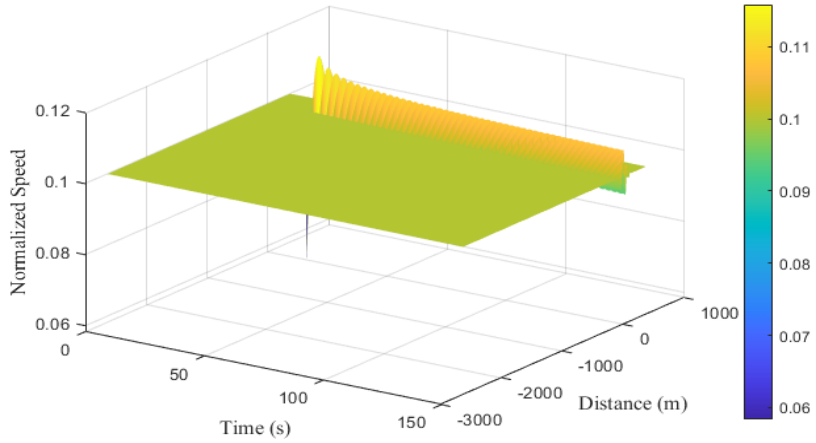

(a)

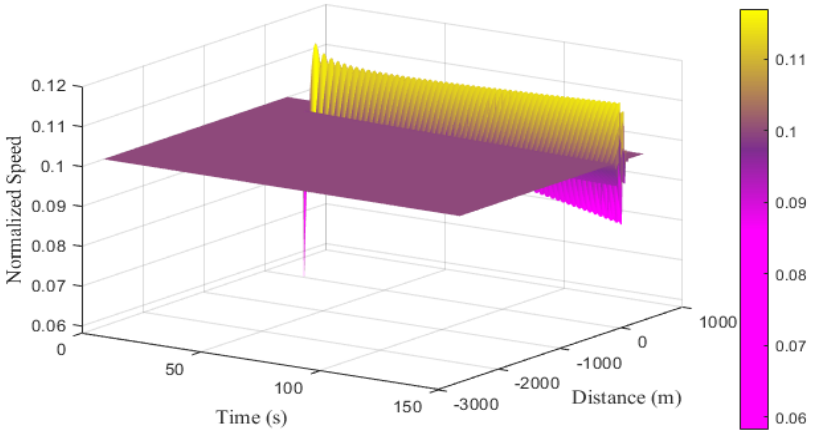

(b)

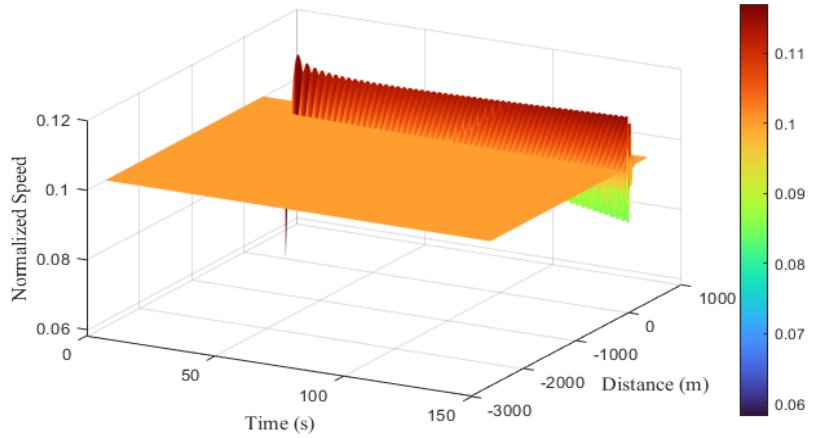

(c)

Figure 3.9 Normalized speed for the ID model over a 3000 m circular road, **(a)** $\delta = 1$, **(b)** $\delta = 4$, **(c)** $\delta = 20$.

Figure 3.9 gives the normalized speed for the ID model with $v_{max} = 20$ m/s and $\delta = 1,\ 4,$ and 20. When $\delta = 1$, the speed is 0.10 until 15.0 s and then increases to 0.11 at 21.0 s. The speed oscillates between 0.09 and 0.10 from 118.0 s to 149.5 s as shown in Figure 3.9a. When $\delta = 4$, the speed is 0.09 until 15.0 s, decreasing to 0.05 at 15.5 s, and then increasing to 0.11 at 19.5 s. It oscillates between 0.08 and 0.11 from 122.5 s to 149.5 s as shown in Figure 3.9b. When $\delta = 20$, the speed is 0.1 until 15.0 s, decreasing to 0.05 at 15.5 s, and then increasing to 0.11 at 20.5 s. It oscillates between 0.08 and 0.11 from 118.5 s to 150.0 s as indicated in Figure 3.9c. For all the values of δ, there are road segments where the speed is constant such as between -2590.0 m and -322.0 m at 148.0 s when $\delta = 1$, between -2498.0 m and -292.0 m at 147.0 s when $\delta = 4$, and between -2594.0 m and -374.0 m at 149.0 s when $\delta = 20$.

The results for the proposed model indicate that pavement condition influences traffic flow as expected. In particular, the flow increases with speed as shown in Figures 3.2–3.4. The flow with the ID model increases with δ, which is not based on traffic physics. Furthermore, the oscillations in speed with the proposed model vary with the PCI and decrease over time as the PCI increases, which is realistic. Conversely, the oscillations in speed with the ID model are the result of an arbitrary fixed parameter, and they increase over time as δ increases with no justification. This is an inadequate and unrealistic traffic characterization.

3.3 Conclusion

A microscopic traffic flow model was developed based on pavement condition. The PCI was used to characterize traffic behavior. The performance of the proposed model was evaluated and compared with that of the ID model. The results obtained demonstrate that the proposed model provides realistic traffic flow dynamics. In particular, the traffic flow under excellent pavement conditions ($PCI = 100$) is high while the flow under poor pavement conditions ($PCI = 0$) is low, as expected. Conversely, the ID model has a fixed acceleration exponent which does not reflect the relationship between flow and road condition. Furthermore, the oscillations in speed with the proposed model vary according to the pavement condition. They are negligible when the PCI is high, which is expected traffic behavior. In contrast, the ID model produces unrealistic speed oscillations based on δ. The results given indicate that the proposed model can be used in traffic simulators for realistic and effective traffic prediction.

Chapter 4

The Effect of Visibility on Road Traffic During Foggy Weather Conditions

Adverse weather conditions and low intensity illumination cause poor visibility, which can lead to traffic congestion and compromise safety [59], [60]. One natural weather condition that poses a significant risk is fog. When fog forms on the surface, it appears as a cloud that reduces visibility and can lead to accidents on roads that are typically safe [59]. Reduced visibility increases the risk of rear-end crashes and multiple vehicle collisions [61], and results in long traffic queues that take more time to dissipate [62]. It is crucial that drivers be aware of weather conditions and adjust their driving behavior accordingly. Thus, a traffic model is required to characterize driver behavior accurately and realistically during poor visibility conditions.

Road safety is a significant global concern as traffic accidents result in many serious injuries and fatalities. According to the U.S. Federal Highway Administration (FHWA), each year more than 38,700 vehicle accidents happen in foggy conditions, resulting in over 600 fatalities and more than 16,300 injuries [63]. It has been shown that the rate of traffic accidents is 35 times higher in fog compared to clear weather [64].

Drivers obtain almost 90% of their traffic information through vision, and fog can significantly reduce their ability to perceive the surrounding environment [65]. The reduced visibility conditions caused by fog result in velocity (speed) reduction and increased delay. It has been reported that the velocity (speed) drops by 3.89 m/s when visibility is below 160 m [66]. The average distance headway is reduced by 19% and 33% in light and dense fog, respectively, compared to clear weather conditions [67]. Furthermore, fog can cause stop-and-go traffic behavior, which increases delay and thus fuel consumption [68].

Here, a microscopic traffic model is proposed to provide realistic traffic characterization based on the visibility in fog. The stability of the proposed model is analyzed and compared with the ID model. Results are presented which demonstrate that the proposed model realistically characterizes traffic behavior during foggy weather conditions.

The remainder of the chapter is structured as follows. Section 4.1 presents the ID and proposed models. The stability of these models is examined in Section 4.2 and their performance is evaluated in Section 4.3. Finally, Section 4.5, concludes the chapter.

4.1 Traffic Models

The acceleration in the ID model is given by

$$\frac{dv}{dt} = a_{max}\left(1 - \left(\frac{v}{v_{max}}\right)^{\delta} - \left(\frac{D}{s}\right)^{2}\right), \tag{4.1}$$

where D can be expressed as [26]

$$D = s_j + \tau v + \frac{v\Delta v}{2\sqrt{a_{max}b}} \tag{4.2}$$

The acceleration exponent δ is a constant and does not consider traffic physics, leading to an unrealistic and inadequate representation of traffic behavior. In particular, traffic behavior does not vary depending on factors such as reduced visibility due to foggy weather conditions. To address this issue, a variable exponent is proposed to accurately depict traffic behavior in such conditions.

The time required by a driver to react and align to forward traffic conditions is known as the reaction time T_r [69] and the distance covered during this time is known as the distance headway s. Driver reaction is quick for a small distance headway as alignment occurs over a short distance and the driver has a less time to react to avoid a collision [70]. These factors affect driver behavior and vary based on the weather conditions. Thus, the acceleration exponent considering weather can be characterized as

$$\delta = \frac{T_r}{s}\left(\frac{V_d}{V_{d_{\max}}}\right) \tag{4.3}$$

where V_d is the visibility, that is, the distance a driver can see during fog as shown in Figure 4.1, and $V_{d_{\max}}$ is the maximum visibility. According to the international classification of fog visibility [71], visibility can be classified as in Table 4.1. A longer visibility means a driver has more time to react to changes in forward traffic conditions, while a shorter visibility means they have less time to react and avoid potential hazards.

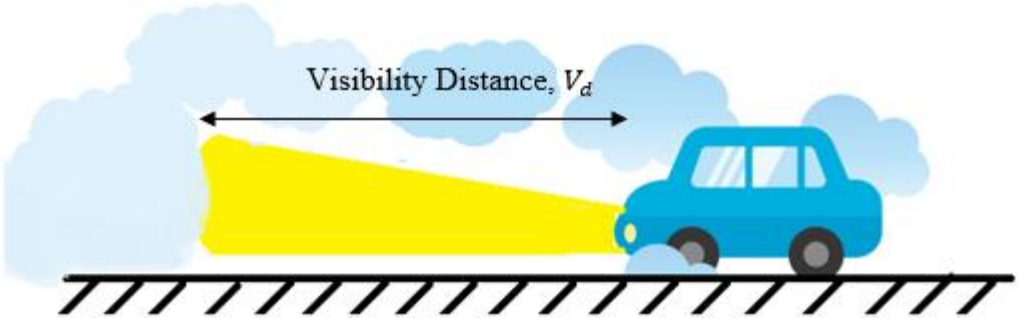

Figure 4.1 Visibility during fog.

Substituting (4.3) in (4.1) gives the proposed model

$$\frac{dv}{dt} = a_{max}\left(1 - \left(\frac{v}{v_{max}}\right)^{\frac{T_r}{s}\left(\frac{V_d}{V_{d\max}}\right)} - \left(\frac{D}{s}\right)^2\right). \tag{4.4}$$

which characterizes traffic based on visibility and so is more accurate and realistic than the ID model. With this model, acceleration varies according to the visibility unlike with the ID model.

Table 4.1 International fog visibility classification [71].

Visibility	**Class**
< 40 m	Dense fog
$40 - 200$ m	Thick fog
$200 - 1000$ m	Low or thin fog

The traffic flow is the product of density and velocity (speed) [31] which gives

$$Q = \frac{v}{s_e} \tag{4.5}$$

At equilibrium $\Delta v = 0$, so the distance headway for the proposed model at equilibrium is given by

$$s_e = \left(s_j + \tau v\right)\left(1 - \left(\frac{v}{v_{max}}\right)^{\frac{T_r}{s}\left(\frac{V_d}{V_{d\max}}\right)}\right)^{-0.5} \tag{4.6}$$

Substituting, (4.6) in (4.5) gives the traffic flow for the proposed model as

$$Q = \frac{v}{(s_j + \tau v)\left(1 - \left(\frac{v}{v_{max}}\right)^{\frac{T_r}{s}\left(\frac{V_d}{V_{d\max}}\right)}\right)^{-0.5}} \tag{4.7}$$

This shows that the flow with the proposed model is based on visibility. In clear weather, it is large as $V_d = V_{d_{\max}}$, whereas in foggy weather the flow is smaller as $V_d < V_{d_{\max}}$.

4.2 Traffic Models Stability

In this section, the stability of the ID and proposed models is evaluated over a circular road of length 2200 m for 250 s. The ID model is evaluated for $\delta = 1, 4$ and 40 and the proposed model is evaluated for $V_d = 30, 100, 300, 500, 700$ and 1000 m as fog reduces visibility to below 1000 m [71]. The time headway for both models is 1 s [35], and the minimum and maximum acceleration are 0.5 m/s^2 and 3 m/s^2, respectively [36]. The distance headway is 5 m [72], the vehicle length is 4.5 m [73], and the jam spacing is 2 m [26]. According to the Ottawa Safety Council [74], the average driver reaction time is 2.5 s, so $T_r = 2.5$ s. The initial equilibrium velocity (speed) is set to 18 m/s and a disturbance is induced at 20 s. The number of vehicles on the road is 51. The parameters are summarized in Table 4.2.

Table 4.2 Stability analysis parameters.

Parameter	**Value**
Initial equilibrium velocity (speed)	18 m/s
Time headway for the ID and proposed models, τ	1 s
Distance headway for the proposed model, s	5 m
Reaction time of a driver, T_r	2.5 s
Jam spacing, s_j	2 m
Maximum acceleration, a_{max}	0.5 m/s^2
Minimum acceleration (deceleration), b	3 m/s^2
Vehicle length, L	4.5 m
Time step size, Δt	0.5 s
Acceleration exponent, δ	$1, 4,$ and 40

Visibility, V_d	$30, 100, 300, 500, 700$ and 1000 m
Maximum visibility distance, $V_{d_{\max}}$	1000 m

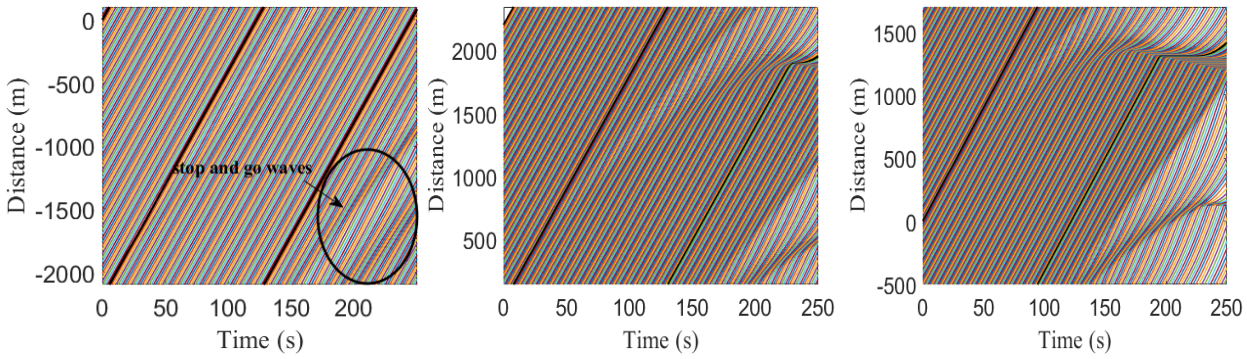

(a) **(b)** **(c)**

Figure 4.2 Vehicle trajectories with the ID model over time and space on a 2200 m circular road, **(a)** $\delta = 1$, **(b)** $\delta = 4$, **(c)** $\delta = 40$.

Figure 4.2 shows that with the ID model, the disturbance propagates into stop-and-go waves. Further, a larger value of δ results in greater traffic amplitudes. This is because acceleration and deceleration are more frequent, making the model unstable. In contrast to the ID model, Figure 4.3 shows that with the proposed model amplification does not occur so it is stable. Disturbances are dissipated as expected preventing stop-and-go traffic from occurring.

The unstable behavior of the ID model is due to the constant δ which is not based on traffic physics and so has no connection to real-world traffic. Conversely, the proposed model is stable even under foggy weather conditions because it is based on actual traffic parameters.

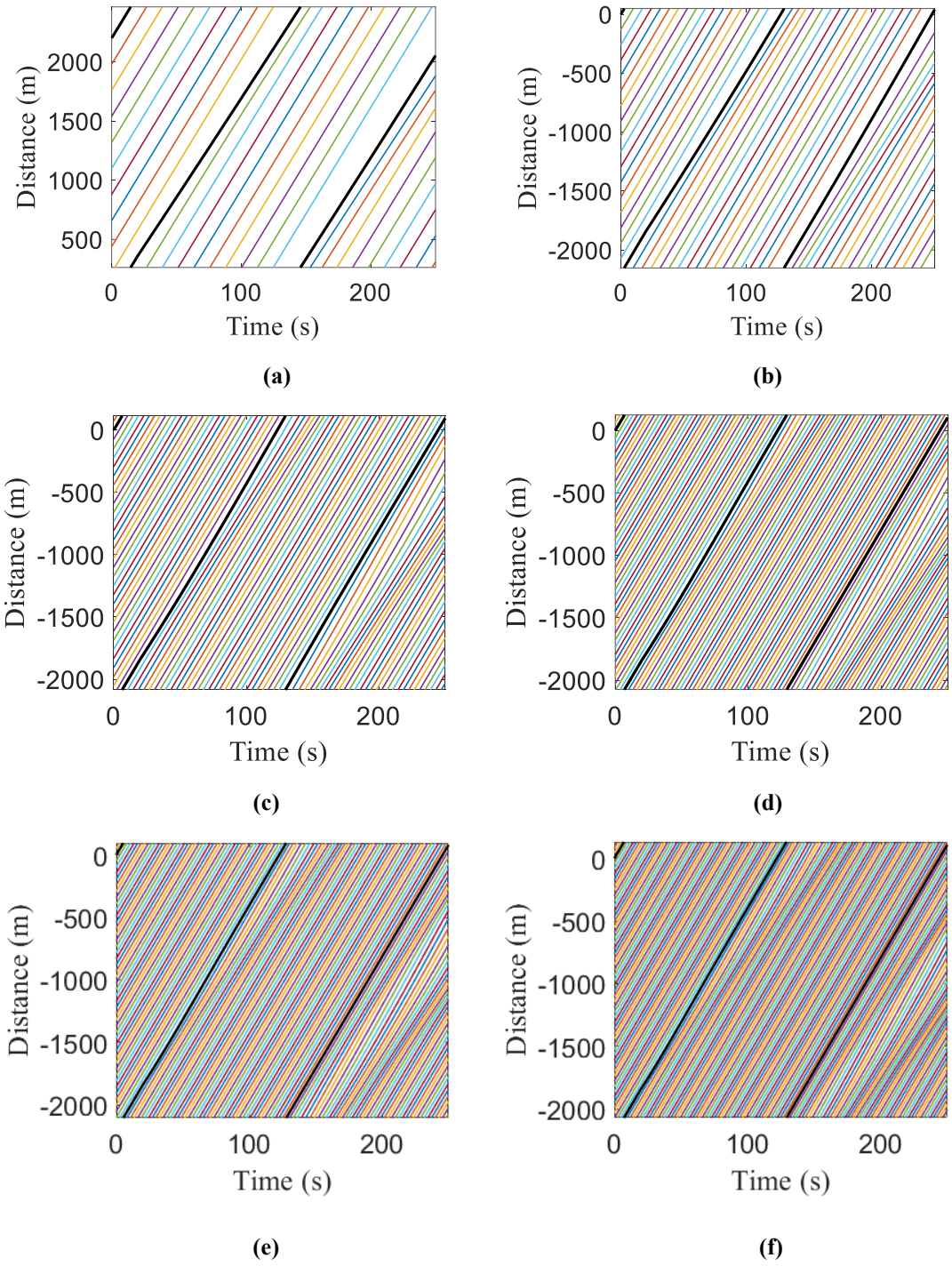

Figure 4.3 Vehicle trajectories with the proposed model over time and space on a 2200 m circular road, **(a)** $V_d = 30$ m, **(b)** $V_d = 100$ m, **(c)** $V_d = 300$ m, **(d)** $V_d = 500$ m, **(e)** $V_d = 700$ m and **(f)** $V_d = 1000$ m.

4.3 Traffic Models Performance

The performance of the ID and proposed models is evaluated over a 2200 m circular road for 250 s using the explicit Euler scheme with a time step of 0.5 s. The simulation parameters are given in Table 4.3. The maximum velocity (desired speed) is set to 30 m/s [47]. As previously, the ID model is evaluated for $\delta = 1, 4$, and 40, and the proposed model for $V_d = 30, 100, 300, 500, 700$ and 1000 m. The time headway for both models is 1 s [35], and the minimum and maximum acceleration are 0.5 m/s^2 and 3 m/s^2, respectively [36]. The distance headway is 5 m [72], the vehicle length is 4.5 m [73], the jam spacing is 2 m [26], and $T_r = 2.5$ s. The number of vehicles on the road is 51.

Table 4.3 Simulation parameters.

Parameter	**Value**
Maximum velocity (desired speed), v_{max}	30 m/s
Time headway for the ID and proposed model, τ	1 s
Distance headway for the proposed model, s	5 m
Reaction time of a driver, T_r	2.5 s
Jam spacing, s_j	2 m
Maximum acceleration, a_{max}	0.5 m/s^2
Minimum acceleration (deceleration), b	3 m/s^2
Vehicle length, L	4.5 m
Time step size, Δt	0.5 s
Acceleration exponent, δ	$1, 4,$ and 40
Visibility, V_d	$30, 100, 300, 500, 700$ and 1000 m
Maximum visibility distance, $V_{d(\max)}$	1000 m

4.3.1 ID Model Performance

Figure 4.4 presents the velocity (speed) evolution over time and space with the ID model on a 2200 m circular road. The initial queue velocity (speed) is zero which indicates congestion. For $\delta = 1$, the queue dissipates at 89.0 s as shown in Figure 4.4a and the velocity (speed) after dissipation is 11.95 m/s at 143.0 s. For $\delta = 4$ and 40, the queue dissipates at 90.0 s as shown in Figures 4.4b and 4.4c. The corresponding velocity (speed) after dissipation ranges between $8.62 - 5.90$ m/s and $6.88 - 1.37$ m/s, respectively, as shown in Table 4.4. However, for both $\delta = 4$ and 40 a queue again develops at 217.0 s and 164.5 s, respectively, and persists until 250.0 s.

To illustrate the queue length changes, the vehicle trajectories over time and space for the ID model are presented in Figure 4.5. The black trajectory represents the 1st vehicle while the others represent the following 50 vehicles. The results are summarized in Table 4.5. This shows that the queue length changes with δ, and the length is longer for a larger value of δ.

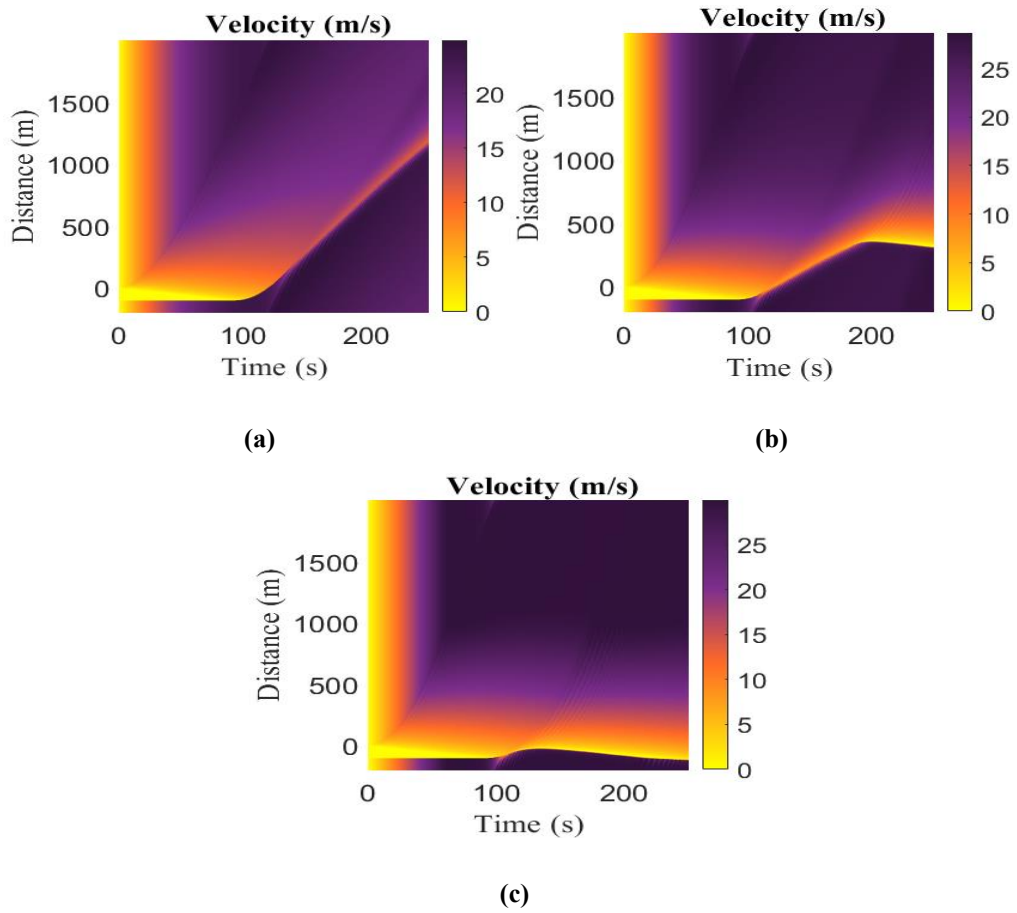

Figure 4.4 Velocity (speed) evolution with the ID model over time and space on a 2200 m circular road, **(a)** $\delta = 1$, **(b)** $\delta = 4$, **(c)** $\delta = 40$.

Table 4.4 ID model velocity (speed) and time during and after the queue.

Acceleration exponent δ	**Time for which congestion occurs (s)**	**Velocity (speed) after congestion dissipates (m/s)**	**Time of velocity (speed) after congestion dissipates (s)**
1	$0 - 89.0$	11.95	143.0
4	$0 - 90.0$ and $217.0 - 250.0$	$8.62 - 5.90$	$129.0 - 194.0$
40	$0 - 90.0$ and $164.5 - 250.0$	$6.88 - 1.37$	$112.5 - 151.5$

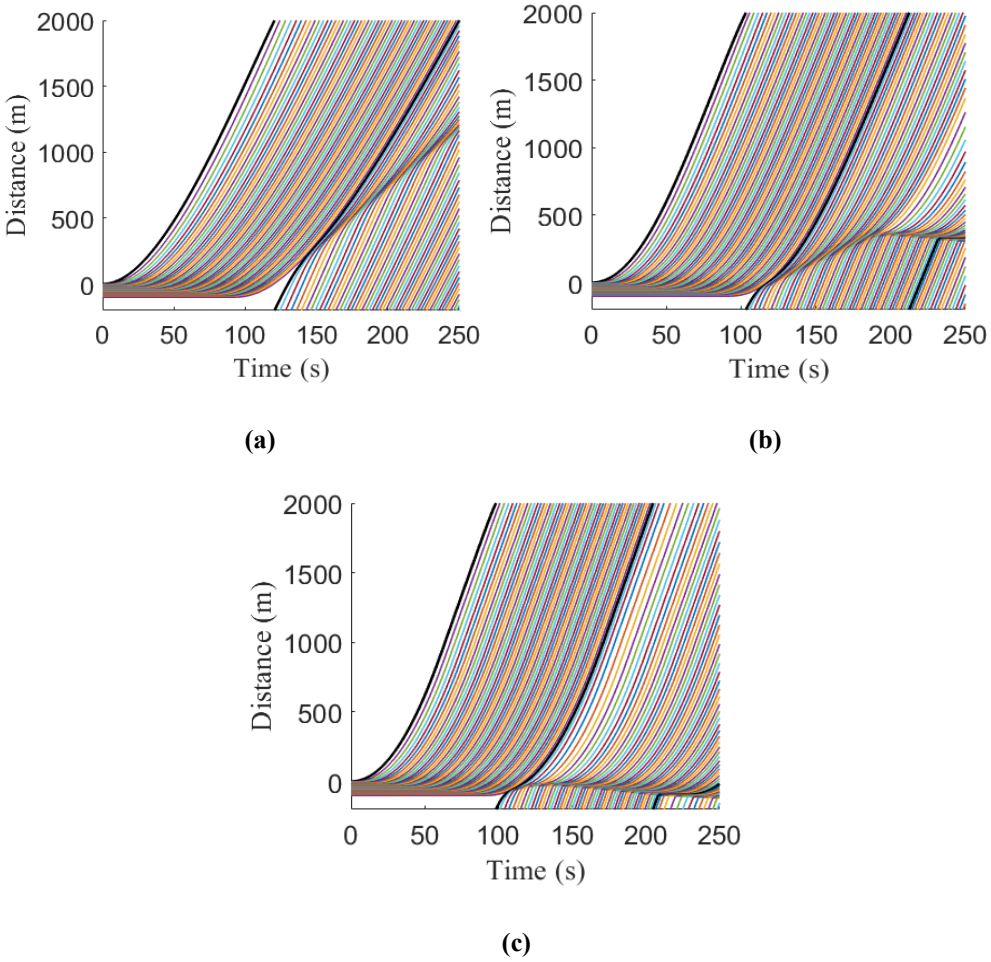

Figure 4.5 Vehicle trajectories over time and space for the ID model on a 2200 m circular road, **(a)** $\delta = 1$, **(b)** $\delta = 4$, **(c)** $\delta = 40$.

Table 4.5 Queue length of the 1st, 23rd, and 51st vehicles for the ID model.

Acceleration exponent δ	Queue length of the 1st vehicle (s)	Queue length of the 23rd vehicle (s)	Queue length of the 51st vehicle (s)
1	1.50	46.0	89.0
4	2.50	48.5	90.0
40	3.50	49.0	90.0

Figure 4.6 presents the evolution of acceleration over time with the ID model at $\delta = 1, 4,$ and 40. This shows that acceleration first decreases and then increases. The acceleration starts at 0.5 m/s^2 and the decrease is greater with a larger value of δ. The variations increase with δ so they are greatest for $\delta = 40$ ranging between 0.5 m/s^2 and -3 m/s^2.

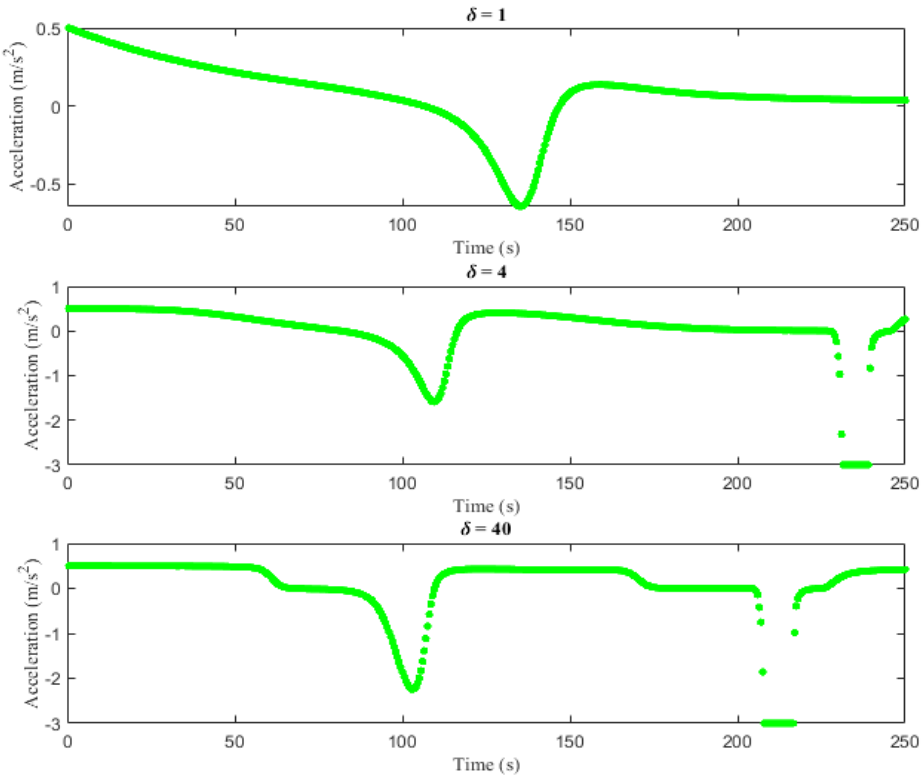

Figure 4.6 Acceleration temporal evolution of a single vehicle for the ID model on a 2200 m circular road.

4.3.2 Proposed Model Performance

Figure 4.7 presents the time and space velocity (speed) evolution of the queue for the proposed model on a 2200 m circular road. The congestion results are summarized in Table 4.6. For $V_d = 30$ m, the queue does not dissipate, and congestion occurs from $0 - 250$ s between -96 m and -6 m as shown in Figure 4.7a. For $V_d = 100$ m, the queue does not dissipate. At 0 s, the velocity (speed) between -87 m and -3 m is 0 m/s while at 250.0 s it is 0 m/s from -87 m to -51 m, as shown in Figure 4.7b. For $V_d = 300$ m, the queue dissipates at 201.5 s while for $V_d = 500$, it dissipates at 152.0 s. The corresponding velocity (speed) after the queue dissipates is 1.36 m/s and 4.74 m/s as shown in Figures 4.7c and 4.7d, respectively. For $V_d = 700$ m and 1000 m, the queue dissipates at 127.5 s and 108.0 s, respectively. The corresponding velocity (speed) after the queue dissipates is 6.29 m/s and 8.53 m/s as shown in Figures 4.7e and 4.7f, respectively. These results indicate that the velocity (speed) increases with an increase in visibility, as expected.

Table 4.6 Proposed model velocity (speed) and time during and after the queue.

Fog	Visibility, V_d (m)	Time for which congestion occurs (s)	Velocity (speed) after congestion dissipates (m/s)	Time of velocity (speed) after congestion dissipates (s)
Dense	30	$0 - 250.0$	Queue does not dissipate	-
Thick	100	$0 - 250.0$	Queue does not dissipate	-
Thin	300	$0 - 201.5$	1.36	224.0
	500	$0 - 152.0$	4.74	184.0
	700	$0 - 127.5$	6.29	163.5
	1000	$0 - 108.0$	8.53	152.5

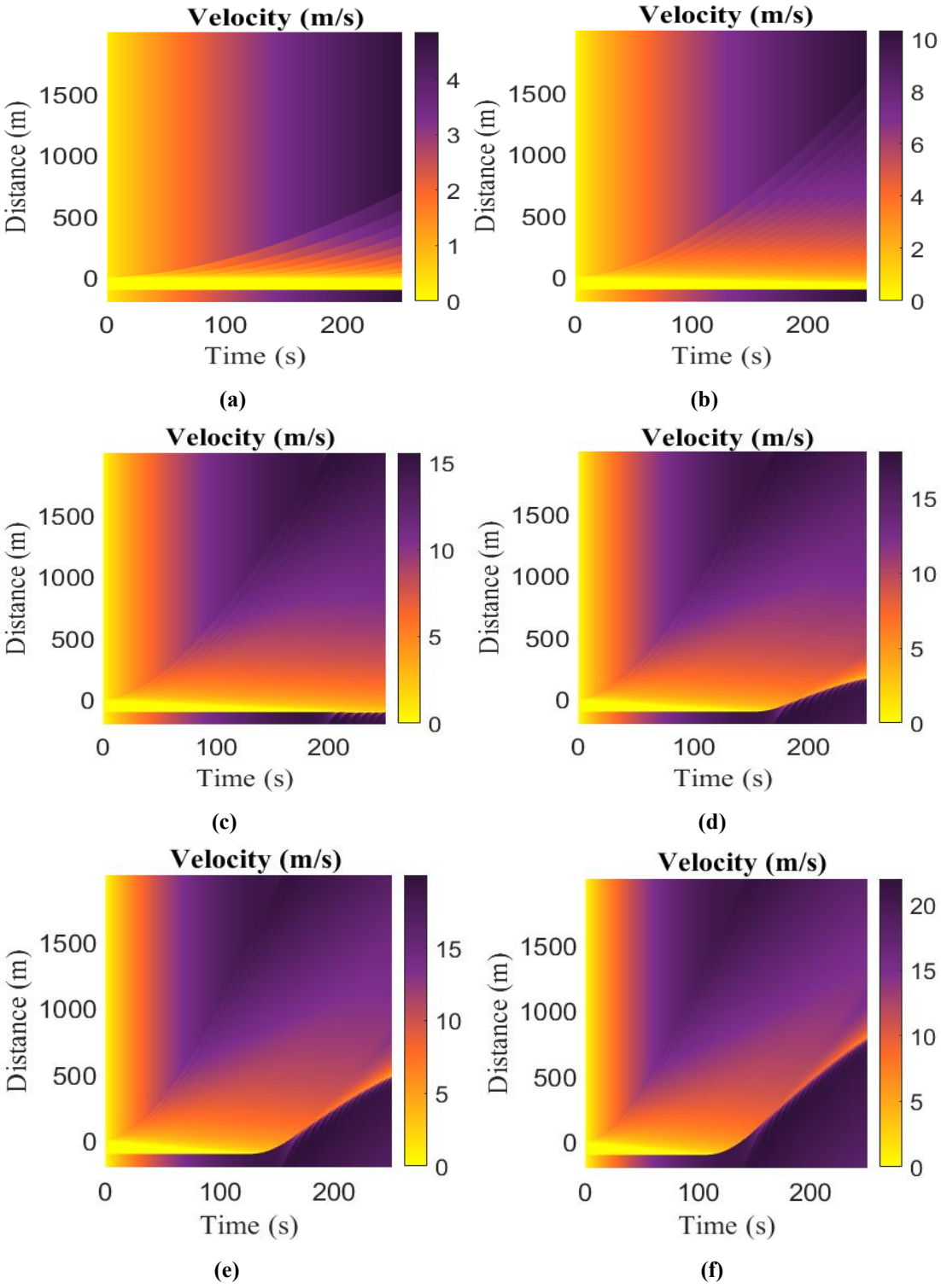

Figure 4.7 Velocity (speed) evolution over time and space for the proposed model on a 2200 m circular road, **(a)** $V_d = 30$ m, **(b)** $V_d = 100$ m, **(c)** $V_d = 300$ m, **(d)** $V_d = 500$ m, **(e)** $V_d = 700$ m and **(f)** $V_d = 1000$ m.

Figure 4.8 presents the velocity (speed) evolution over time and space with the proposed model on a 2200 m circular road. The black trajectory represents the 1st vehicle while the other trajectories represent the following 50 vehicles. The results are summarized in Table 4.7 and show that the queue length decreases as the visibility V_d increases. For $V_d = 30$ m, the 1st vehicle is in the queue for 22 s, whereas the 23rd and 51st vehicles are in the queue for 250 s, whereas for $V_d = 1000$ m, the 1st vehicle is in the queue for 5 s while the 23rd and 51st vehicles are in the queue for 56 s and 108 s, respectively.

Figure 4.9 presents the temporal evolution of acceleration for the proposed model with $V_d = 30, 100, 300, 500, 700,$ and 1000 m. The initial acceleration is 0.5 m/s^2 and changes over time according to V_d. For $V_d = 30$ and 1000 m the acceleration is approximately constant, while with $V_d = 300, 500, 700,$ and 1000 m there are greater variations. For instance, with $V_d = 300$ m, the acceleration decreases from 0.5 m/s^2 at 0.5 s to 0.2 m/s^2 at 1.5 s and remains relatively constant until 172.5 s. The acceleration then decreases to -2.29 m/s^2 at 208.5 s and then increases to 0.097 m/s^2 at 250 s. Similar patterns are observed for the other values of V_d, 500, 700, and 1000 m, as shown in Figure 4.9.

Table 4.7 Queue length of the 1st, 23rd, and 51st vehicles for the proposed model.

Fog	Visibility V_d (m)	Queue length of the 1st vehicle (s)	Queue length of the 23rd vehicle (s)	Queue length of the 51st vehicle (s)
Dense	30	22.0	250.0	250.0
Thick	100	18.5	229.5	250.0
Thin	300	5.5	111.5	201.5
	500	5.0	72.5	152.0
	700	5.0	64.5	127.0
	1000	5.0	56.0	108.0

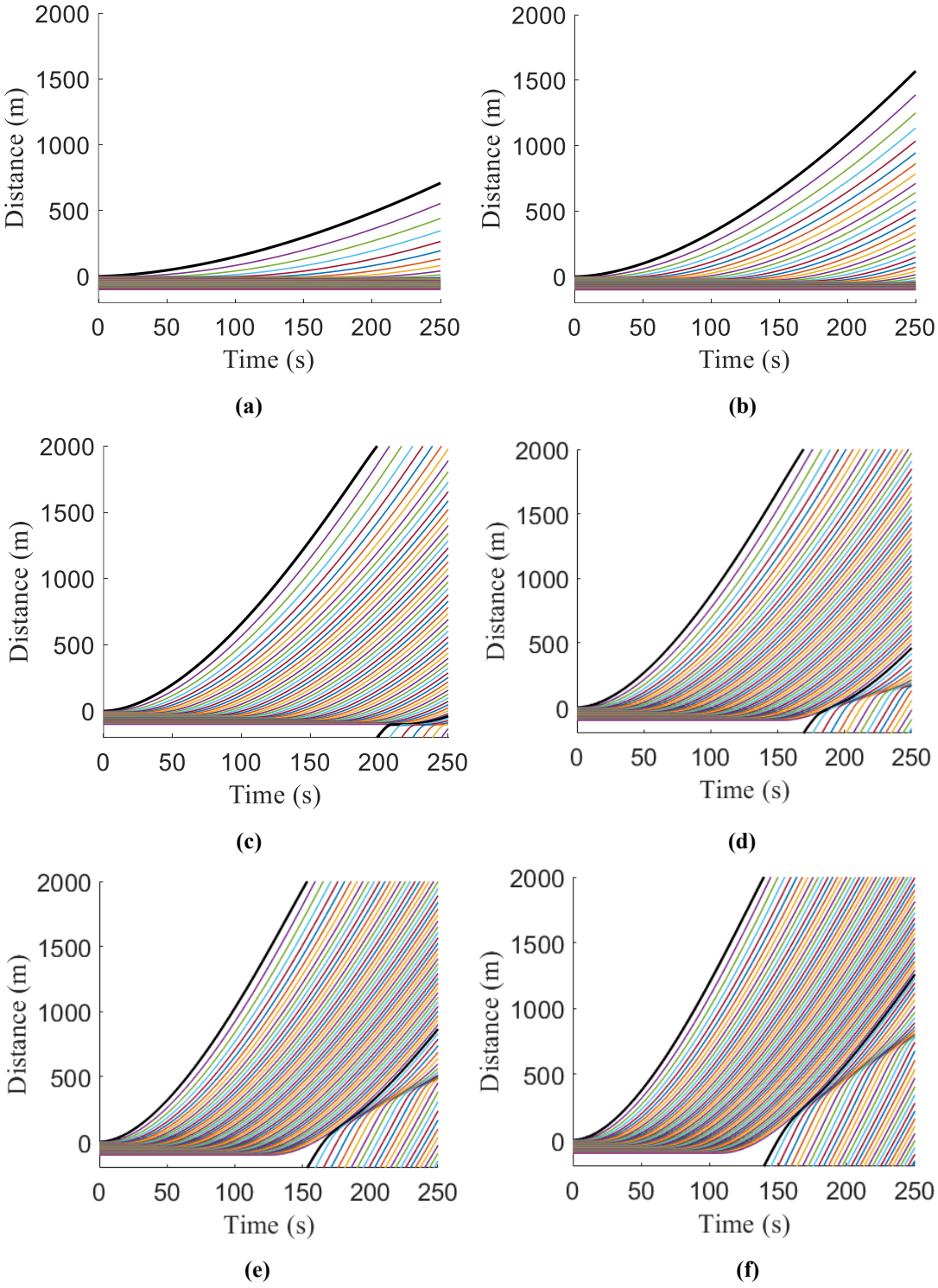

Figure 4.8 Vehicle trajectories over time and space for the proposed model on a 2200 m circular road, **(a)** $V_d = 30$ m, **(b)** $V_d = 100$ m, **(c)** $V_d = 300$ m, **(d)** $V_d = 500$ m, **(e)** $V_d = 700$ m and **(f)** $V_d = 1000$ m.

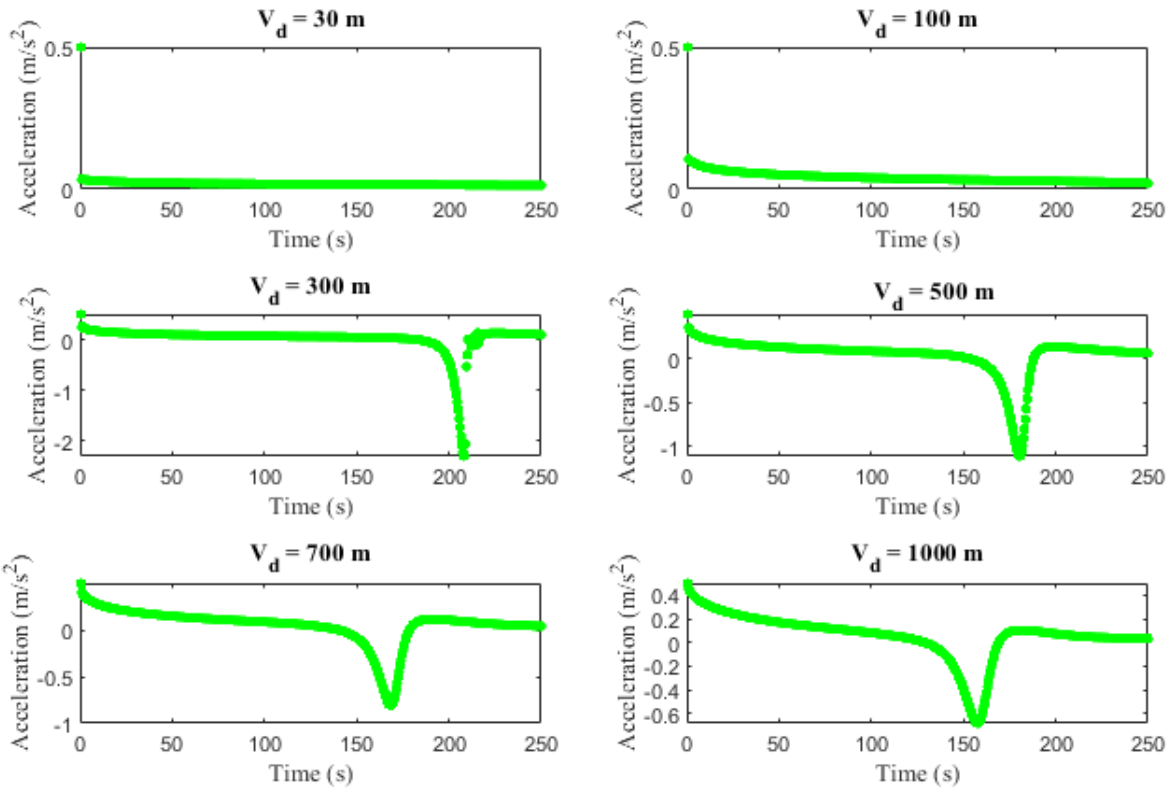

Figure 4.9 Acceleration temporal evolution of a single vehicle for the proposed model on a 2200 m circular road.

These results given in this section illustrate that when there is thin fog, the changes in velocity (speed) are small, as expected. However, with dense fog the visibility is low so these changes are large and cause congestion. This behavior is realistic as in dense fog drivers are unaware of forward traffic conditions and so cannot respond appropriately. Conversely, the velocity (speed) with the ID model is not realistic as it is based on the constant δ. For example, large changes in velocity occur with $\delta = 4$ and 40 and the traffic becomes congested. In addition, the vehicle trajectories for the ID model indicate that as δ increases the time vehicles are in queues increases, while with the proposed model as visibility increases this time decreases. Furthermore, the ID model causes large variations in acceleration which increase with δ, whereas the proposed model has much smaller variations in acceleration.

4.4 Conclusion

Poor visibility due to fog is a significant factor affecting traffic behavior and road safety. Here, a microscopic traffic model was proposed to characterize traffic during foggy weather based on visibility. The proposed model was evaluated for different visibility corresponding to dense, thick, and thin fog on a 2200 m circular road. The results obtained show that in dense fog changes in velocity (speed) are large as the visibility is low, whereas in thin fog the changes are small due to the better visibility, as expected. In contrast, with the ID model large changes in velocity (speed) occur which is unrealistic. Furthermore, as δ increases the time vehicles are in the queue increases. With the proposed model, as visibility increases the time vehicles are in a queue decreases, as expected. In addition, it was shown that the proposed model is more stable as small disturbances do not create stop-and-go traffic.

The proposed model results in small changes in acceleration compared to the ID model. Increased acceleration leads to congestion, higher fuel consumption, and more pollution. Therefore, the proposed model can be used by traffic engineers to provide insights for improved transport network management which will benefit the environment.

Chapter 5

Effect of Human-Driven, Autonomous, and Connected Autonomous Vehicles on Highway Geometric Design Using a Spring-Mass Based Traffic Model

The rapid urbanization worldwide and the increasing number of vehicles have exacerbated traffic problems such as congestion, pollution, and safety. Traditional traffic control and management technologies have had limited effect in mitigating these issues [31]. According to the U.S. Department of Transportation, in 2015, 94% of traffic accidents in the United States were due to human error [8]. Further, about 80% of traffic accident deaths are due to the lack of connectivity between vehicles [11]. Driving systems such as AVs and CAVs have been developed that can reduce or eliminate human error associated with vehicle collisions [75].

Further, highway geometric design plays a critical role in traffic safety, operational efficiency, and vehicle performance, and with the rise of AVs and CAVs, its significance will grow even further [76]. Study shows that AVs require lower geometric design specifications and can lead to lower costs and higher traffic speeds than HVs [77]. The effect of AVs on vertical curves was investigated in [8] by considering the difference in reaction time between AVs and HVs. Whereas the effect of AVs on geometric elements such as sight distance and length of vertical curves was examined in [78] based on the reaction time and acceleration. However, the impact of AVs and CAVs on geometric design, particularly concerning horizontal highway curves still needs to be investigated. Horizontal curves are used on highways for alignment or changes in direction while vertical curves are used to change the slope [79]. Thus, a traffic model needs to be developed to investigate traffic flow on horizontal curves and determine the behavior of AVs and CAVs.

Moreover, various traffic models have been developed as discussed in Chapter 1, however, all of them are based on fluid dynamics theory. Thus, they treat vehicular traffic flow as a compressible fluid based on the principles of fluid dynamics discussed in [80], [81]. However,

vehicle acceleration and deceleration behave like a mechanical system, i.e. a spring-mass system. Thus, a traffic model based on mechanical systems is proposed here. It is used to evaluate the traffic behavior on a horizontal curve. In particular, to compare the behavior of HVs, AVs, and CAVs on a horizontal curve via simulation in MATLAB.

The remainder of this chapter is organized as follows. The traffic models are presented in Section 5.1. The behavior of HVs, AVs, and CAVs is evaluated in Section 5.2, and a conclusion is given in Section 5.3.

5.1 Traffic Models

The ID model is given by [26]

$$\frac{dv}{dt} = a_{max}\left(1 - \left(\frac{v}{v_{max}}\right)^{\delta} - \left(\frac{D}{s}\right)^{2}\right), \tag{5.1}$$

where D is expressed as

$$D = s_j + \tau v + \frac{v\Delta v}{2\sqrt{a_{max}b}} \tag{5.2}$$

As in the ID model, driver response to changes in traffic conditions is characterized by δ, which is a constant. Thus, driver behavior is the same for different traffic conditions including horizontal highway curves, where the driving environment can significantly influence vehicle movement. This results in unsuitable traffic behavior which is not related to traffic physics.

Driver response is affected by the distance required for vehicles to align to changes in traffic conditions. This is analogous to a spring-mass system. When a force is applied to a mass m attached to a spring, the spring stretches. This stores potential energy in the spring which is released as kinetic energy when the force is removed, causing the mass to oscillate. This is analogous to traffic flow as shown in Figure 5.1. When the distance headway s is large, traffic accelerates so the speed increases. When the speed decreases, the distance headway is reduced until the safe distance headway s' is achieved. Thus, s fluctuates around s' according to the speed. When s is larger than s', vehicles accelerate, and they decelerate when s is smaller than s'. Considering this analogy between a spring-mass system and traffic behavior, Hooke's law [82] for traffic flow can be expressed as

$$a = \frac{K}{m}(s - s') \tag{5.3}$$

where a is the acceleration analogous to driver response, m is the vehicle mass, and K is the spring constant. The sensitivity defined as $\xi = \frac{K}{m}$ is analogous to the reaction of a driver to changes in traffic conditions.

Figure 5.1 Spring-mass phenomena in traffic flow.

Research shows that AVs react to changes in traffic conditions much faster than HVs [9]. For example, HV reaction time is in the range $1.1 - 1.6$ s whereas AV reaction time is about 0.5 s and CAV reaction time is only 0.1 s [9].

From (5.3), driver response has the form

$$\xi(s - s') \tag{5.4}$$

A large distance headway results in a small traffic density ρ, whereas the density is maximum when the distance headway is smallest, i.e. $s = 1/\rho$ [47]. Traffic flow Q is the product of speed and density [31], so (5.4) can be expressed as

$$\xi\left(\frac{v}{Q} - s'\right) \tag{5.5}$$

In addition, traffic flow is large with a small time headway τ and vice versa. Thus, flow is inversely proportional to time headway [83], so (5.5) becomes

$$\xi(v\tau - s') \tag{5.6}$$

The change in distance with time results in speed (velocity) change, which gives $S/\tau = v$ [47]. Thus, (5.6) can be written as

$$\xi(S - s') \tag{5.7}$$

and from the equation of motion [84]

$$S = v\tau + \frac{1}{2}a\tau^2 \tag{5.8}$$

Substituting (5.8) in (5.7) gives

$$\xi\left(v\tau + \frac{a\tau^2}{2} - s'\right) \tag{5.9}$$

A vehicle travelling around a horizontal curve develops a centrifugal force [85]

$$F' = \frac{mv^2}{R} \tag{5.10}$$

where R is the radius of the curve which is given by [86], [87]

$$R = \frac{v^2}{g(f + e)} \tag{5.11}$$

In (5.11), $g = 9.8$ m/s^2 is the gravitational acceleration, f is the friction coefficient, and e is the superelevation as shown in Figure 5.2. According to the U.S. FHWA, e ranges from 0.012 m to 0.036 m and is based on parameters such as climate and traffic speed. The value of e for normal weather conditions and high speeds is larger than for adverse weather conditions and low speeds [88].

Figure 5.2 Centrifugal force and highway superelevation.

Substituting (5.11) in (5.10) gives

$$a = g(f + e) \tag{5.12}$$

and substituting this in (5.9), we have

$$\xi\left(v\tau + \frac{\tau^2 g(f+e)}{2} - s'\right) \tag{5.13}$$

The proposed model is obtained by replacing δ in (5.1) with (5.13) which gives

$$\frac{dv}{dt} = a_{max}\left(1 - \left(\frac{v}{v_{max}}\right)^{\xi\left(v\tau + \frac{\tau^2 g(f+e)}{2} - s'\right)} - \left(\frac{D}{s}\right)^2\right). \tag{5.14}$$

With this model, traffic is characterized based on the reaction time and geometric design which is more realistic than the fixed δ in the ID model. Further, traffic behavior varies according to the geometric design whereas the ID model does not consider the type of road.

For the proposed model, traffic flow can be expressed as [89]

$$Q = \frac{v}{s_e} \tag{5.15}$$

where s_e is the distance headway at equilibrium and is given by

$$s_e = (s_j + \tau v)\left(1 - \left(\frac{v}{v_{max}}\right)^{\xi\left(v\tau + \frac{\tau^2 g(f+e)}{2} - s'\right)}\right)^{-\frac{1}{2}} \tag{5.16}$$

Substituting this in (5.15) gives the flow for the proposed model as

$$Q = \frac{v}{(s_j + \tau v)\left(1 - \left(\frac{v}{v_{max}}\right)^{\xi\left(v\tau + \frac{\tau^2 g(f+e)}{2} - s'\right)}\right)^{-\frac{1}{2}}} \tag{5.17}$$

Thus, traffic flow is influenced by the geometric design and reaction time. Vehicles with a large reaction time will behave differently on horizontal curves compared to those with a short reaction time. This is more realistic than the ID model which characterizes traffic flow based on constant δ and so cannot produce acceptable traffic behavior on horizontal curves.

5.2 Traffic Models Performance

In this section, the performance of the proposed model with HVs, AVs, and CAVs is evaluated. In addition, the performance of CAVs is considered with different time headway τ values and compared with the ID model for $\delta = 1, 4,$ and 80. Results are obtained for a 1300 m circular road

and time duration 150 s using the explicit Euler scheme with time step 0.5 s [47]. The friction coefficient employed is 0.7 which is a typical value for dry roads [90], [91] and the maximum speed (desired speed) is 30 m/s [47]. The maximum acceleration and deceleration are 0.73 m/s^2 and 1.67 m/s^2, respectively [26]. The time headway adjusts based on the traffic conditions and is typically between 0.5 s and 2.6 s [92]. The vehicle length is 4.5 m [73] and the maximum normalized density is $\frac{1}{s_j} = 0.2$. Spacing during traffic jams varies between 2 m and 7m [26], [47], so 5 m is used here. The simulation parameters are given in Table 5.1.

Table 5.1 Simulation parameters.

Parameter	**Value**
Maximum speed (desired speed), v_{max}	30 m/s
Time headway, τ	0.5, 1, 2 and 2.5 s
Maximum acceleration, a_{max}	0.73 m/s^2
Friction coefficient, f	0.7
Superelevation rate, e	0.036 m
Spacing during jam, s_j	5 m
Minimum acceleration (deceleration), b	1.67 m/s^2
Vehicle length, L	4.5 m
Reaction time of HVs, ξ	1.6 s
Reaction time of AVs, ξ	0.5 s
Reaction time of CAVs, ξ	0.1 s
Maximum normalized density, $\rho_m = \frac{1}{s_j}$	0.2
Acceleration exponent, δ	1, 4 and 80
Time step size, Δt	0.5 s

5.2.1 Performance with HVs, AVs, and CAVs

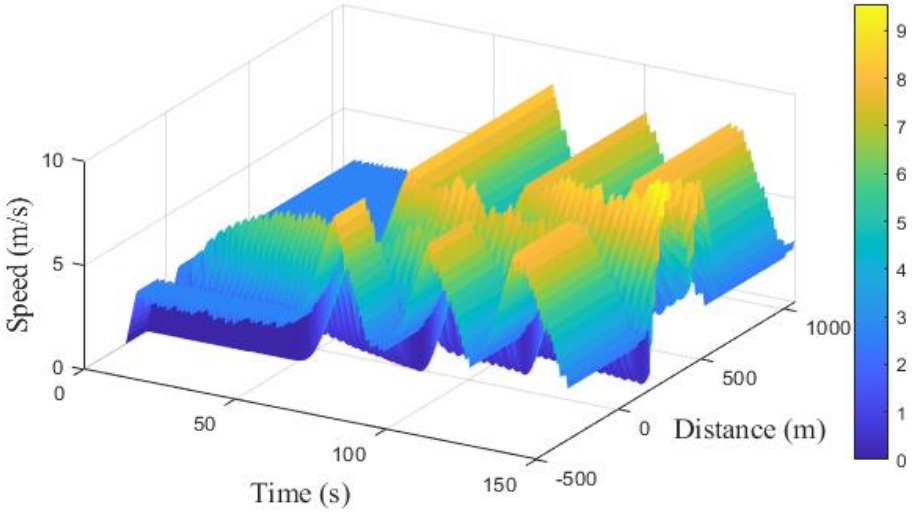

Figure 5.3 Temporal and spatial speed with HVs ($\xi = 1.6$ s) at time headway τ of 1 s over a 1300 m circular road.

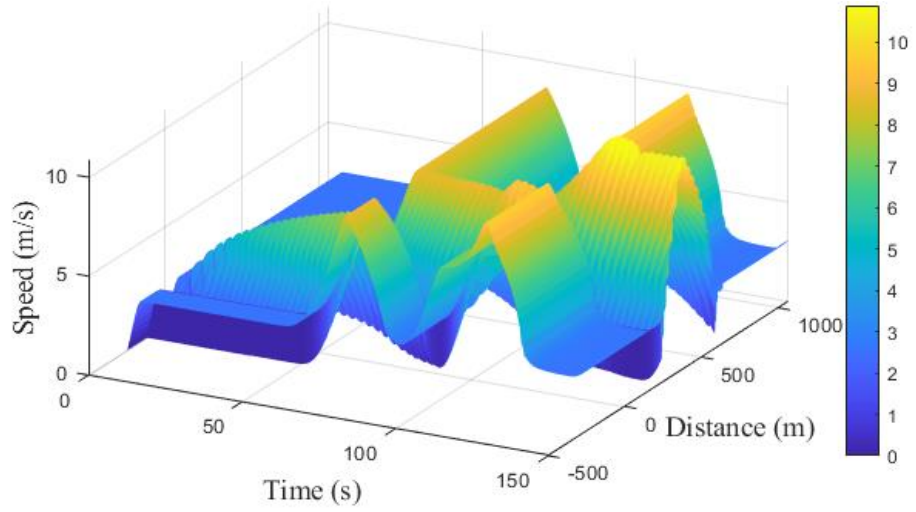

Figure 5.4 Temporal and spatial speed with AVs ($\xi = 0.5$ s) at time headway τ of 1 s over a 1300 m circular road.

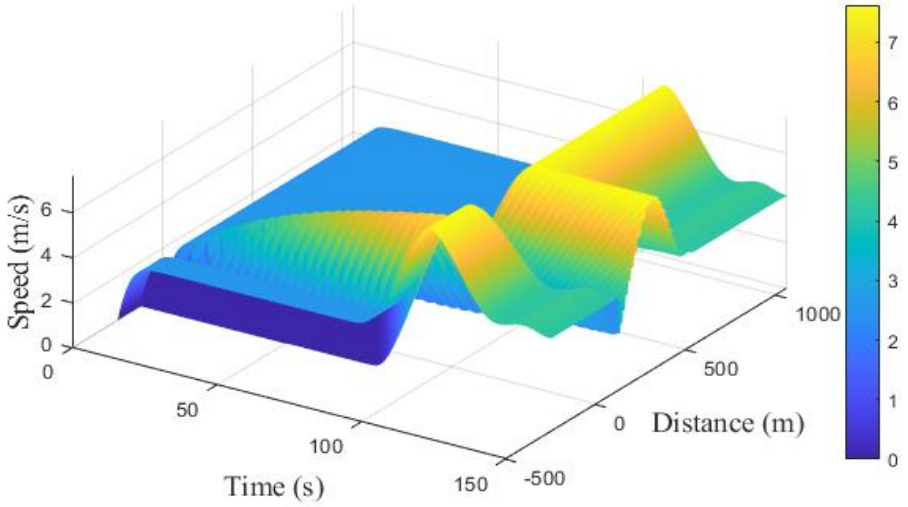

Figure 5.5 Temporal and spatial speed with CAVs ($\xi = 0.1$ s) at time headway τ of 1 s over a 1300 m circular road.

The speed over a 1300 m circular road for 150 s with HVs, AVs, and CAVs is given in Figures 5.3, 5.4, and 5.5, respectively. These results show that the speed oscillates over time and space but the oscillations are greater with HVs and AVs. The oscillations are smaller with automated vehicles, particularly CAVs. Further, the highest speed with HVs is 9.4 m/s, AVs is 10.7 m/s, and CAVs is 7.6 m/s. Thus, CAVs provide the best performance.

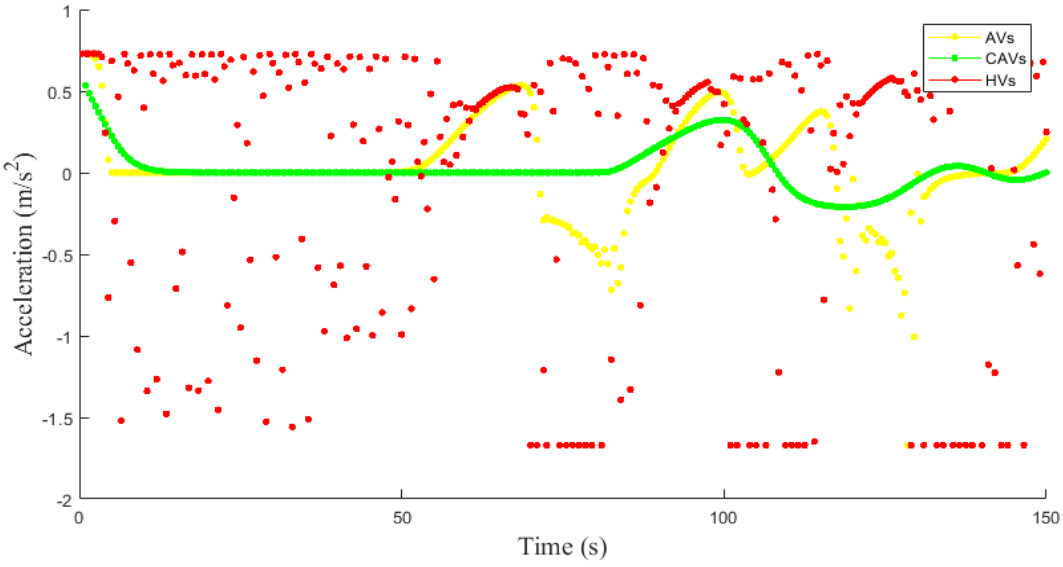

Figure 5.6 Temporal acceleration with HVs ($\xi = 1.6$ s), AVs ($\xi = 0.5$ s), and CAVs ($\xi = 0.1$ s) for time headway $\tau = 1$ s over a 1300 m circular road.

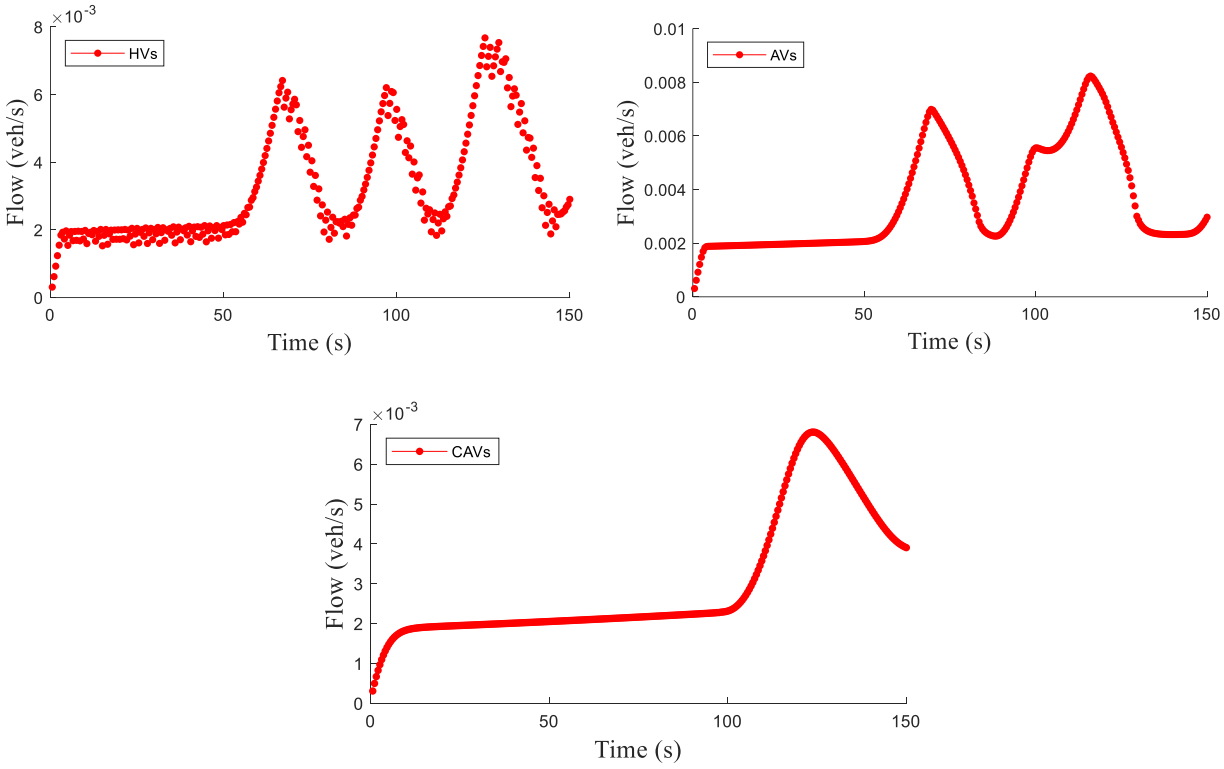

Figure 5.7 Temporal flow with HVs ($\xi = 1.6$ s), AVs ($\xi = 0.5$ s), and CAVs ($\xi = 0.1$ s) for time headway $\tau = 1$ s over a 1300 m circular road.

Figures 5.6 and 5.7 give the proposed model acceleration and flow, respectively, with HVs, AVs, and CAVs for 150 s. These results show that the oscillations in acceleration and flow with HVs are large. For example, the acceleration varies between 0.73 m/s^2 and -1.67 m/s^2 from 0 s to 150 s. The acceleration oscillations with AVs are much smaller, i.e. between 0.53 m/s^2 and -1.00 m/s^2 from 53.5 s to 150 s. The corresponding flow varies between 0.002 and 0.009 from 56.0 s to 150 s and this is similar to the results for HVs. With CAVs the oscillations in acceleration are minimal and the acceleration is approximately 0.002 m/s^2 from 16.0 s to 81.0 s.

The results presented in this section show that AVs tend to maintain higher speeds on horizontal curves compared to HVs and CAVs. This is because AVs follow predefined rules and algorithms without human intervention and thus can navigate curves at higher speeds. However, at higher speeds horizontal curves can lead to traffic accidents as these curves are designed to facilitate gradual turns rather than fast maneuvers. Vehicles with higher speeds can misjudge the curvature, increasing the risk of accidents. HVs have lower speeds compared to AVs as drivers choose to reduce their speed due to safety concerns or uncertainty about the road ahead. However,

HV speed oscillations are larger due to driver reaction to various road conditions. CAVs have slower and more stable speeds compared to AVs and HVs as they prioritize safety and efficiency over speed. This results in smaller oscillations due to their ability to communicate with other vehicles and infrastructure.

Figures 5.6 and 5.7 show that the variations in acceleration and flow with CAVs are much smaller than with HVs and AVs. Overall, the results obtained show that CAVs have better performance on the horizontal curves compared to HVs and AVs.

5.2.2 Comparison of Proposed Model and ID Model

In this section, the traffic behavior of the proposed model considering CAVs and the ID model is examined. The CAVs are chosen as they have superior performance on horizontal curves. The simulation parameters in Table 5.1 are employed and a platoon of 25 vehicles is considered. Figure 5.8 gives the spatial and temporal evolution of speed with CAVs for $\tau = 0.5, 1, 2,$ and 2.5 s. When $\tau = 0.5$ s, the speed is zero, which results in congestion as the vehicles are not moving. At $\tau = 1$ s, congestion occurs from 0 s to 85.0 s. The vehicles move slowly and the maximum speed is 7.4 m/s. With $\tau = 2$ s, the congestion dissipates after 65.0 s and the vehicles move at speeds from 6.6 m/s to 17.2 m/s. At $\tau = 2.5$ s, the vehicles accelerate rapidly and reach a maximum speed of 21.2 m/s. There is no congestion after 70.5 s. Figures 5.8 indicate that an increase in τ results in an increase in speed.

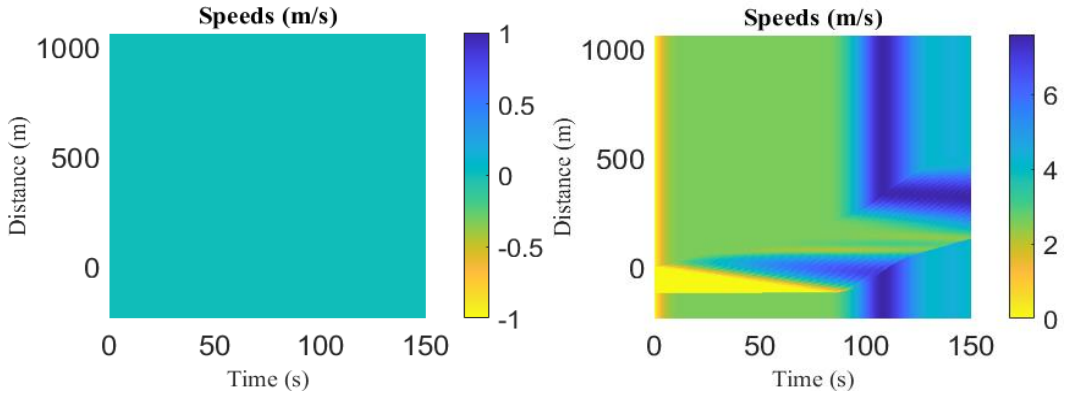

(a) **(b)**

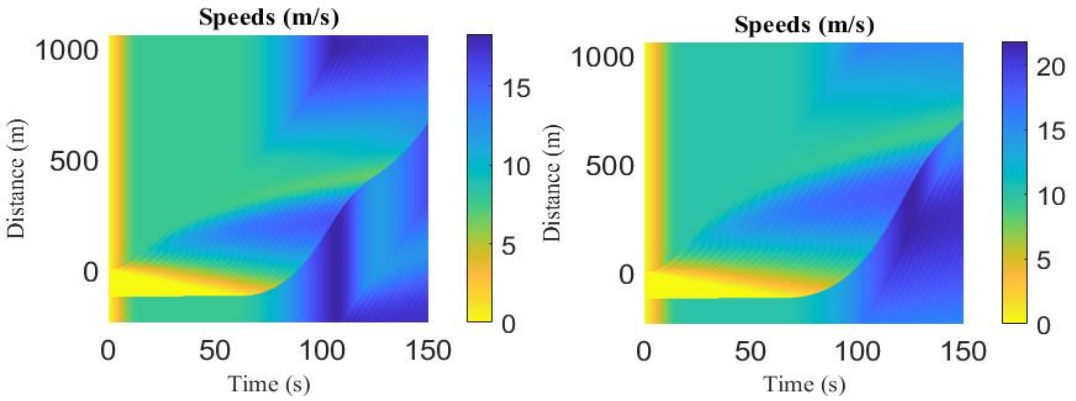

Figure 5.8 CAVs speed with proposed model over time and space for, **(a)** $\tau = 0.5$ s **(b)** $\tau = 1$ s, **(c)** $\tau = 2$ s, and **(d)** $\tau = 2.5$ s.

Figure 5.9 depicts the spatial and temporal evolution of speed with the ID model for $\delta = 1, 4$ and 80. When $\delta = 1$, congestion occurs from 0 s to 57.5 s. After congestion, vehicles move slowly, and the maximum speed is 23.5 m/s. At $\delta = 4$, the congestion dissipates after 58 s and the vehicles move at speeds from 11.8 m/s to 27.5 m/s. At $\delta = 80$, congestion occurs from 0 s to 58 s, however, congestion occurs again from 140 s and increases over time. Figures 5.9 indicate that an increase in δ results in an increase in speed and traffic congestion appears, which is not a representative of real traffic dynamics.

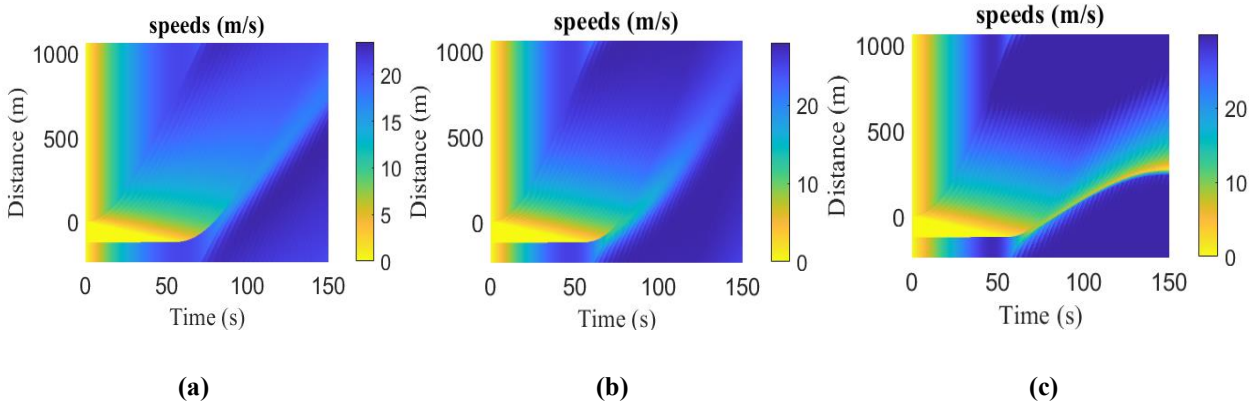

Figure 5.9 ID model speed over time and space for, **(a)** $\delta = 1$, **(b)** $\delta = 4$, and **(c)** $\delta = 80$.

5.3 Conclusion

The traditional traffic models are all based on fluid dynamics, however, vehicle acceleration and deceleration behave like a spring-mass system. In this work, a microscopic traffic model was

developed based on Hooke's law for a spring-mass system to improve the ID model by addressing its limitations, such as the unrealistic assumption of a constant exponent δ and the dependence on fluid dynamics. This new model was used to investigate the behavior of HVs, AVs, and CAVs on horizontal curves as they are crucial for traffic safety and operational efficiency. Simulation results indicate that CAVs perform better than HVs and AVs on horizontal curves. In particular, the speed with CAVs is lower and more stable which allows for safer maneuvering. CAVs also have smaller speed and flow oscillations which reduces the probability of congestion. This is because CAVs can coordinate with other vehicles and infrastructure to adjust speeds and maintain safe distance headway, resulting in a smooth flow. CAVs also have smaller acceleration and deceleration on horizontal curves which reduces fuel consumption and consequently traffic emissions, contributing towards a more sustainable environment. Furthermore, the comparison between the proposed model and the ID model highlights that the new model outperforms the ID model and provides more accurate and realistic traffic behavior.

Chapter 6

The Effect of Connected Autonomous Vehicles at Bottlenecks and the Impact of Cyberattacks

Traffic bottlenecks significantly reduce the safety and efficiency of transportation systems [93]–[95]. At bottlenecks, flow is restricted due to accidents, reduced speed limits, and lane merging and closure [93], [96], which lowers road capacity. When the upstream traffic demand surpasses the bottleneck capacity, vehicles form a queue upstream, leading to congestion [97], [98]. Further, when a downstream vehicle approaches a bottleneck, the speed is reduced resulting in shockwaves. These waves propagate upstream and increase the risk of collisions [96]. Traffic congestion due to bottlenecks causes delays, which according to the U.S. Urban Mobility Report has doubled from 1982 to 2019 [99]. To address this issue, safety management and control measures such as ramp metering, variable speed limit (VSL) control, and dynamic routing have been adopted [94], [96]. However, their effectiveness is limited by the VSL range and maximum queue length permitted on a ramp [93].

The recent introduction of CAVs has led to the development of methods to improve traffic flow efficiency at bottlenecks [100]. These typically involve CAV trajectory planning and merging control, and have been shown to provide effective congestion control [101], [102]. Connected vehicles can obtain downstream traffic information beyond visual perception, and can increase road capacity and decrease emissions by reducing time headway and improving reaction time and sensitivity to changing traffic conditions [103]. However, the connected vehicle environment is susceptible to cybersecurity threats.

Therefore, this chapter presents a microscopic traffic model to investigate the behavior of CAVs at bottlenecks considering cyberattacks. This is based on data collected from a sensor node installed on University Road in Peshawar, Pakistan. This is the main city road that connects various government organizations and educational institutions. Thus, creates the highest traffic volumes in the city which results in frequent bottlenecks. The data are analyzed as in [104] and the traffic parameters are integrated with the ID model to obtain a new model. The performance of the proposed and ID models is evaluated over a circular road.

The rest of this chapter is structured as follows. Section 6.1 details cyberattacks in CAVs and Section 6.2 presents the traffic models. The proposed and ID models are evaluated in Section 6.3, and Section 6.4 concludes the chapter.

6.1 Connected Autonomous Vehicle (CAV) Cyberattacks

Cyberattacks on CAVs attempt to exploit vulnerabilities in vehicle software, digital systems, and/or communication networks to disrupt functionality, compromise safety, and/or gain unauthorized access to sensitive data [105]. The potential attacks are spoofing, denial-of-service (DOS), malware injection, and jamming [106], [107]. Spoofing can compromise GPS data to corrupt vehicle navigation [108]. A DOS attack can overload systems to degrade services such as communication. Vehicle control can be lost due to malware. Incorrect data can be communicated to neighboring vehicles, which can lead to accidents [109]. Thus, robust cybersecurity measures are required to address these attacks and assess their impact on traffic dynamics.

The threshold (intensity) of a cyberattack is determined based on the impact of an attack on the system, the potential for propagation, and the cumulative effect. The factors considered are attacked exposed surface (ES), severity impact (SI), propagation rate (PR), detection latency (DT), impact scope (IS), and recovery time (RT) [107], [109]–[111]. This includes the potential number of interfaces and systems that can be attacked, the impact on safety and function, the speed and spread of the attack, the time taken to detect the attack, the vehicles and infrastructure affected, and the time taken to recover. The cyberattack intensity is expressed as

$$c = w_1 ES + w_2 SI + w_3 PR + w_4 \frac{1}{DT} + w_5 \frac{1}{RT} + w_6 IS \tag{6.1}$$

where w_1, w_2, w_3, w_4, w_5, and w_6 are weights based on the severity and importance of the factors. ES and SI are integers, PR is the percentage of the systems affected, DT and RT are measured in minutes, and IS ranges from 1 to 10. A larger value of c indicates a more severe attack. The factors considered are $ES = 6$, $SI = 7$, $PR = 67.21\%$, $DT = 3$ min, $RT = 21$ min, and $IS = 10$. The corresponding weights are $w_1 = 1$, $w_2 = 1.4$, $w_3 = 1.1$, $w_4 = 0.7$, $w_5 = 0.7$ and $w_6 = 1$. This results in $c = 100$ so the attack is severe. If the propagation rate is reduced to $PR = 3.57\%$, the cyberattack severity is $c = 30$. These intensity values are considered here to evaluate the impact of cyberattacks on traffic.

6.2 Traffic Models

The ID model is defined as [26]

$$\frac{dv}{dt} = a_{max}\left(1 - \left(\frac{v}{v_{max}}\right)^{\delta} - \left(\frac{D}{s}\right)^{2}\right), \tag{6.2}$$

where D is given by [26]

$$D = s_j + \tau v + \frac{v\Delta v}{2\sqrt{a_{max}b}} \tag{6.3}$$

The driver response with the ID model depends on the constant δ. Thus, driver behavior is the same for all traffic conditions, regardless of whether the traffic is moving freely or experiencing a bottleneck, which is not realistic. Actual driver behavior varies according to the traffic conditions. Near a bottleneck, drivers become cautious and reduce their speed, whereas in free-flow traffic, drivers are more aggressive and can maintain high speeds. Therefore, δ should vary with changes in flow and density to reflect real-world traffic behavior. Further, the ID model was developed to simulate human-driven vehicle dynamics and so does not adequately account for the advanced communication and cooperative abilities of CAVs, which is crucial in complex traffic environments. This model also does not capture the decision-making and coordination behavior of CAVs in scenarios like bottlenecks.

Here, an acceleration exponent δ for realistic characterization of traffic at bottlenecks is proposed based on changes in traffic density and flow. The flow Q and density ρ were obtained from a sensor node installed at University Road, Peshawar, with GPS coordinates 33.99841270487691 latitude and 71.47962908395094 longitude [104]. Data were collected for a week from $9{:}00$ AM to $4{:}00$ PM which corresponds to high traffic volumes in the area and so provides the most important traffic conditions. The flow and density were measured and transferred to the ThingSpeak cloud platform. Regression analysis was performed to model the relationship between Q and ρ. Linear, exponential, polynomial, logarithmic, and power models were considered. It was determined that a second-order polynomial provides the best fit and is given by [104]

$$Q = -44.34\rho^2 + 80.02\rho + 1.628 \tag{6.4}$$

This indicates that as density increases, the traffic flow becomes congested, which indicates a bottleneck. Differentiating (6.4) with respect to density gives

$$\frac{dQ}{d\rho} = -88.68\rho + 80.02$$

A larger distance headway results in fewer vehicles on the road, and therefore the density is small. Conversely, a small distance headway means vehicles are closely packed, so the density is high. Therefore, substituting $\rho = 1/s$ [47], we obtain

$$\frac{dQ}{d\rho} = -\frac{88.68}{s} + 80.02 \tag{6.5}$$

Driver reaction also affects traffic at bottlenecks [112] and is influenced by the ratio of distance headway s to desired distance headway D [113]. Thus, the proposed acceleration exponent δ is

$$\delta = \left(-\frac{88.68}{s} + 80.02\right)\left(\frac{s}{D}\right)\xi \tag{6.6}$$

where ξ is the CAV reaction time. This is smaller than the reaction time for human-driven vehicles as sensors and communication technology are used to process and respond to traffic conditions much faster than humans. CAVs have a reaction time of approximately 0.1 s, which is almost instantaneous. This is due to their ability to exchange data continuously and rapidly with other vehicles and infrastructure in the environment [9].

The value of $\frac{s}{D}$ is between 0 and 1. When $\frac{s}{D} = 0$, there is no velocity change. In this case, density is maximum, i.e., there is congestion with minimal vehicle movement. When $\frac{s}{D} = 1$, velocity changes occur quickly so the traffic flow is smooth and the maximum speed is attained. When $s \ll D$, vehicles are closely packed, which can create bottlenecks. Substituting (6.6) in (6.2), the proposed model for bottlenecks is obtained as

$$\frac{dv}{dt} = a_{max}\left(1 - \left(\frac{v}{v_{max}}\right)^{\left(-\frac{88.68}{s}+80.02\right)\left(\frac{s}{D}\right)\xi} - \left(\frac{D}{s}\right)^2\right), \tag{6.7}$$

This model characterizes traffic flow at bottlenecks based on the reaction time and distance headway and is more realistic than the constant δ in the ID model. With the proposed model, traffic behavior at bottlenecks varies according to the reaction time and distance headway whereas the ID model produces similar behavior for all traffic conditions. Further, the proposed model can account for CAVs dynamically adjusting their headway and speed based on traffic conditions, leading to better flow and less congestion, which is not possible with the ID model. It can also characterize CAV reactions to bottlenecks.

Traffic flow is given by $Q = v/s_e$ [31], where s_e is expressed as

$$s_e = (s_j + \tau v)\left(1 - \left(\frac{v}{v_{max}}\right)^{\left(-\frac{88.68}{s}+80.02\right)\left(\frac{s}{D}\right)\xi}\right)^{-\frac{1}{2}} \tag{6.8}$$

This shows that with the proposed model, distance headway between vehicles at equilibrium is based on the reaction time of CAVs and is more realistic than the constant δ in the ID model. The flow for the proposed model is then

$$Q = \frac{v}{(s_j + \tau v)\left(1 - \left(\frac{v}{v_{max}}\right)^{\left(-\frac{88.68}{s}+80.02\right)\left(\frac{s}{D}\right)\xi}\right)^{-\frac{1}{2}}} \tag{6.9}$$

CAV behavior can be affected by cyberattacks. In a connected vehicle environment, vehicle alignment relies on real-time data exchange, particularly the distance headway information communicated between vehicles. When this information is accurate and readily accessible, the system functions normally, enabling vehicles to effectively adjust their speed and behavior [114]. Conversely, if the distance headway is inaccurate or unavailable due to cyberattacks, the system does not function properly. This results in inefficient vehicle behavior and delayed reactions [114]. Thus, the impact of these attacks in the proposed model (6.7) can be expressed as

$$\frac{dv}{dt} = a_{max}\left(1 - \left(\frac{v}{v_{max}}\right)^{\left(-\frac{88.68}{s}+80.02\right)\left(\frac{s}{D}\right)\xi} - \left(\frac{D}{s}\right)^2\right) + c\left(\frac{s}{D}\right)\xi \tag{6.10}$$

where c is the cyberattack intensity that ranges between 0 and 100. $c = 0$ indicates that the vehicles behave normally, whereas $c = 100$ signifies that the vehicles are affected significantly by the attack. During a cyberattack, the distance headway and reaction time are manipulated so the information communicated in the system is corrupted.

6.3 Performance

The performance of the proposed and ID models is evaluated on a 1000 m circular road for 200 s using the Euler technique. The proposed model is evaluated for a platoon of 40 CAVs with time headway 1 s, jam spacing 1.5 m [115], and reaction time 0.1 s [9]. The ID model is evaluated for a platoon of 36 vehicles with time headway 2 s [116] and jam spacing 2 m [26] so the platoons have the same length. The number of vehicles on the road was obtained by dividing the road length by the equilibrium distance headway s_e. The value of s/D ranges between 0 and 1, so here 0.2, 0.5, and 0.8 are used. δ is set to 1, 4, and 100. To assess the impact of cyberattacks, the intensity from (6.1) is 30 and 100. The simulation parameters are given in Table 6.1 and the circular road considered is illustrated in Figure 6.1.

Table 6.1 Simulation parameters.

Parameter	**Value**
Maximum speed (desired speed) for the ID model, v_{max}	30 m/s [53]
Maximum speed (desired speed) for the proposed model, v_{max}	20 m/s [32]
Time headway for the proposed model, τ	1 s
Time headway for the ID model, τ	2 s
Maximum acceleration, a_{max}	0.73 m/s^2 [26]
Jam spacing for the proposed model, s_j	1.5 m
Maximum normalized density for the proposed model, $\rho_m = 1/s_j$	0.67
Jam spacing for the ID model, s_j	2 m
Maximum normalized density for the ID model, $\rho_m = 1/s_j$	0.5
Minimum acceleration (deceleration), b	1.67 m/s^2 [26]
Vehicle length, L	4.5 m
CAV reaction time, ξ	0.1 s
Ratio of distance headway to desired distance headway, s/D	0.2, 0.5, and 0.8
Time step size, Δt	0.5 s [47]
Cyberattack intensity, c	30 and 100

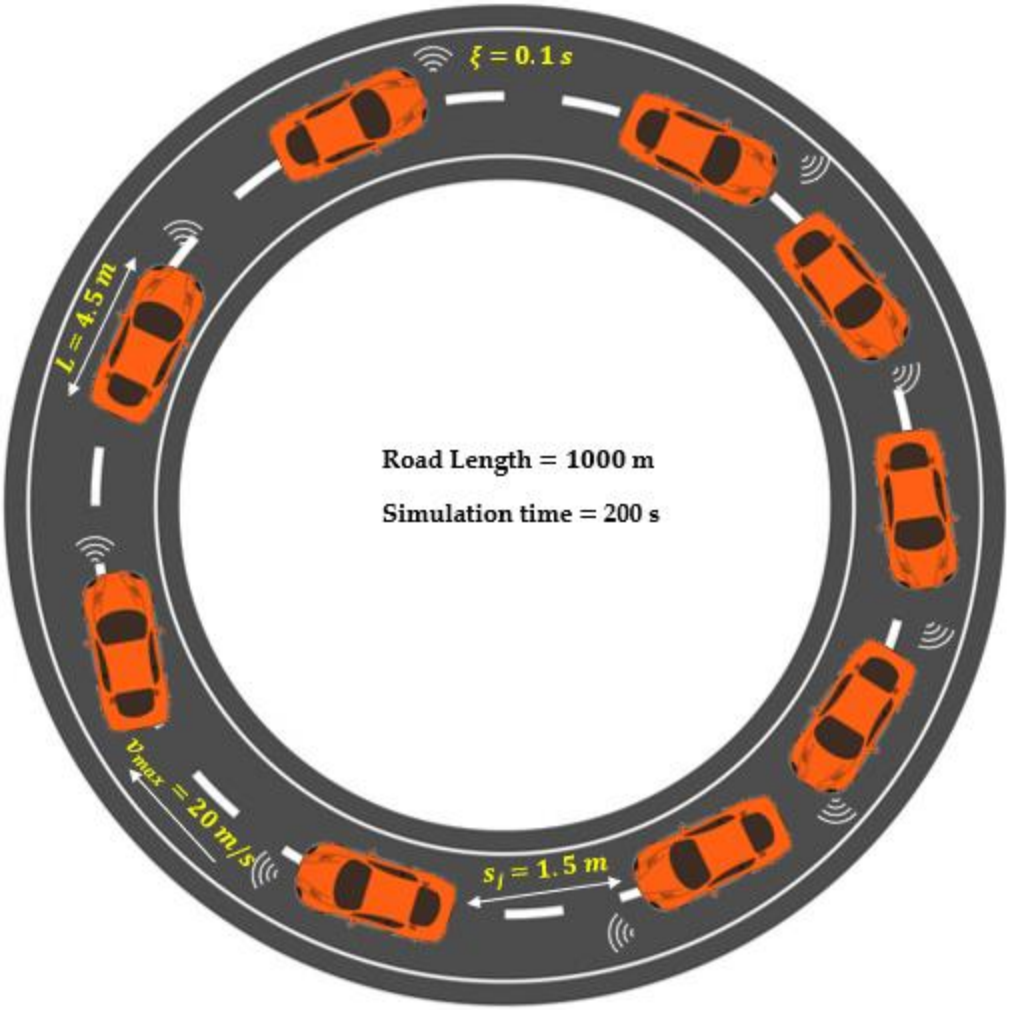

Figure 6.1 The simulation environment with a circular road.

Figure 6.2 presents the flow versus density with the proposed and ID models for $s/D = 0.2, 0.5$, and 0.8, and $\delta = 1, 4$, and 100, and the results are summarized in Tables 6.2 and 6.3, respectively. These show that with the proposed model, the maximum flow increases as s/D increases, whereas the critical density decreases. Similar behavior is observed with the ID model as δ increases. However, the road capacity with the proposed model is higher. As the density increases, the distance headway decreases, and thus s/D is smaller. In dense traffic ($s/D = 0.2$), the capacity with the proposed model is 1.4 times higher than the capacity with the ID model for $\delta = 100$.

Table 6.2 Maximum traffic flow and critical density for the proposed model.

s/D	Maximum Traffic Flow (veh/s)	Critical Density
0.2	0.67	0.11
0.5	0.83	0.08
0.8	0.86	0.07

Table 6.3 Maximum traffic flow and critical density for the ID model.

Acceleration Exponent δ	Maximum Traffic Flow (veh/s)	Critical Density
1	0.38	0.05
4	0.45	0.03
100	0.48	0.01

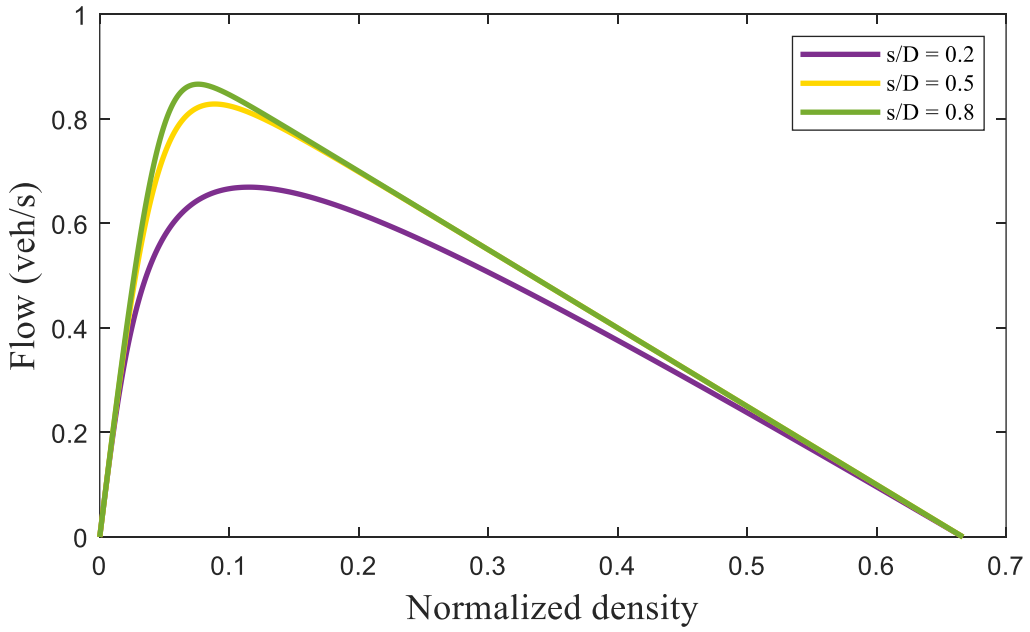

(a)

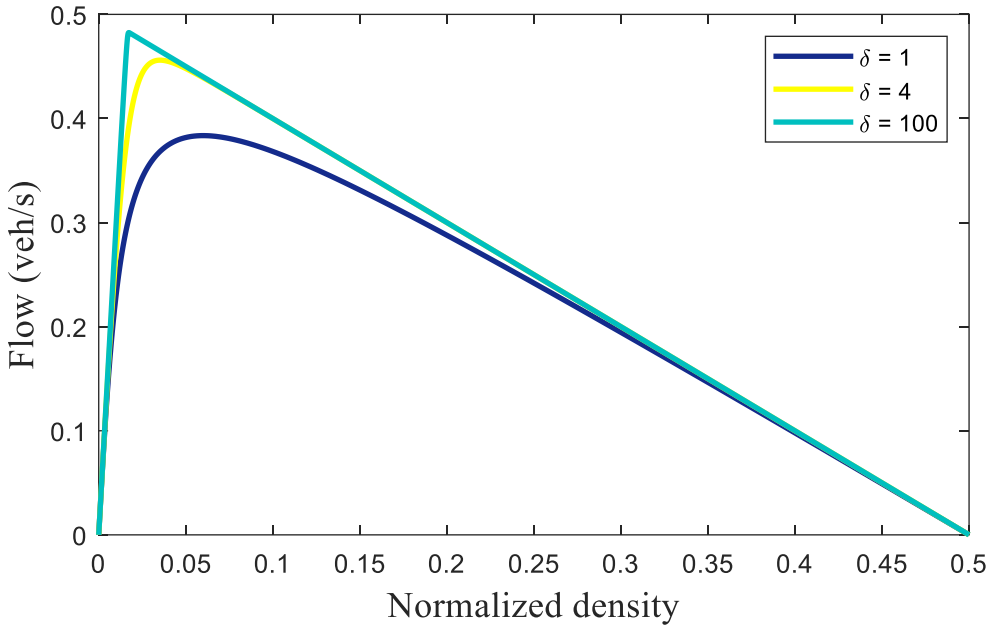

(b)

Figure 6.2 Fundamental diagram with the **(a)** proposed model and **(b)** ID model.

Figure 6.3 presents the proposed model speed behavior on a 1000 m circular road for $s/D = 0.2, 0.5$, and 0.8. This shows that as s/D increases, i.e., traffic approaches free flow and the speed becomes smooth over time, which is realistic. Conversely, with the ID model, traffic does not evolve towards a constant speed, and the variations increase over time and space with an increase in δ, as indicated in Figure 6.4. Figure 6.3a shows that with $s/D = 0.2$, the speed is between 17.9 m/s and 16.7 m/s from 1.0 s to 31.0 s, and there are small variations in speed. As s/D increases, these variations decrease, and at $s/D = 0.8$, the speed is approximately 17.9 m/s from 77.0 s to 200 s. With the ID model, for $\delta = 1$, the speed varies between 9.9 m/s and 10.2 m/s from -1000 m to 0 m at 196.0 s as shown in Figure 6.4a. As δ increases, the variations in speed increase, and with $\delta = 100$, the speed is between 9.6 m/s and 10.6 m/s with a difference of 1 m/s from -1000 m to 0 m at 198.0 s as indicated in Figure 6.4c. This shows that the variations in speed are smaller with the proposed model. Further, both the proposed and ID models have a temporary decrease in speed due to the disturbance at 30.5 s. However, the proposed model recovers more quickly from this disturbance as the variations in speed are smaller.

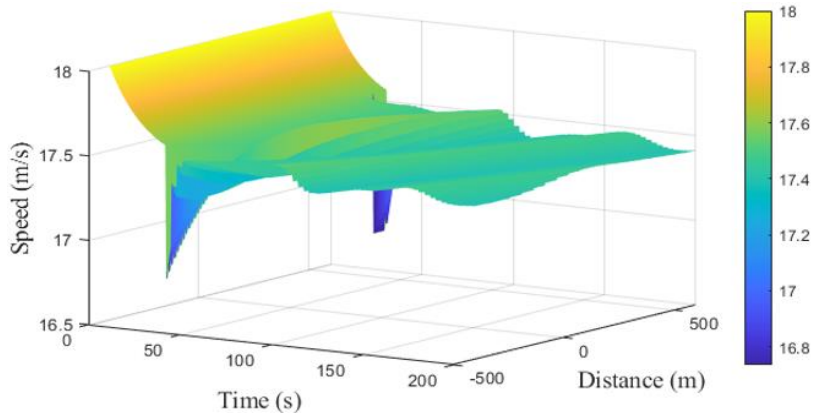

(a)

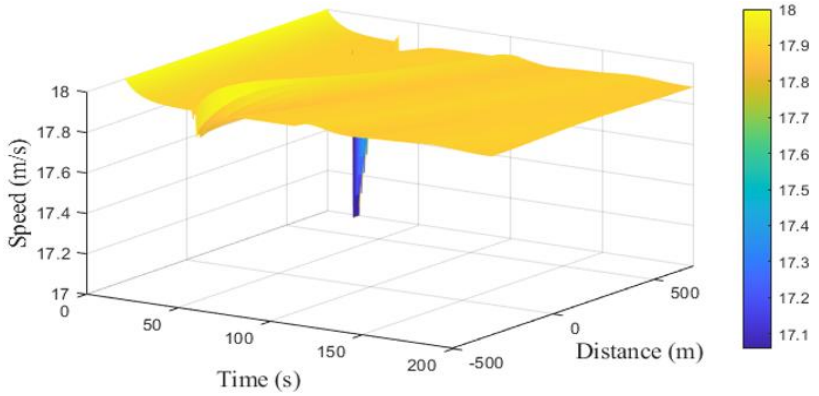

(b)

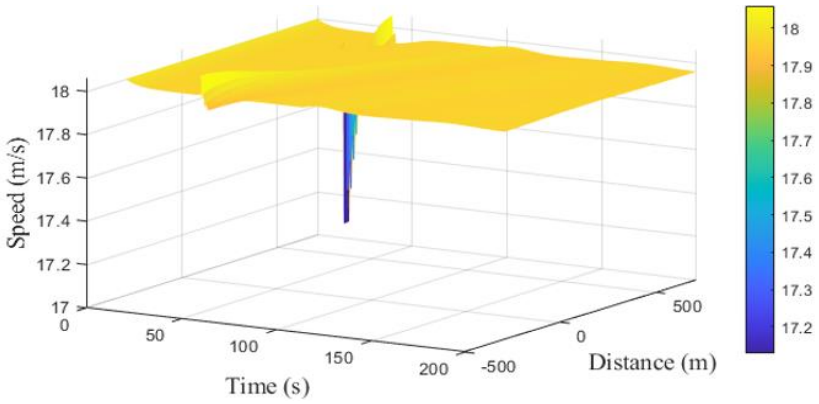

(c)

Figure 6.3 Traffic speed behavior with the proposed model for **(a)** $\frac{s}{D} = 0.2$, **(b)** $\frac{s}{D} = 0.5$, and **(c)** $\frac{s}{D} = 0.8$ on a 1000 m circular road.

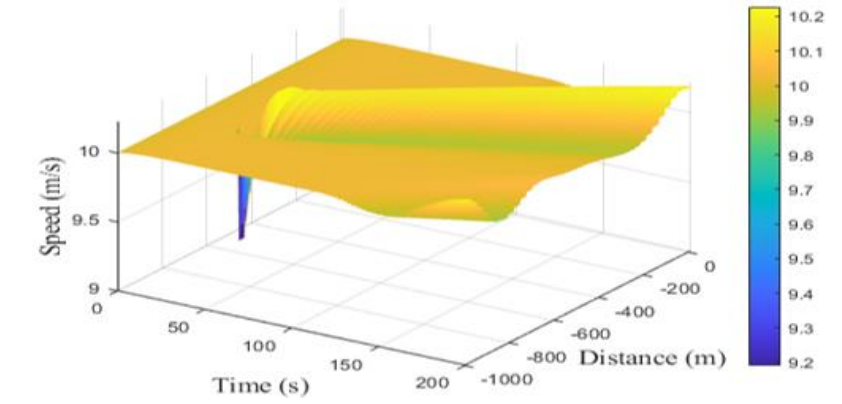

(a)

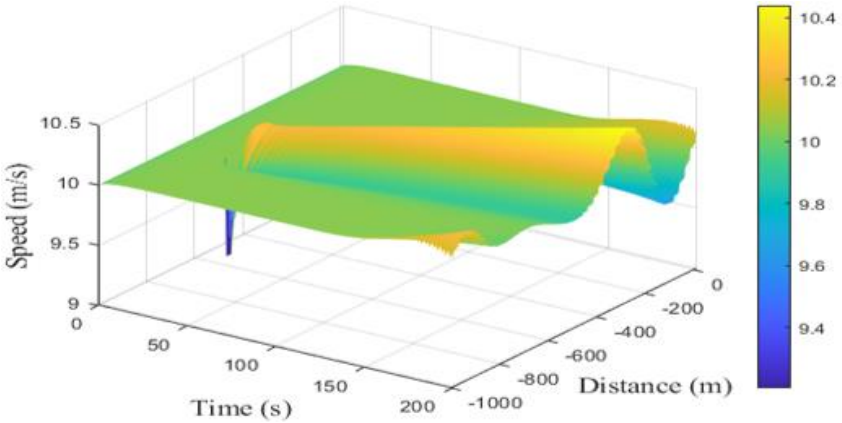

(b)

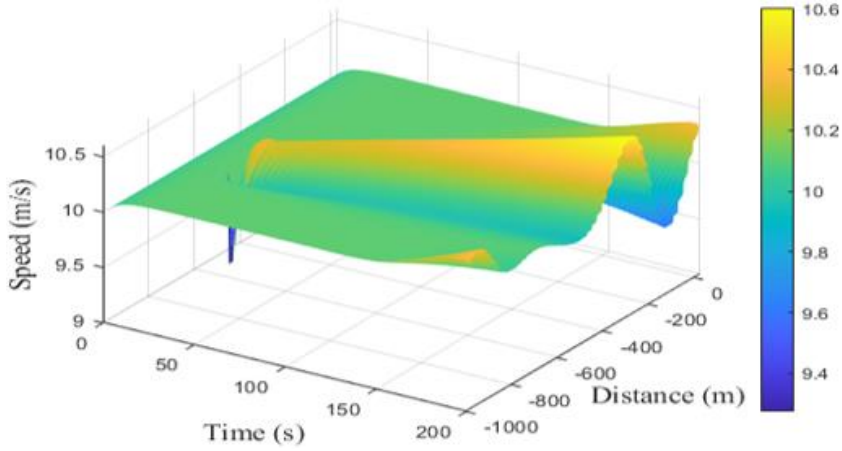

(c)

Figure 6.4 Traffic speed behavior with the ID model for **(a)** $\delta = 1$, **(b)** $\delta = 4$, and **(c)** $\delta = 100$ on a 1000 m circular road.

Figure 6.5 presents the traffic acceleration on a 1000 m circular road for $s/D = 0.2, 0.5$, and 0.8. This shows that when $s/D = 0.2$, CAV acceleration variations are small and range from 0.07 m/s^2 to -0.05 m/s^2 at 1.0 s. This is because, in high-density traffic, CAVs operate at slower speeds and are required to stop frequently. Conversely, at moderate ($s/D = 0.5$) and low ($s/D = 0.8$) densities, CAV acceleration varies between 0.21 m/s^2 and -0.18 m/s^2, and 0.30 m/s^2 and -0.30 m/s^2, respectively, at 1.0 s. This is because a decrease in density reduces CAV constraints due to surrounding vehicles. This allows the CAVs to accelerate to higher speeds. However, for all values of s/D, the variations in acceleration and deceleration decrease over time and are almost zero at 200 s. This is because CAVs can quickly stabilize their speeds and spacing due to their excellent reaction time. In addition, the adaptive behavior of CAVs based on sensor inputs such as radar and LiDAR allows them to adjust their speeds and distances relative to their surroundings. Conversely, the ID model results in larger acceleration and deceleration that increase over time as shown in Figure 6.6. With $\delta = 1$, the acceleration varies between 0.01 m/s^2 and -0.02 m/s^2 at 200 s. These variations increase with δ as with $\delta = 4$ and 100, it is between 0.06 m/s^2 and -0.08 m/s^2 and 0.1 m/s^2 to -0.1 m/s^2, respectively, at 200 s.

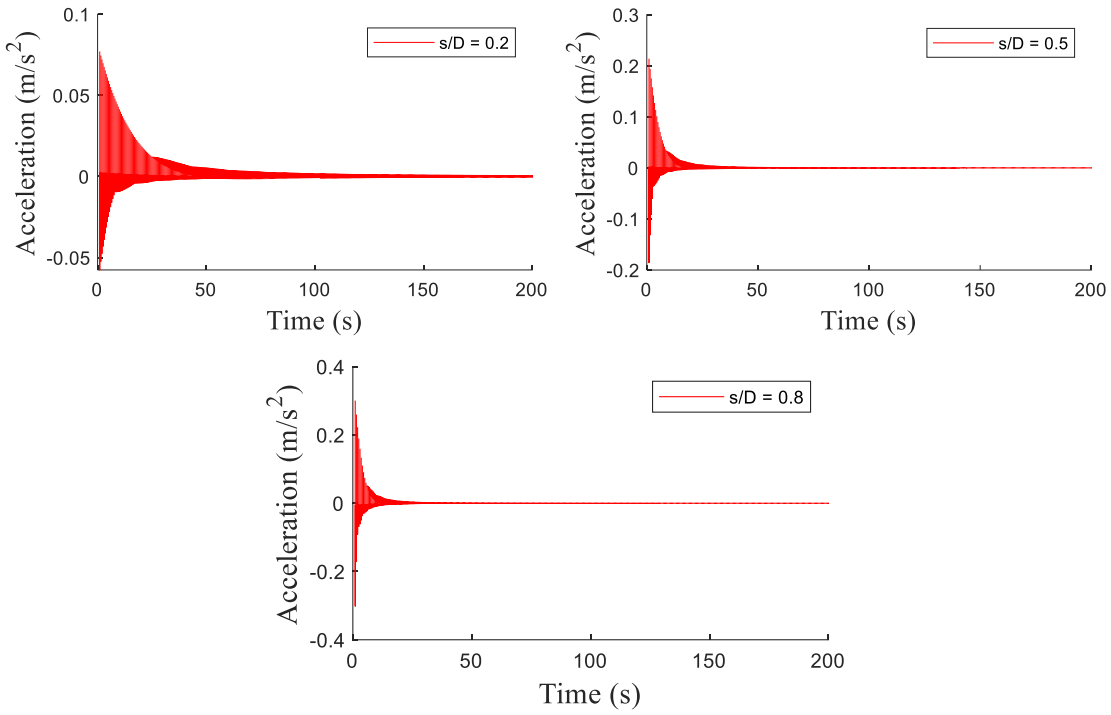

Figure 6.5 CAV acceleration evolution over time with the proposed model for $s/D = 0.2, 0.5$, and 0.8 on a 1000 m circular road.

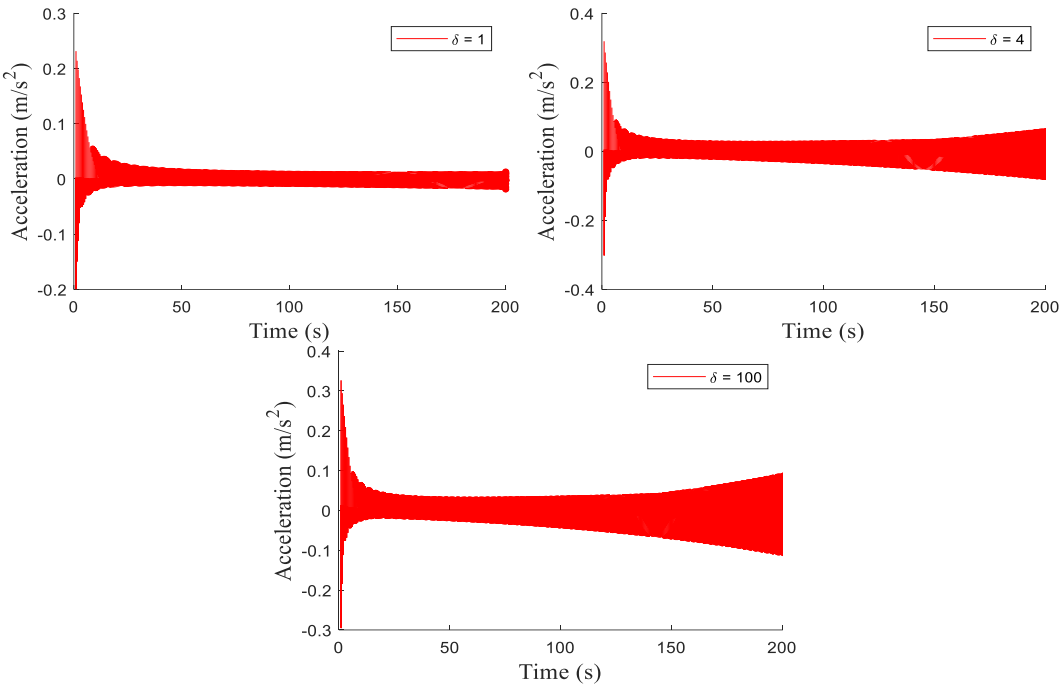

Figure 6.6 Temporal evolution of vehicle acceleration with the ID model for $\delta = 1, 4$, and 100 on a 1000 m circular road.

Figures 6.7 and 6.8 show the traffic flow behavior on a 1000 m circular road with the proposed and ID models, respectively. Figure 6.7 indicates that the flow with the proposed model increases as the density decreases. In dense traffic ($s/D = 0.2$), at -22 m, the maximum flow is 0.75 veh/s at 80.0 s. At a lower density ($s/D = 0.5$), at -26 m, the maximum flow is 0.83 veh/s at 73.5 s, whereas for $s/D = 0.8$, it is 0.91 veh/s at -20 m and -79.0 s. Figure 6.8 shows that the maximum flow with the ID model for $\delta = 1$ is 0.95 veh/s at -75.0 m and 100 s. For $\delta = 4$, the maximum flow is 7.5 veh/s and there are variations from 58.0 s to 187.0 s between -84 m and -138 m, and from 167.5 s to 200 s between 837 m and 864 m. When $\delta = 100$, the maximum flow is 11.2 veh/s with variations from 56.0 s to 182.0 s between -27 m and -138 m, and from 163.0 s to 200 s between 849 m and 858 m. This shows that an increase in δ increases the traffic flow as well as the variations.

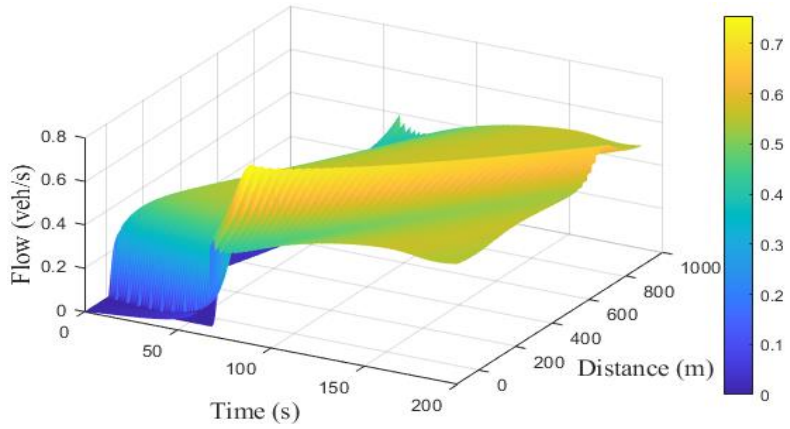

(a)

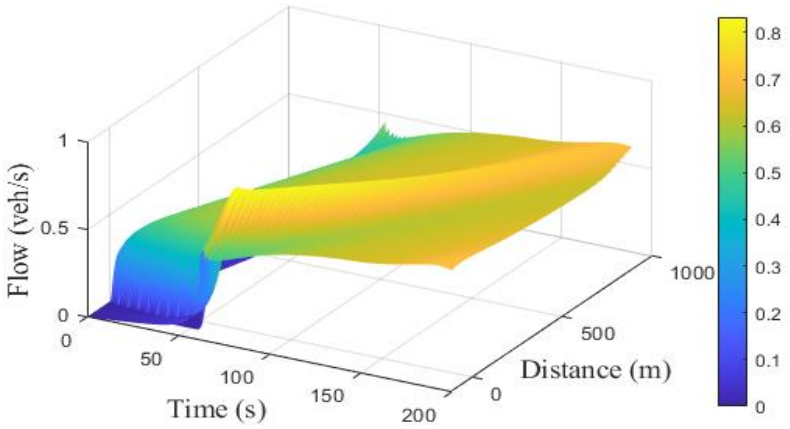

(b)

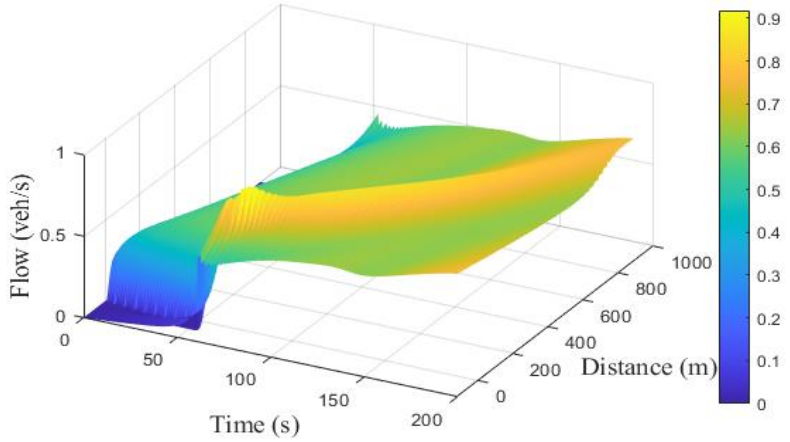

(c)

Figure 6.7 Traffic flow behavior of CAVs on a 1000 m circular road with the proposed model for **(a)** $\frac{s}{D} = 0.2$, **(b)** $\frac{s}{D} = 0.5$, and **(c)** $\frac{s}{D} = 0.8$.

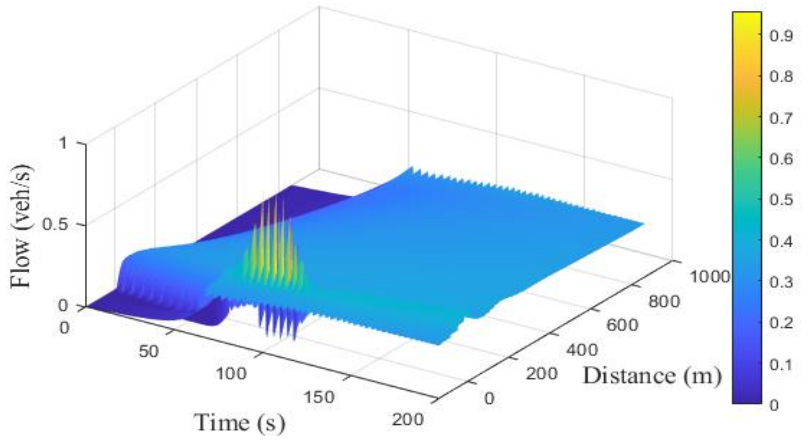

(a)

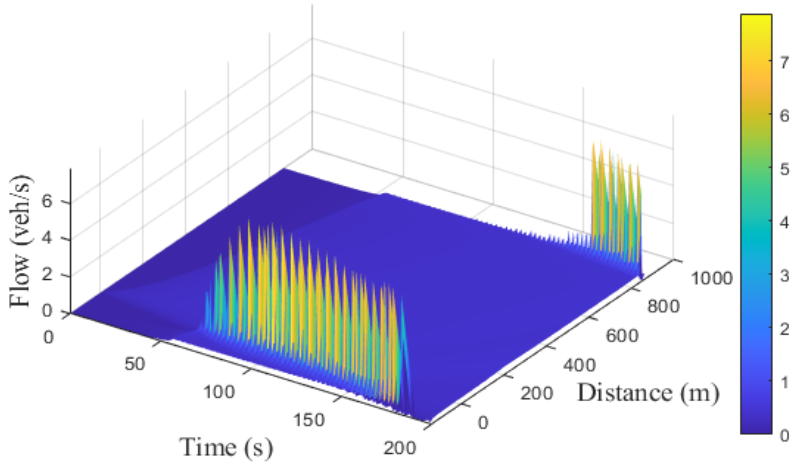

(b)

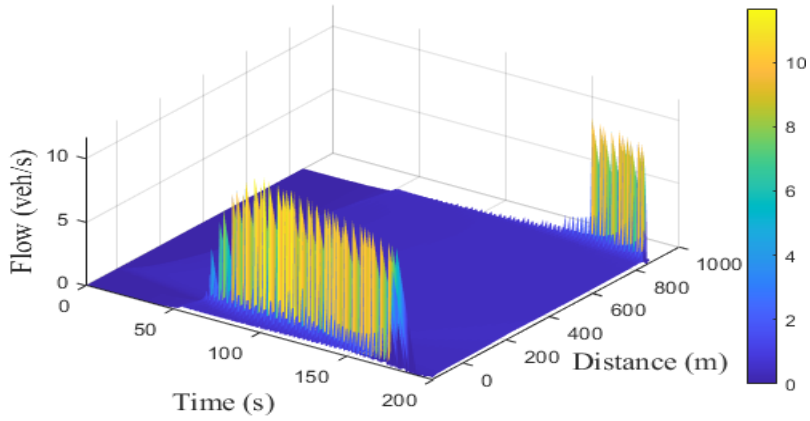

(c)

Figure 6.8 Traffic flow behavior on a 1000 m circular road with the ID model for **(a)** $\delta = 1$, **(b)** $\delta = 4$, and **(c)** $\delta = 100$.

Figure 6.9 presents the CAV flow behavior under a cyberattack at $c = 100$ on a 1000 m circular road with the proposed model. This shows that the attack produces significant traffic variations, resulting in vehicle clusters at regular intervals. Further, the traffic flow increases as the density decreases. In dense traffic ($s/D = 0.2$), the maximum flow is 1.50 veh/s, whereas at lower densities ($s/D = 0.5$ and 0.8), the maximum flow is 2.39 veh/s and 3.26 veh/s, respectively. Figure 6.10 presents the corresponding CAV flow behavior under a cyberattack at $c = 30$. This indicates that a smaller cyberattack intensity produces smaller variations in flow as the impact is less pronounced. It also shows that the flow with $c = 30$ is smaller than at $c = 100$. Further, the flow increases as the density decreases. In dense traffic ($s/D = 0.2$), the maximum flow is 0.90 veh/s, whereas at lower densities ($s/D = 0.5$ and 0.8), the maximum flow is 1.33 veh/s and 1.65 veh/s, respectively.

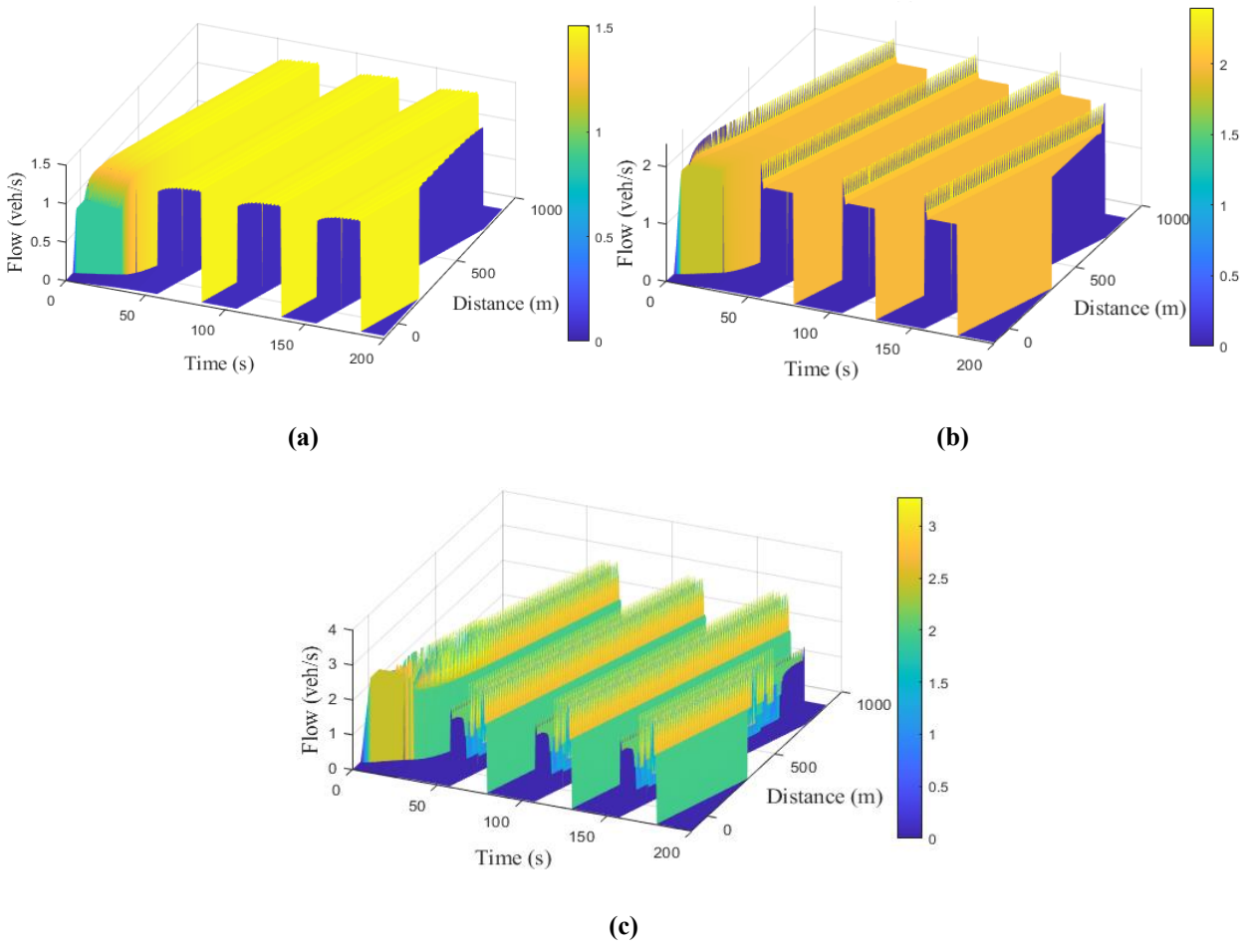

Figure 6.9 Traffic flow behavior of CAVs on a 1000 m circular road with the proposed model under a cyberattack at $c = 100$ for **(a)** $\frac{s}{D} = 0.2$, **(b)** $\frac{s}{D} = 0.5$, and **(c)** $\frac{s}{D} = 0.8$.

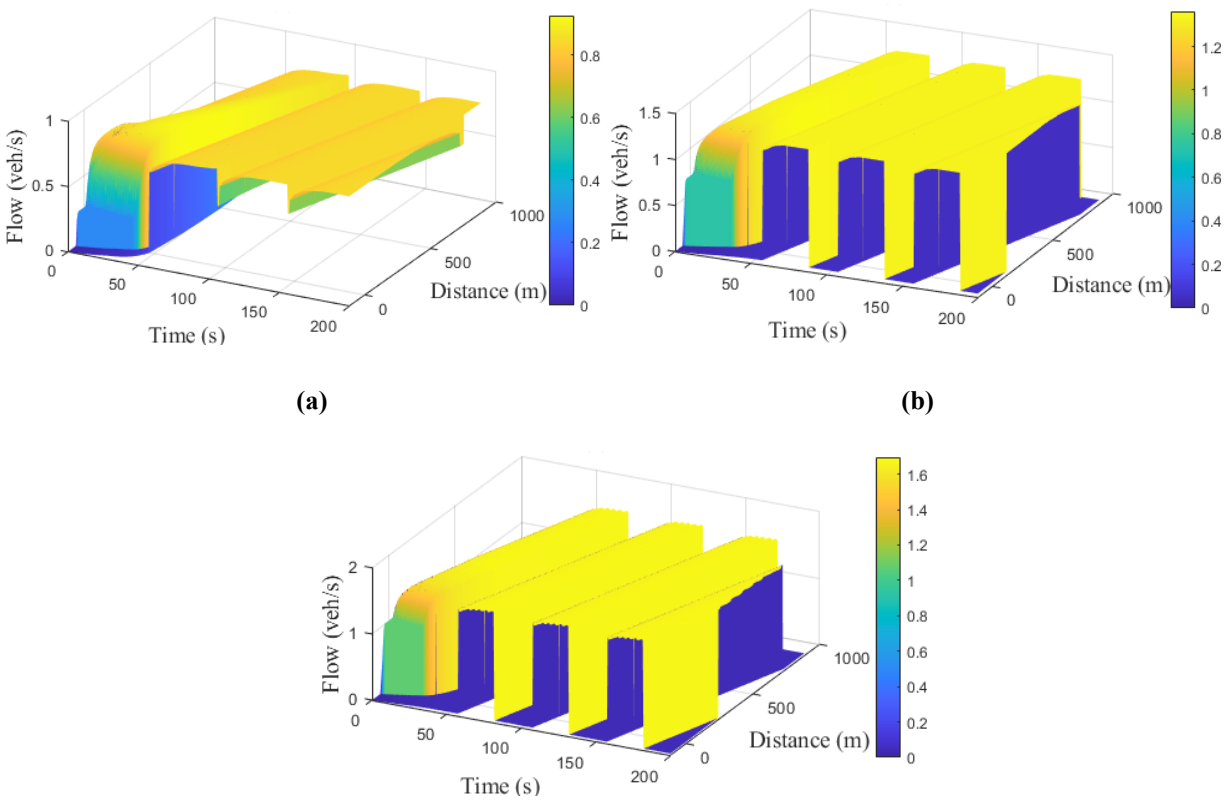

Figure 6.10 Traffic flow behavior of CAVs on a 1000 m circular road with the proposed model under a cyberattack at $c = 30$ for **(a)** $\frac{s}{D} = 0.2$, **(b)** $\frac{s}{D} = 0.5$, and **(c)** $\frac{s}{D} = 0.8$.

6.3.1 Discussion

The results presented indicate that the road capacity with the proposed model is higher than with the ID model. Further, the variations in speed with the proposed model are small, and an approximately constant speed is achieved over time, which is realistic. Conversely, the ID model results in large speed variations that increase with δ, so the traffic behavior is unrealistic. These variations produce significant acceleration and deceleration that increase over time as shown in Figure 6.6. Conversely, with the proposed model, the CAVs exhibit small variations in acceleration and deceleration that decrease over time. These variations are greater at lower densities (high s/D) due to the increased freedom of movement, while at higher densities (low s/D), the variations are smaller due to the need for closer coordination and smoother driving behavior.

With the proposed model, a lower density results in increased traffic flow, which is consistent with traffic dynamics. With the ID model, the flow increases as δ increases, which results in

unrealistic behavior as δ does not represent real traffic dynamics. Moreover, the maximum speed with the proposed model is 18.0 m/s, but with the ID model, it is only 10.6 m/s as shown in Figure 6.4c. The proposed model can incorporate CAVs, whereas the ID model is only applicable to HVs. This results in greater efficiency as CAVs can communicate and coordinate their behavior.

The results for cyberattacks show that the proposed model produces realistic traffic flows. The variations are large when the attack intensity is high and small when the intensity is low. Thus, the proposed model can be used to effectively analyze and manage cybersecurity threats.

6.4 Conclusion

A microscopic model was developed to characterize traffic behavior at a bottleneck and evaluate the performance under cyberattacks. The results obtained show that the proposed model provides a realistic characterization of traffic at bottlenecks. In particular, the traffic flow is low in dense traffic ($s/D = 0.2$) and increases as the density decreases ($s/D = 0.5$ and 0.8), as expected. Conversely, the flow with the ID model is based on a constant δ and the flow increases with δ, resulting in unrealistic traffic characterization. Further, the ID model produces large speed variations and thus high acceleration and deceleration. With the proposed model, the variations in speed and acceleration are small and decrease over time. Further, the traffic capacity is higher than with the ID model. These results indicate that the proposed model can be used to reduce vehicle emissions and thus pollution. The results obtained indicate that the proposed model produces larger traffic flows and variations when the cyberattack intensity is higher. Thus, it provides realistic traffic flow behavior under cyberattacks and thus can effectively manage the corresponding disruptions.

Chapter 7

Effect of Driver Energy-Saving Awareness on Energy Consumption

Climate change and air pollution are significant global challenges that are now critical concerns [117]. Transportation contributes substantially to energy consumption and emissions, exacerbating these problems. According to the International Energy Agency (IEA), in 2021 the transportation sector was responsible for almost 30% of the total energy consumption in major countries [118], leading to over 8000 Mt of CO_2 emissions [119]. Road transportation accounts for 75% of this energy [120]. The global energy consumption by transportation is estimated to increase to 151 quadrillion Btu by 2040, indicating an increase of 44 quadrillion Btu from 2015 [121]. In Canada, from 1990 to 2017, the total energy consumption in the transport sector increased by 41%, and the associated greenhouse gas (GHG) emissions increased by 40% from 131.3 Mt to 182.1 Mt [122]. Therefore, achieving energy conservation and emission reduction in urban road transportation is crucial to mitigate climate change.

Ongoing energy concerns have prompted drivers to increasingly adopt driving strategies that reduce energy consumption. The goal is to limit vehicle movement to reduce fuel costs. However, traditional traffic models cannot effectively characterize the effect of driver energy-saving behavior on traffic flow. Therefore, they cannot accurately and realistically depict real-world traffic dynamics considering energy concerns. Thus, a new model is required to better predict the energy consumption characteristics of traffic flows.

In this chapter, a microscopic energy consumption model is developed considering driver energy-saving awareness. First, the relationship between energy consumption and traffic flow parameters is established. Then, the performance of the proposed and ID models is examined. The results obtained demonstrate the advantages of the proposed model.

The rest of the chapter is organized as follows. Section 7.1 introduces the proposed energy consumption model considering driver energy-saving awareness, Section 7.2 provides a

performance investigation of the proposed model alongside that of the ID model. Some concluding remarks are given in Section 7.3.

7.1 Energy Consumption Model

Acceleration in the ID model is expressed as [26]

$$\frac{dv}{dt} = a_{max}\left(1 - \left(\frac{v}{v_{max}}\right)^{\delta} - \left(\frac{D}{s}\right)^{2}\right), \tag{7.1}$$

where D is given by [26]

$$D = s_j + \tau v + \frac{v\Delta v}{2\sqrt{a_{max}b}} \tag{7.2}$$

The ID model driver response is based on a constant δ, meaning that driver behavior does not vary with traffic conditions, and thus energy-saving driving behavior is ignored. Thus, this model cannot depict real-world traffic dynamics.

The proposed traffic model characterizes driver energy-saving awareness using vehicle energy conservation [123] as follows

$$E = \left\{\int I\left(ma_{max}v(t) + mg\sin\theta v(t) + 0.5\rho_{air}A_dA\left(v(t)\right)^3 + fmg\cos\theta v(t)\right)dt + Bdt\right\} \tag{7.3}$$

which is based on the principle of energy conservation. It is used during acceleration and deceleration to evaluate the changes in kinetic energy K_e and potential energy P_e, and the energy consumption due to air resistance A_e, road friction F_e, and vehicle internal systems I_e. From [123], we have

$$K_e = \int ma_{max}v(t)dt$$

$$P_e = \int mg\sin\theta v(t)dt$$

$$A_e = \int 0.5\rho_{air}A_dA(v(t))^3dt$$

$$F_e = \int fmg\cos\theta v(t)dt$$

$$I_e = E - K_e - P_e - A_e - F_e$$

where E is the total energy consumption, m is the vehicle mass, g is gravitational acceleration, θ is the slope of the road, ρ_{air} is the air density, A_d is the air drag coefficient, A is the vehicle front area, f is the friction coefficient, and a_{max} is the maximum acceleration vehicles can attain and is based on driver behavior, i.e. it is large with an aggressive driver and small when a driver is cautious. Differentiating (7.3) gives the instantaneous energy consumption power as

$$E_p = I(ma_{max}v + mg\sin\theta v + 0.5\rho_{air}A_dAv^3 + fmg\cos\theta v) + B \tag{7.4}$$

where B is the vehicle braking energy consumption intensity coefficient, and I is the vehicle internal energy consumption intensity coefficient.

Vehicle energy consumption is influenced by driver awareness of energy conservation [119]. Energy-conscious drivers adjust vehicle speed to reduce energy consumption, whereas traditional drivers ignore this consideration [119]. Thus, considering driver energy conservation awareness γ, δ can be expressed as

$$\delta = (1-\gamma)(I(ma_{max}v + mg\sin\theta v + 0.5\rho_{air}A_dAv^3 + fmg\cos\theta v) + B) \tag{7.5}$$

where γ ranges from 0 to 1. When $\gamma = 1$, the driver has full awareness of energy conservation, meaning that the lowest amount of energy possible is consumed by their vehicle. When $\gamma = 0$, the driver has no awareness of energy conservation, meaning that the most energy is consumed [119]. Vehicle energy consumption is also impacted by traffic density [124], so

$$\delta = (1-\gamma)(I(ma_{max}v + mg\sin\theta v + 0.5\rho_{air}A_dAv^3 + fmg\cos\theta v) + B \times \rho \tag{7.6}$$

Traffic flow is the product of density and speed, $Q = \rho v$ [31], which gives

$$\delta = \frac{(1-\gamma)(I(ma_{max}v + mg\sin\theta v + 0.5\rho_{air}A_dAv^3 + fmg\cos\theta v) + B) \times Q}{v} \tag{7.7}$$

The traffic flow is large with a small time headway τ, and a larger time headway decreases the flow [83]. Therefore (7.7) can be expressed as

$$\delta = \frac{(1-\gamma)(I(ma_{max}v + mg\sin\theta v + 0.5\rho_{air}A_dAv^3 + fmg\cos\theta v) + B)}{v\tau} \tag{7.8}$$

Acceleration is the change in speed with respect to time, $a_{max} = v/\tau$ [47]. Therefore

$$\delta = \frac{(1-\gamma)(I(ma_{max}v + mg\sin\theta v + 0.5\rho_{air}A_dAv^3 + fmg\cos\theta v) + B)}{a_{max}\tau^2} \tag{7.9}$$

Substituting (7.9) in (7.1) gives the proposed energy consumption model

$$\frac{dv}{dt} = a_{max}\left(1 - \left(\frac{v}{v_{max}}\right)^{\frac{(1-\gamma)(I(ma_{max}v+mg\sin\theta v+0.5\rho_{air}A_dAv^3+fmg\cos\theta v)+B)}{a_{max}\tau^2}} - \left(\frac{D}{s}\right)^2\right), \tag{7.10}$$

This model characterizes energy consumption to reflect driver behavior in terms of energy-saving consciousness. Thus, it can predict traffic flow dynamics in an energy-saving driving environment more realistically compared to the ID model.

Traffic density is $\rho = 1/s_e$ [47], where s_e is the steady-state distance headway, that is when $\Delta v = 0$, and is given by

$$s_e = (s_j + v\tau)\left(1 - \left(\frac{v}{v_{max}}\right)^{\frac{(1-\gamma)(I(ma_{max}v+mg\sin\theta v+0.5\rho_{air}A_dAv^3+fmg\cos\theta v)+B)}{a_{max}\tau^2}}\right)^{-\frac{1}{2}} \tag{7.11}$$

From [31], traffic flow is

$$Q = \frac{v}{s_e} \tag{7.12}$$

By substituting (7.11) in (7.12), the flow for the proposed model becomes

$$Q = \frac{v\left(1 - \left(\frac{v}{v_{max}}\right)^{\frac{(1-\gamma)(I(ma_{max}v+mg\sin\theta v+0.5\rho_{air}A_dAv^3+fmg\cos\theta v)+B)}{a_{max}\tau^2}}\right)^{\frac{1}{2}}}{(s_j + v\tau)} \tag{7.13}$$

This indicates that the traffic flow in the proposed model is based on driver energy consumption awareness. Thus, the flow will vary according to the level of driver energy conservation awareness. This is more realistic than the ID model, which characterizes traffic flow based on a constant δ and cannot adequately characterize traffic in an energy-saving driving environment.

7.2 Performance

The proposed and ID models are evaluated over a 1000 m circular road (periodic boundary conditions) for 700 s. First, the energy consumption characteristics of traffic flow are examined using the proposed model, and then the results with the proposed and ID models are compared. The maximum speed (desired speed) v_{max} is set to 30 m/s [47], the maximum acceleration for the proposed and ID models is 1.3 m/s^2 and 1.4 m/s^2, respectively, and the deceleration is 2 m/s^2 [33]. The value of γ is between 0 and 1, so here 0.1, 0.5, and 0.9 are employed. The acceleration exponent is typically 4 [26], so here $\delta = 4$ is used. For the ID model, a platoon of 61 vehicles with a jam spacing of 2 m [26] is considered. For the proposed model, a platoon of 17 vehicles with a jam spacing of 5 m is used so the platoon lengths would be same. The simulation parameters are provided in Table 7.1.

Table 7.1 Simulation parameters.

Parameter	**Value**
Maximum speed (desired speed), v_{max}	30 m/s
Time headway for ID model, τ	1.6 s [26]
Time headway for energy consumption model, τ	2 s [113]
Maximum acceleration for the ID model, a_{max}	1.4 m/s^2
Maximum acceleration for the proposed model, a_{max}	1.3 m/s^2
Driver energy conservation awareness, γ	0.1, 0.5 and 0.9
Jam spacing for energy consumption model, s_j	5 m
Jam spacing for ID model, s_j	2 m
Minimum acceleration (deceleration), b	2 m/s^2
Vehicle internal energy consumption intensity coefficient, I	6.609 [119]
Vehicle mass, m	1550 kg [119]
Gravitational acceleration, g	9.8 m/s^2 [125]
Air density, ρ_{air}	1.1691 kg/m^3 [119]
Air drag coefficient, A_d	0.31 [119]
Friction coefficient, f	0.0095 [126]

Vehicle front area, A	2.51 m^2 [127]
Braking energy consumption intensity coefficient, B	52,408 J/s [119]
Vehicle length, L	4.5 m [73]
Acceleration exponent, δ	4
Maximum normalized density for energy consumption model, $\rho_m = 1/s_j$	0.2
Maximum normalized density for ID model, $\rho_m = 1/s_j$	0.5
Time step size, Δt	0.5 s

7.2.1 Energy Consumption Characteristics of Traffic

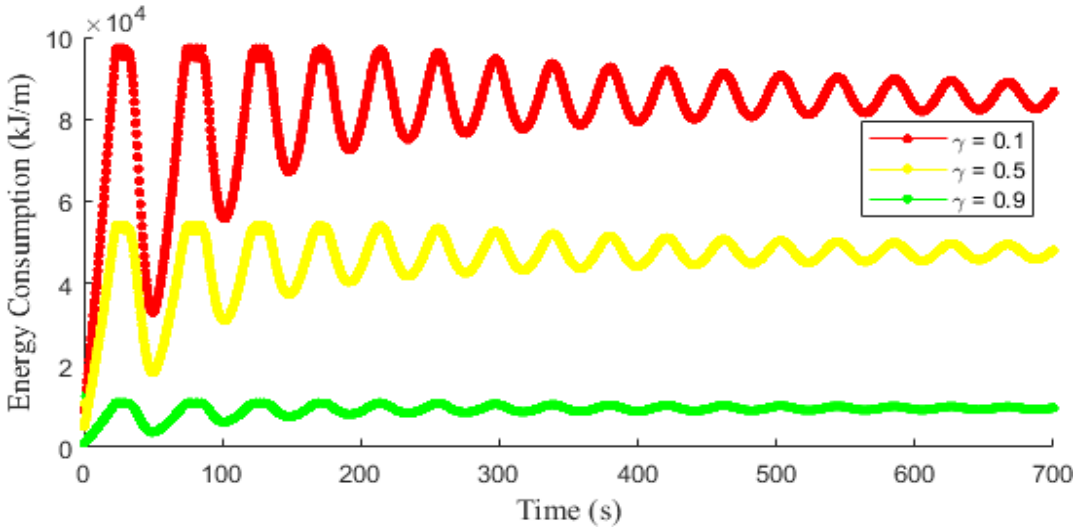

Figure 7.1 Energy consumption evolution of traffic on a 1000 m road.

Figure 7.1 presents the per meter energy consumption over time obtained by using the proposed model on a 1000 m road for $\gamma = 0.1, 0.5,$ and 0.9. When driver awareness of energy conservation was low ($\gamma = 0.1$), the energy consumption was high with large fluctuations. On the other hand, with a higher awareness of energy conservation ($\gamma = 0.9$), energy consumption was low, with small fluctuations that decreased over time. Figure 7.1 indicates that, for all values of γ, the fluctuations in energy consumption became smaller as the drivers employed energy-saving behavior, such as maintaining near-constant speeds and avoiding abrupt acceleration or deceleration.

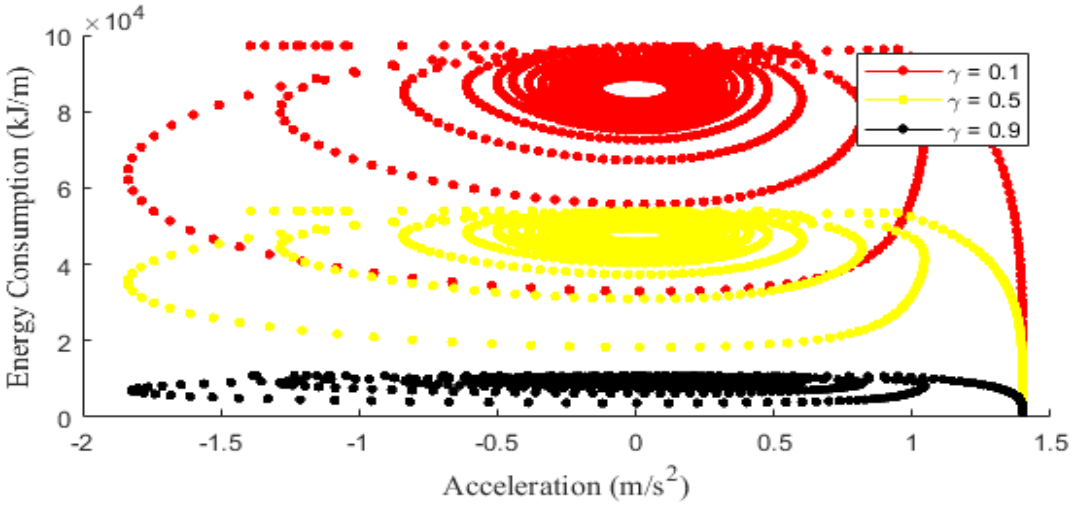

Figure 7.2 The relationship between energy consumption and acceleration for $\gamma = 0.1, 0.5$ and 0.9.

Figures 7.2, 7.3, and 7.4 present the relationship between energy consumption and acceleration, flow, and headway, respectively for $\gamma = 0.1, 0.5$, and 0.9. Figure 7.2 shows that, with a higher driver energy-saving awareness ($\gamma = 0.9$), vehicle energy consumption was more closely distributed within a somewhat circular region compared to lower driver energy-saving awareness ($\gamma = 0.1$), which had a more diverse energy consumption. This indicates that a high γ results in energy use which is more consistent owing to a smoother driving behavior involving fewer speed fluctuations. Conversely, with a low γ, energy consumption was high and more erratic due to irregular driving behavior. Moreover, when $\gamma = 0.1$, energy consumption was high due to greater acceleration and deceleration variations, whereas when $\gamma = 0.9$ energy consumption was low owing to smaller acceleration and deceleration variations. Thus, a higher γ means that drivers make gradual speed adjustments and avoid unnecessary braking and acceleration, a behavior that conserves energy.

Figure 7.3 shows an increase in energy consumption variations due to an increase in traffic flow. This is because the flow significantly affects the driving patterns. As the number of vehicles on the road increased and the traffic flow became higher, drivers were required to adjust their speeds more frequently to adapt to the surrounding traffic. This resulted in more frequent acceleration and deceleration, in turn increasing both the number and magnitude of variations in energy consumption. Figure 7.3 also indicates that a high driver awareness ($\gamma = 0.9$) resulted in lower energy consumption with smaller variations, even with a higher traffic flow. Conversely,

when driver awareness was low ($\gamma = 0.1$), the energy consumption was large with greater variations, particularly with a higher traffic flow. This is confirmed by the greater variation in energy consumption.

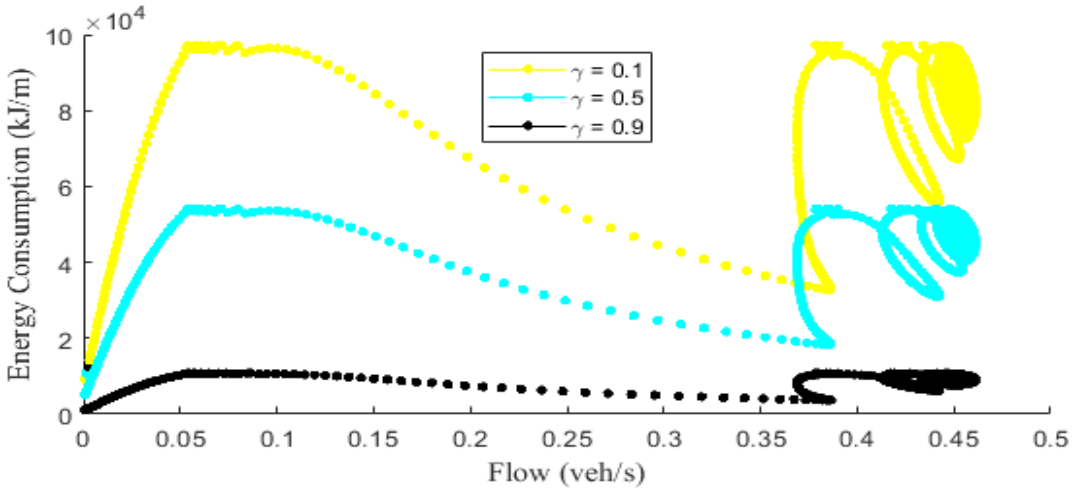

Figure 7.3 The relationship between energy consumption and flow for $\gamma = 0.1, 0.5$ and 0.9.

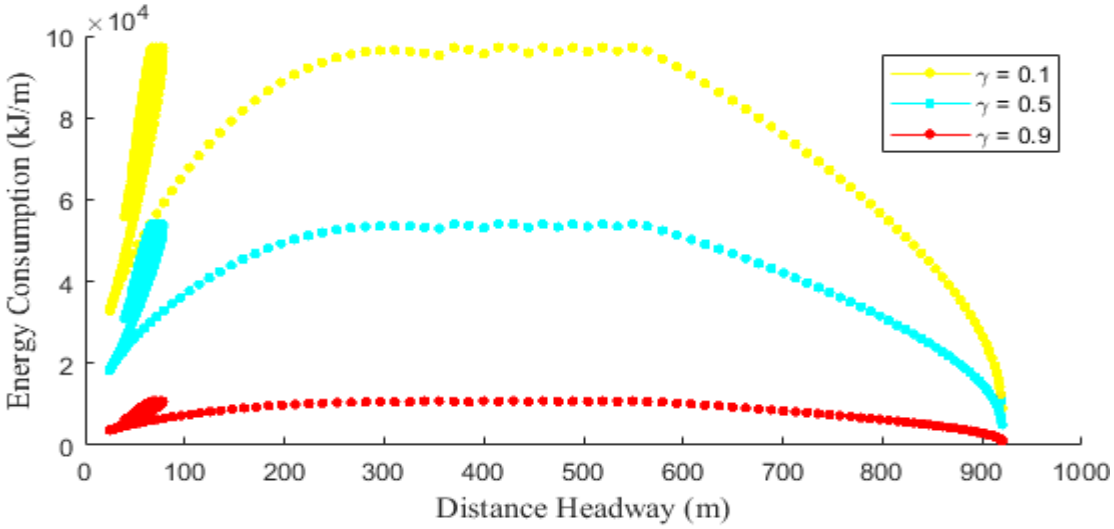

Figure 7.4 The relationship between energy consumption and distance headway for $\gamma = 0.1, 0.5$ and 0.9.

Figure 7.4 shows that, in general, energy consumption decreased with increasing distance headway for all values of γ. This is because an increase in distance headway allowed drivers to maintain vehicle speed and react slowly to changing conditions. Thus, a larger distance headway

reduced acceleration and deceleration, leading to a smoother traffic flow and lower energy consumption. Figure 7.4 also indicates that with higher awareness, $\gamma = 0.9$, energy consumption was low with smaller variations. This illustrates how energy-saving driving techniques reduce energy usage. With a lower energy-saving awareness ($\gamma = 0.1$), although a large distance headway did lead to a reduction in energy consumption, the variations were greater, resulting in less efficient energy usage. Thus, energy consumption was higher compared to the $\gamma = 0.9$ scenario.

7.2.2 Comparison of Proposed Model and ID Model

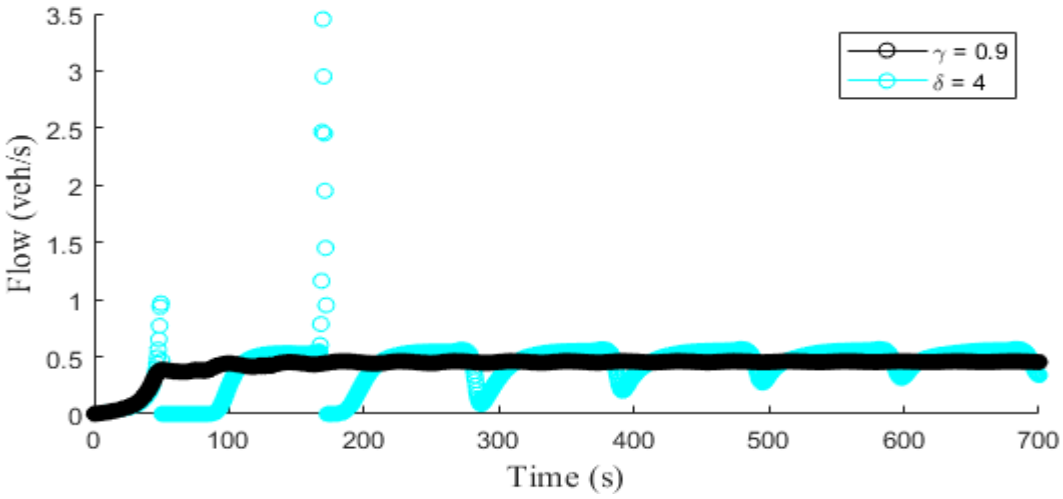

Figure 7.5 Temporal flow evolution with the proposed ($\gamma = 0.9$) and ID ($\delta = 4$) models.

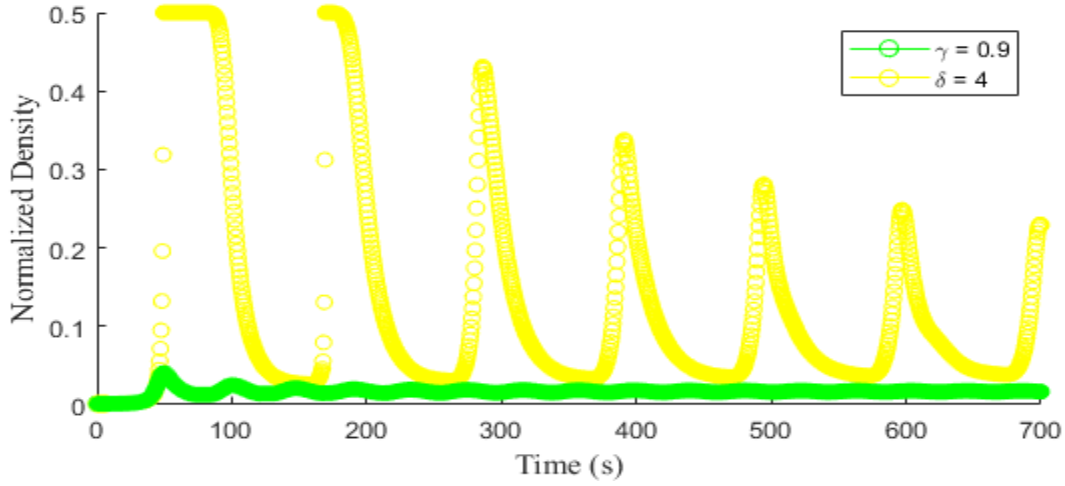

Figure 7.6 Temporal density evolution with the proposed ($\gamma = 0.9$) and ID ($\delta = 4$) models.

Figures 7.5 and 7.6 present the traffic flow and density evolution over time, respectively, with $\gamma = 0.9$ (proposed model) and $\delta = 4$ (ID model). These results show that the variations in both flow and density with $\delta = 4$ were large, whereas when $\gamma = 0.9$ these variations were negligible and the flow and density became approximately constant over time.

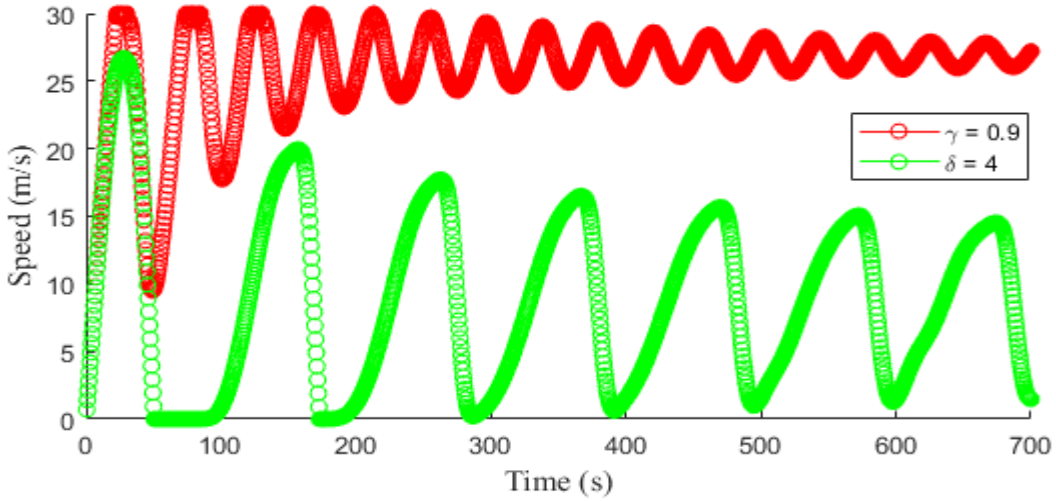

Figure 7.7 Temporal evolution of speed with the proposed ($\gamma = 0.9$) and ID ($\delta = 4$) models.

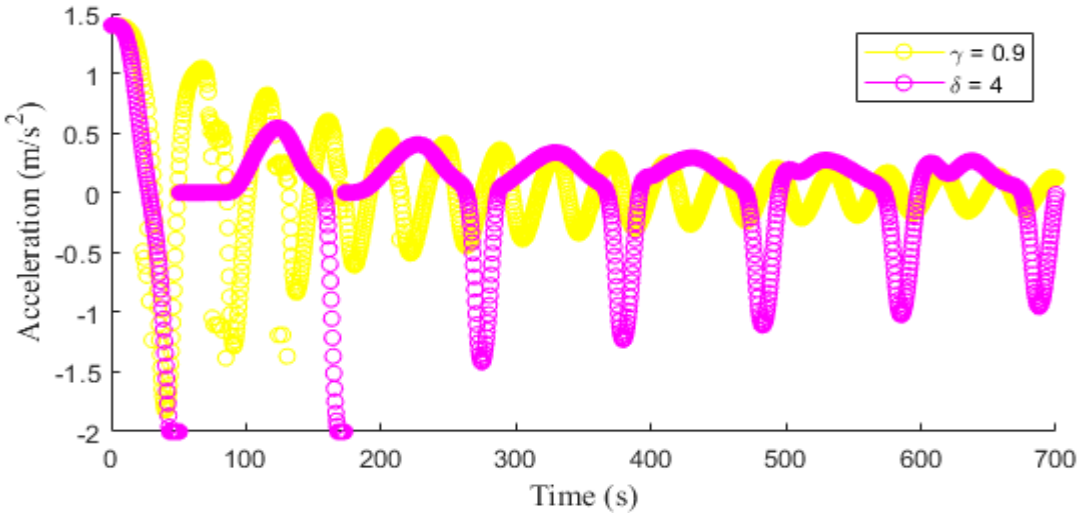

Figure 7.8 Temporal evolution of acceleration with the proposed ($\gamma = 0.9$) and ID ($\delta = 4$) models.

Figures 7.7 and 7.8 present the temporal speed and acceleration evolution, respectively, with $\gamma = 0.9$ (proposed model) and $\delta = 4$ (ID model). Figure 7.7 shows that $\gamma = 0.9$ resulted in higher

speeds with smaller variations which decreased over time. Conversely, $\delta = 4$ led to lower speeds which decreased over time with larger variations that diminished less. Figure 7.8 indicates that, with $\gamma = 0.9$, the variations in acceleration and deceleration were small and decreased over time. On the other hand, $\delta = 4$ resulted in large acceleration and deceleration variations which did not decrease over time.

The results presented in Section 7.2.1 indicate that the vehicle energy consumption was low in all cases when driver energy-saving awareness was high ($\gamma = 0.9$), whereas the energy consumption was significantly higher when this awareness was low ($\gamma = 0.1$). Based on the physics of vehicle motion and its effect on energy consumption, vehicle acceleration requires substantially more energy than maintaining a constant speed. Thus, drivers with low energy-saving awareness ($\gamma = 0.1$) consume more energy during stop-and-go traffic due to the more frequent stops and starts. Conversely, more aware drivers ($\gamma = 0.9$) adopt energy-saving techniques such as gradual braking to conserve energy, reducing stop-and-go waves.

The results in Section 7.2.2 illustrate that the proposed energy consumption model results in smaller variations in traffic flow, speed, and density compared to the ID model. In addition, greater speeds are achieved with less acceleration and deceleration, leading to better energy consumption. Conversely, the ID model produces lower speeds with more acceleration and deceleration variations, causing higher fuel consumption. Moreover, the traffic density in the ID model is high, whereas the proposed model results in lower traffic density.

7.3 Conclusion

Energy concerns such as global warming underscore the importance of traffic energy savings. This chapter introduces a microscopic traffic model that incorporates driver energy-saving awareness and energy consumption. The constant δ, representing driver behavior in the ID model, is replaced with an exponent reflecting energy consumption and driver energy-saving consciousness. It is shown that the ID model yields unrealistic traffic behavior because it cannot characterize changes in driver behavior. Conversely, the proposed model can realistically predict traffic flow dynamics in an energy-saving driving environment. Results are presented which show that, as driver energy conservation awareness increases, the energy consumption associated with traffic flow, acceleration, and headway decreases. Further, a driver with higher energy-saving awareness ($\gamma = 0.9$) uses less energy compared to a driver with low awareness ($\gamma = 0.1$).

Compared to the ID model, the proposed model results in smaller variations in traffic speed, flow, and density. It also leads to a smoother traffic flow and improved traffic efficiency, highlighting the importance of adopting energy-aware driving practices in traffic management strategies. Further, greater speeds with fewer acceleration and deceleration variations are achieved in the proposed model, substantially reducing fuel consumption.

Chapter 8
Conclusions

This chapter provides a summary of the contributions to traffic modeling presented in this dissertation. A concise overview of the achievements is given and their significance is highlighted.

8.1 Contributions

This study investigated microscopic modeling for traffic flow characterization and CAV behavior, with the objective of developing realistic traffic models and improving traffic safety, efficiency, and pollution control. The contributions to traffic modeling are as follows.

1. A microscopic traffic model was proposed that characterizes driver response according to reaction and sensitivity. The proposed model was compared to the state-of-the-art ID model and shown to have better stability. The proposed model generates a smooth traffic flow and can be integrated into CAVs and ACC systems for efficient and effective traffic management. In addition, it can be used in advanced driver assistant systems (ADASs) to ensure traffic safety by providing information about driver behavior. The proposed model can also be employed in automated driving systems (ADSs) for realistic traffic characterization.

2. A microscopic traffic model was developed that incorporates vehicle vibrations due to pavement conditions. The pavement condition is evaluated using the PCI. The proposed model provides realistic traffic flow dynamics compared to the ID model. Further, it can predict traffic behavior in real-time to help ACC systems better anticipate and adapt to changes in traffic conditions. An ACC system guided by the proposed model can adjust vehicle speed and following distance in response to the observed traffic density.

3. A microscopic traffic model was proposed to characterize traffic during foggy weather based on visibility. The proposed model results in realistic traffic behavior when compared to the ID model and is stable even in foggy weather. It can reduce fuel

consumption and pollution resulting from traffic congestion and can therefore be used by traffic engineers to provide insights for improved transport network management which will benefit the environment. The proposed model can also be incorporated into traffic simulators for realistic traffic prediction during foggy weather.

4. A traffic model was developed from a spring-mass system theory perspective to investigate traffic dynamics on horizontal highway curves. The proposed model was utilized to evaluate the behavior of HVs, AVs, and CAVs on horizontal curves. CAVs had better performance compared to HVs and AVs, leading to a better understanding of safety and efficiency on horizontal road segments. It was shown that CAVs improve energy efficiency and emission reduction, contributing to an effective and environmentally sustainable transportation system.

5. A microscopic traffic model was developed to characterize CAV behavior at a bottleneck and evaluate the performance under cyberattacks. The proposed model provides realistic traffic flow behavior, and reduces vehicle emissions and thus pollution. It can be employed by transportation agencies and planners for traffic control, safety, and forecasting when bottleneck conditions exist and there is malicious behavior. Further, it can be used as an alternative or to complement traditional traffic control techniques such as VSL to provide adaptive CAV control based on reaction time and distance headway.

6. A microscopic traffic model was introduced that incorporates driver energy-saving awareness and energy consumption. The proposed model can realistically predict traffic flow dynamics in an energy-saving driving environment. It was shown that this model reduces fuel consumption and can be employed to conserve energy and reduce fuel cost and vehicle emissions, thereby decreasing the overall carbon footprint of traffic and contributing to a more sustainable environment.

8.2 Future Work

There are several interesting research challenges in the field of microscopic traffic flow characterization. A brief outline of these problems is given below.

1. The range of scenarios analyzed in Chapter 5 can be expanded to include various road geometries and environmental conditions. This will increase the applicability and improve the effectiveness in real-world scenarios. Further, this will lead to the development of more comprehensive and robust traffic models.

2. Evaluating the impact of cyberattacks in a mixed traffic flow is another interesting problem as more CAVs and HVs co-exist. Thus, a traffic model can be developed to evaluate the impact of cyberattacks at various CAV penetration rates in mixed traffic. Integrating the CAV penetration rate into a cyberattack model is essential to understand how traffic dynamics are affected. This will help in evaluating how CAVs and HVs respond when under these attacks.

3. Global traffic demands contribute significantly to the rapid increase in CO_2 emissions. CAVs can be deployed to reduce these emissions and thus the environmental impact. This requires that a traffic model to characterize CO_2 emissions from CAVs be developed.

4. Investigating the effect of CAVs under foggy weather conditions is another research direction. Fog reduces the performance of the sensors CAVs rely on such as LiDAR, radar, and cameras, and thus affects traffic safety and efficiency. Therefore, a traffic model to characterize CAV behavior in foggy weather should be developed.

Bibliography

[1] B. S. Kerner, and S. L. Klenov, “A theory of traffic congestion at moving bottlenecks,” *J. Physics A Math. Theor.*, vol. 43, art. 425101, 2010.

[2] J. Long, Z. Gao, H. Ren, and A. Lian, “Urban traffic congestion propagation and bottleneck identification,” *Sci. China F Inform. Sci.*, vol. 51, pp. 948–964, 2008.

[3] J. A. Laval, and L. Leclercq, “A mechanism to describe the formation and propagation of stop-and-go waves in congested freeway traffic,” *Philos. Trans. R. Soc. A Math. Phys. Eng. Sci.*, vol. 368, no. 1928, pp. 4519–4541, 2010.

[4] K. Chung, J. Rudjanakanoknad, and M. J. Cassidy, “Relation between traffic density and capacity drop at three freeway bottlenecks,” *Transp. Res. Part B Methodol.*, vol. 41, no. 1, pp. 82–95, 2007.

[5] K. Yuan, V. L. Knoop, L. Leclercq, and S. P. Hoogendoorn, “Capacity drop: A comparison between stop-and-go wave and standing queue at lane-drop bottleneck,” *Transp. B Transp. Dyn.*, vol. 5, no. 2, pp. 145–158, 2017.

[6] A. M. Rao and K. R. Rao, “Measuring urban traffic congestion-a review,” *Int. J. Traffic Transp. Eng.*, vol. 2, no. 4, pp. 286–305, 2012.

[7] R. C. Carlson, I. Papamichail, and M. Papageorgiou, “Local feedback-based mainstream traffic flow control on motorways using variable speed limits,” *IEEE Trans. Intell. Transp. Syst.*, vol. 12, no. 4, pp. 1261–1276, 2011.

[8] J. Khoury, K. Amine, and R. Abi Saad, “An initial investigation of the effects of a fully automated vehicle fleet on geometric design,” *J. Adv. Transp.*, vol. 2019, art. 6126408, 2019.

[9] T. Vranken, B. Sliwa, C. Wietfeld, and M. Schreckenberg, “Adapting a cellular automata model to describe heterogeneous traffic with human-driven, automated, and communicating automated vehicles,” *Phys. A Stat. Mech. its Appl.*, vol. 570, art. 125792, 2021.

[10] L. Ma, S. Qu, J. Ren, and X. Zhang, “Mixed traffic flow of human-driven vehicles and

connected autonomous vehicles: String stability and fundamental diagram," *Math. Biosci. Eng.*, vol. 20, pp. 2280–2295, 2022.

[11] M. M. Rana and K. Hossain, "Connected and autonomous vehicles and infrastructures: A literature review," *Int. J. Pavement Res. Technol.*, vol. 16, no. 2, pp. 264–284, 2023.

[12] M. Rahman, M. R. Islam, M. Chowdhury, and T. Khan, "Development of a connected and automated vehicle longitudinal control model," *arXiv*, 2019, doi: 10.13140/RG.2.2.35436.51847.

[13] D. Milakis, "Long-term implications of automated vehicles: An introduction," *Transp. Rev.*, vol. 39, no. 1, pp. 1–8, 2019.

[14] A. Talebpour and H. S. Mahmassani, "Influence of connected and autonomous vehicles on traffic flow stability and throughput," *Transp. Res. Part C Emerg. Technol.*, vol. 71, pp. 143–163, 2016.

[15] Q. Wang, B. Li, Z. Li, and L. Li, "Effect of connected automated driving on traffic capacity," in *Chinese Automation Congress*, Jinan, China, 2017, pp. 633–637.

[16] D. Chen, S. Ahn, M. Chitturi, and D. A. Noyce, "Towards vehicle automation: Roadway capacity formulation for traffic mixed with regular and automated vehicles," *Transp. Res. Part B Methodol.*, vol. 100, pp. 196–221, 2017.

[17] P. Bansal and K. M. Kockelman, "Forecasting Americans' long-term adoption of connected and autonomous vehicle technologies," *Transp. Res. Part A Policy Pract.*, vol. 95, pp. 49–63, 2017.

[18] F. Ali, Z. H. Khan, K. S. Khattak, T. A. Gulliver, and A. B. Altamimi, "A microscopic traffic model incorporating vehicle vibrations due to pavement condition," *Mathematics*, vol. 11, no. 24, art. 4911, 2023.

[19] Z. H. Khan, W. Imran, S. Azeem, K. S. Khattak, T. A. Gulliver, and M. S. Aslam, "A macroscopic traffic model based on driver reaction and traffic stimuli," *Appl. Sci.*, vol. 9, no. 14, art. 2848, 2019.

[20] Z. H. Khan, T. A. Gulliver, and K. S. Khattak, "A novel macroscopic traffic model based

on distance headway," *Civ. Eng. J.*, vol. 7, pp. 32–40, 2021.

[21] F. Ali, Z. H. Khan, K. S. Khattak, and T. A. Gulliver, "The effect of visibility on road traffic during foggy weather conditions," *IET Int. Transp. Syst*., vol. 18*,* no.1, pp. 47-57, 2024.

[22] L. A. Pipes, "An operational analysis of traffic dynamics," *J. Appl. Phys.*, vol. 24, no. 3, pp. 274–281, 1953.

[23] A. Reuschel, "Vehicle movements in a platoon," *Oesterreichisches Ingenieur-Archir*, vol. 4, pp. 193–215, 1950.

[24] F. Ali, Z. H. Khan, A. B. Altamimi, K. S. Khattak, and T. A. Gulliver, "A microscopic traffic model considering time headway and distance headway," *Appl. Sci.*, vol. 13*,* no. 12, art. 7234, 2023.

[25] G. F. Newell, "Nonlinear effects in the dynamics of car following," *Oper. Res.*, vol. 9, no. 2, pp. 209–229, 1961.

[26] M. Treiber, A. Hennecke, and D. Helbing, "Congested traffic states in empirical observations and microscopic simulations," *Phys. Rev. E - Stat. Physics, Plasmas, Fluids, Relat. Interdiscip. Top.*, vol. 62, no. 2, pp. 1805–1824, 2000.

[27] G. F. Newell, "A simplified car-following theory: A lower order model," *Transp. Res. Part B Methodol.*, vol. 36, no. 3, pp. 195–205, 2002.

[28] M. Bando, K. Hasebe, A. Nakayama, A. Shibata, and Y. Sugiyama, "Dynamical model of traffic congestion and numerical simulation," *Phys. Rev. E*, vol. 51, no. 2, pp. 1035–1042, 1995.

[29] D. Helbing and B. Tilch, "Generalized force model of traffic dynamics," *Phys. Rev. E - Stat. Physics, Plasmas, Fluids, Relat. Interdiscip. Top.*, vol. 58, no. 1, pp. 133–138, 1998.

[30] P. G. Gipps, "A behavioural car-following model for computer simulation," *Transp. Res. Part B*, vol.15, pp. 105–111, 1981.

[31] Z. Cao, L. Lu, C. Chen, and X. U. Chen, "Modeling and simulating urban traffic flow mixed with regular and connected vehicles," *IEEE Access*, vol. 9, pp, 10392–10399, 2021.

[32] W. Dahui, W. Ziqiang, and F. Ying, "Hysteresis phenomena of the intelligent driver model

for traffic flow," *Phys. Rev. E - Stat. Nonlinear, Soft Matter Phys.*, vol. 76, no. 1, pp. 2–8, 2007.

[33] A. Kesting, M. Treiber, and D. Helbing, "Enhanced intelligent driver model to access the impact of driving strategies on traffic capacity," *Philos. Trans. R. Soc. A Math. Phys. Eng. Sci.*, vol. 368, no. 1928, pp. 4585–4605, 2010.

[34] S. Yang, "Enlarged stopping distance to improve vehicle discharge at urban signalised intersections," Ph.D. thesis, Queensland University of Technology, Brisbane, QLD, Australia, 2013.

[35] T. Kovács, K. Bolla, R. A. Gil, C. Fábián, and L. Kovács, "Parameters of the intelligent driver model in signalized intersections," *Teh. Vjesn*., vol. 23, pp. 1469–1474, 2016.

[36] M. Liebner, M. Baumann, F. Klanner, and C. Stiller, "Driver intent inference at urban intersections using the intelligent driver model," in *IEEE Intelligent Vehicle Symposium*, Madrid, Spain, 2012.

[37] P. Liu and W. Fan, "Exploring the impact of connected and autonomous vehicles on freeway capacity using a revised intelligent driver model," *Transp. Plan. Technol.*, vol. 43, no. 3, pp. 279–292, 2020.

[38] Y. Li, Z. Li, H. Wang, W. Wang, and L. Xing, "Evaluating the safety impact of adaptive cruise control in traffic oscillations on freeways," *Accid. Anal. Prev.*, vol. 104, pp. 137–145, 2017.

[39] W. J. Schakel, B. Van Arem, and B. D. Netten, "Effects of cooperative adaptive cruise control on traffic flow stability," in *International IEEE Conference on Intelligent Transportation Systems*, Funchal, Portugal, 2010.

[40] V. Milanés and S. E. Shladover, "Modeling cooperative and autonomous adaptive cruise control dynamic responses using experimental data," *Transp. Res. Part C Emerg. Technol.*, vol. 48, pp. 285–300, 2014.

[41] A. Jafaripournimchahi, Y. Cai, H. Wang, L. Sun, and J. Weng, "Integrated-hybrid framework for connected and autonomous vehicles microscopic traffic flow modelling," *J. Adv. Transp.*, vol. 2022, art. 2253697, 2022.

[42] R. Malinauskas, “The intelligent driver model: analysis and application to adaptive cruise control,” Ph.D. thesis, Clemson University, Clemson, SC, USA, 2014.

[43] M. Rahman, M. R. Islam, M. Chowdhury, and T. Khan, “A physics-based longitudinal driver model for automated vehicles,” *IEEE Access*, vol. 10, pp. 80883–80899, 2022.

[44] B. A. Zielke, R. L. Bertini, and M. Treiber, “Empirical measurement of freeway oscillation characteristics: an international comparison,” *Transp. Res. Rec.*, vol. 2088, no. 1, pp. 57–67, 2008.

[45] M. Treiber and A. Kesting, “Evidence of convective instability in congested traffic flow: A systematic empirical and theoretical investigation,” *Procedia-Social Behav. Sci.*, vol. 17, pp. 683–701, 2011.

[46] H. Yeo and A. Skabardonis, “Understanding stop-and-go traffic in view of asymmetric traffic theory,” in Transportation and Traffic Theory 2009, pp. 683–701, Springer: Boston, MA, USA, 2009.

[47] F. Kessels, Traffic flow modelling: Introduction to traffic flow theory through a genealogy of models, Springer: Cham, Switzerland, 2019.

[48] J. Wang, R. Chai, and X. Xue, “The effects of stop-and-go wave on the immediate follower and change in driver characteristics,” *Procedia Eng.*, vol. 137, pp. 289–298, 2016.

[49] Z. H. Khan and T. A. Gulliver, “A macroscopic traffic model based on anticipation,” *Arab. J. Sci. Eng.*, vol. 44, no. 5, pp. 5151–5163, 2019.

[50] M. Treiber and A. Kesting, Traffic flow dynamics: Data, models and simulation, Springer: Berlin, Germany, 2013.

[51] S. Hallerbach, Y. Xia, U. Eberle, and F. Koester, “Simulation-based identification of critical scenarios for cooperative and automated vehicles,” *SAE Int. J. Connect. Autom. Veh.*, vol. 1, pp. 93–106, 2018.

[52] S. Feng, Y. Zhang, S. E. Li, Z. Cao, H. X. Liu, and L. Li, “String stability for vehicular platoon control: Definitions and analysis methods,” *Annu. Rev. Control*, vol. 47, pp. 81–97, 2019.

[53] O. Derbel, T. Peter, H. Zebiri, B. Mourllion, and M. Basset, “Modified intelligent driver model for driver safety and traffic stability improvement, ” *IFAC Proc.*, vol. 46, pp. 744–749, 2013.

[54] R. Kumar, S. K. Suman, and G. Prakash, “Evaluation of pavement condition index using artificial neural network approach,” *Transp. Dev. Econ.*, vol. 7, no. 2, pp. 1–15, 2021.

[55] F. Ali, Z. H. Khan, K. S. Khattak, and T. A. Gulliver, “A microscopic traffic flow model characterization for weather conditions,” *Appl. Sci.*, vol. 12, no. 24, art. 12981, 2022.

[56] “Accidents caused by poor road quality and conditions in DC | Gilman & Bedigian.” Available online: https://www.gilmanbedigian.com/accidents-caused-by-poor-road-quality-and-conditions-in-dc/ (accessed on 23 September 2022).

[57] A. M. Sohail, K. S. Khattak, A. Iqbal, Z. H. Khan, and A. Ahmad, “Cloud-based detection of road bottlenecks using OBD-II telematics,” in *International Multitopic Conference*, Islamabad, Pakistan, 2019.

[58] A. Ahmed, D. Ngoduy, M. Adnan, and M. A. U. Baig, “On the fundamental diagram and driving behavior modeling of heterogeneous traffic flow using UAV-based data,” *Transp. Res. Part A Policy Pract.*, vol. 148, pp. 100–115, 2021.

[59] F. A. Majeed *et al.*, “Smart traffic management system for foggy weather conditions,” in *Advances in Science and Engineering Technology International Conferences*, Dubai, United Arab Emirates, 2019.

[60] K. Dahmane, P. Duthon, F. Bernardin, M. Colomb, F. Chausse, and C. Blanc, “Weathereye-proposal of an algorithm able to classify weather conditions from traffic camera images,” *Atmosphere (Basel).*, vol. 12, art. 717, 2021.

[61] Y. Wu, M. Abdel-Aty, L. Wang, and M. S. Rahman, “Improving flow and safety in low visibility conditions by applying connected vehicles and variable speed limits technologies,” *in Transportation Research Board Annual Meeting,* Washington DC, USA, art. 19-02734, 2019.

[62] F. Ali, Z. H. Khan, F. A. Khan, K. S. Khattak, and T. A. Gulliver, “A new driver model based on driver response,” *Appl. Sci.*, vol. 12, no. 11, art. 5390, 2022.

[63] U.S. Department of Transportation, Federal Highway Administration, Road weather management program, "Low visibility". Available online: https://ops.fhwa.dot.gov/weather/weather_events/low_visibility.htm (accessed on 26 February 2023).

[64] Y. Wang, L. Liang, and L. Evans, "Fatal crashes involving large numbers of vehicles and weather," *J. Safety Res.*, vol. 63, pp. 1–7, 2017.

[65] B. Gong, F. Wang, C. Lin, and D. Wu, "Modeling HDV and CAV mixed traffic flow on a foggy two-lane highway with cellular automata and game theory model," *Sustainability*, vol. 14, no. 10, art. 5899, 2022.

[66] M. Kyte, Z. Khatib, P. Shannon, and F. Kitchener, "Effect of environmental factors on free-flow speed," *US Natl. Acad. Sci. Transp. Res. Board*, vol. 18, no. 1, pp. 10–25, 2000.

[67] K. L. M. Broughton, F. Switzer, and D. Scott, "Car following decisions under three visibility conditions and two speeds tested with a driving simulator," *Accid. Anal. Prev.*, vol. 39, no. 1, pp. 106–116, 2007.

[68] R. E. Stern *et al.*, "Dissipation of stop-and-go waves via control of autonomous vehicles: Field experiments," *Transp. Res. Part C Emerg. Technol.*, vol. 89, pp. 205–221, 2018.

[69] Z. H. Khan, "Traffic modelling for intelligent transportation systems," Ph.D. dissertation, University of Victoria, Victoria, BC, Canada, 2016.

[70] F. Ali, Z. H. Khan, K. S. Khattak, T. A. Gulliver, and A. N. Khan, "A microscopic heterogeneous traffic flow model considering distance headway," *Mathematics*, vol. 11, no. 1, art. 184, 2023.

[71] A. A. Khan, M. Fatima, S. Arshad, and K. Khan, "Spatio-temporal analysis of hazardous fog: A case study of Bahawalpur, Pakistan," *Arab World Geogr.*, vol. 17, no. 4, pp. 357–375, 2014.

[72] W. Imran, Z. H. Khan, T. A. Gulliver, K. S. Khattak, S. Saeed, and M. S. Aslam, "Macroscopic traffic flow characterization for stimuli based on driver reaction," *Civ. Eng. J.*, vol. 7, no. 1, pp. 1–13, 2021.

[73] "How long is a car? (Average car length according to types)."Available online: https://www.smartmotorist.com/average-car-length (accessed on 8 May 2022).

[74] Ottawa Safety Council, "On the road to safety." Available online: https://www.ottawasafetycouncil.ca/ (accessed on 3 March 2023).

[75] S. Lam, J. Taghia, and J. Katupitiya, "Evaluation of a transportation system employing autonomous vehicles," *J. Adv. Transp.*, vol. 50, no. 8, pp. 2266–2287, 2016.

[76] "Future highways–Automated vehicles," SunCam online continuing education course, Wellington, FL, USA, 2022. Available online: https://s3.amazonaws.com/suncam/docs/208.pdf (accessed on 14 March 2024).

[77] S. Pham, L. Truong, and N. Nguyen, "Impacts of autonomous vehicles on road and pavement design," in *Australasian Transport Research Forum,* Brisbane, QLD, Australia, 2021.

[78] S. Wang and B. Yu, "Impacts on the geometric design of highway from non-autonomous to autonomous vehicles," in *Transportation Research Board Annual Meeting*, Washington DC, USA, 2019.

[79] Testbook, "Different types of curves in surveying." Available online: https://testbook.com/civil-engineering/different-types-of-curves-in-surveying (accessed on 14 March 2024).

[80] A. Abbas, A. Khan, T. Abdeljawad, and M. Aslam, "Numerical simulation of variable density and magnetohydrodynamics effects on heat generating and dissipating Williamson Sakiadis flow in a porous space: Impact of solar radiation and Joule heating," *Heliyon*, vol. 9, no. 11, 2023.

[81] A. Abbas *et al.*, "Effect of non-uniform heat rise/fall and porosity on MHD Williamson hybrid nanofluid flow over incessantly moving thin needle," *Heliyon*, vol. 10, no. 1, 2024.

[82] Y. Li, W. Chen, S. Peeta, X. He, T. Zheng, and H. Feng, "An extended microscopic traffic flow model based on the spring-mass system theory," *Mod. Phys. Lett. B*, vol. 31, no. 09, art. 1750090, 2017.

[83] H. Halim, S. A. Adisasmita, M. I. Ramli, and S. H. Aly, "The relationship of volume and headway on heterogen traffic conditions in Makassar City," in *IOP Conference Series: Earth and Environmental Science*, vol. 419, art. 012105, 2020.

[84] The physics hypertextbook, "Equations of motion." Available online: https://physics.info/motion-equations/ (accessed on 14 March 2024).

[85] ESE notes, "Transition curves and length of transition curve 2.20." Available online: https://esenotes.com/transition-curves-length-of-transition-curve/ (accessed on 21 February 2024).

[86] BigRentz, "What is superelevation and how does it keep roads safer?" Available online: https://www.bigrentz.com/blog/superelevation (accessed on 13 February 2024).

[87] G. Xu *et al.*, "The influence of the pavement friction coefficient evolution caused by traffic flow on the risk of motorway horizontal curves," *PLoS One*, vol. 17, no. 8, art. e0266519, 2022.

[88] Federal Highway Administration, "Mitigation strategies for design exceptions - superelevation." Available online: https://safety.fhwa.dot.gov/geometric/pubs/mitigationstrategies/chapter3/3_superelevation.cfm (accessed on 13 February 2024).

[89] F. Ali, Z. H. Khan, K. Khattak, and T. A. Gulliver, "Evaluating the effect of road surface potholes using a microscopic traffic model," *Appl. Sci.*, vol. 2023, art. 8677, 2023.

[90] A. Kordani, O. Rahmani, A. Nasiri, and S. Boroomandrad, "Effect of adverse weather conditions on vehicle braking distance of highways," *Civ. Eng. J.*, vol. 4, pp. 46–57, 2018.

[91] Physics 101, "The friction of automobile tires." Available online: http://boson.physics.sc.edu/~rjones/phys101/tirefriction.html (accessed on 17 February 2024).

[92] M. Taieb-Maimon and D. Shinar, "Minimum and comfortable driving headways: Reality versus perception," *Hum. Factors*, vol. 43, no. 1, pp. 159–172, 2001.

[93] Y. Di, W. Zhang, H. Ding, X. Zheng, and B. Ran, "Cooperative control of dynamic CAV

dedicated lanes and vehicle active lane changing in expressway bottleneck areas," *Phys. A Stat. Mech. its Appl.*, vol. 638, art. 129623, 2024.

[94] X. Qu, L. Li, Z. Yi, P. Mao, and M. Yang, "Traffic flow modeling of freeway variable speed limit control based on the big data of driving behavior," *J. Adv. Transp.*, vol. 2020, art. 8859494, 2020.

[95] S. Li, T. Wang, H. Ren, B. Shi, X. Kong, J. Chai, and X. Wang, "Variable speed limit strategies based on the macro hierarchical control traffic flow model," *J. Adv. Transp.*, vol. 2021, art. 9910097, 2021.

[96] Y. Li, Y. Shi, J. Lee, C. Yuan, and B. Wang, "Safety effects of connected and automated vehicle-based variable speed limit control near freeway bottlenecks considering driver's heterogeneity," *J. Adv. Transp.*, vol. 2022, art. 996623, 2022.

[97] H. Ding, L. Zhang, J. Chen, X. Zheng, H. Pan, and W. Zhang, "MPC-based dynamic speed control of CAVs in multiple sections upstream of the bottleneck area within a mixed vehicular environment," *Phys. A Stat. Mech. its Appl.*, vol. 613, art. 128542, 2023.

[98] C. Zhang, N. R. Sabar, E. Chung, A. Bhaskar, and X. Guo, "Optimisation of lane-changing advisory at the motorway lane drop bottleneck," *Transp. Res. Part C Emerg. Technol.*, vol. 106, pp. 303–316, 2019.

[99] S. E Seilabi, M. Pourgholamali, S. X. He, and S. Labi, "Managing dedicated lanes for connected and autonomous vehicles to address bottleneck congestion considering morning peak commuter departure choices," *SSRN Elect. J.,* 2022. https://doi.org/10.2139/ssrn.4142516.

[100] H. H. S. N. Subraveti, A. Srivastava, S. Ahn, V. L. Knoop, and B. van Arem, "On lane assignment of connected automated vehicles: strategies to improve traffic flow at diverge and weave bottlenecks," *Transp. Res. Part C Emerg. Technol.*, vol. 127, art. 103126, 2021.

[101] Y. Di, W. Zhang, H. Ding, X. Zheng, and H. Bai, "Integrated control for mixed CAV and CV traffic flow in expressway merge zones combined with variable speed limit, ramp metering, and lane changing," *J. Transp. Eng. Part A Syst.*, vol. 149, no. 2, art. 4022140, 2023.

[102] H. Ding, Y. Di, X. Zheng, H. Bai, and W. Zhang, “Automated cooperative control of multilane freeway merging areas in connected and autonomous vehicle environments,” *Transp. B Transp. Dyn.*, vol. 9, no. 1, pp. 437–455, 2021.

[103] A. Talebpour, H. S. Mahmassani, and A. Elfar, “Investigating the effects of reserved lanes for autonomous vehicles on congestion and travel time reliability,” *Transp. Res. Rec.*, vol. 2622, no. 1, pp. 1–12, 2017.

[104] A. Khan, K. Khattak, Z. H. Khan, T. A. Gulliver, and A. Zakhil, “Edge computing for effective and efficient traffic characterization,” *Sensors*, vol. 23, pp. 1–20, 2023.

[105] S. Ghosh, N. Saha, and T. Roy, “A cyberattack detection-isolation algorithm for CAV under changing driving environment,” *IEEE Trans. Intell. Transp. Syst.*, vol. 25, pp. 19646–19657, 2024.

[106] J. Reilly, S. Martin, M. Payer, and A. M. Bayen, “Creating complex congestion patterns via multi-objective optimal freeway traffic control with application to cyber-security,” *Transp. Res. Part B Methodol.*, vol. 91, pp. 366–382, 2016.

[107] I. McManus and K. Heaslip, “The impact of cyberattacks on efficient operations of CAVs,” *Front. Futur. Transp.*, vol. 3, art. 792649, 2022.

[108] J. Petit and S. E. Shladover, “Potential cyberattacks on automated vehicles,” *IEEE Trans. Intell. Transp. Syst.*, vol. 16, no. 2, pp. 546–556, 2014.

[109] Z. Sun, R. Liu, H. Hu, D. Liu, and Z. Yan, “Cyberattacks on connected automated vehicles: A traffic impact analysis,” *IET Intell. Transp. Syst.*, vol. 17, no. 2, pp. 295–311, 2023.

[110] T. Wang *et al.*, “Impact evaluation of cyberattacks on connected and automated vehicles in mixed traffic flow and its resilient and robust control strategy,” *Sensors*, vol. 23, no. 1, art. 74, 2022.

[111] K. L. Thomson, “Cybersecurity: reducing the attack surface,” Inaugural Lecture; Nelson Mandela University: Gqeberha, South Africa, 2021. Available online: https://lectures.mandela.ac.za/lectures/media/Store/documents/Inaugural%20lectures/Full-lecture-of-Prof-KL-Thomson.pdf (accessed on 15 December 2024).

[112] A. Morgan, B. Cesme, and B. Schroeder, “How connected and automated vehicles may change freeway capacities”, Kittelson & Associates: Orlando, FL, USA, 2019. Available online: https://www.kittelson.com/ideas/how-connected-automated-vehicles-may-change-freeway-capacities/ (accessed on 15 December 2024).

[113] F. Ali, Z. H. Khan, T. A. Gulliver, K. S. Khattak, and A. B. Altamimi, “A microscopic traffic model considering driver reaction and sensitivity,” *Appl. Sci.*, vol. 13, no. 13, art. 7810, 2023.

[114] S. Yadav and P. Redhu, “Analysis of passing behavior on car-following model under the influence of cyberattacks,” *Nonlinear Dyn.*, vol. 112, no. 9, pp. 7269–7289, 2024.

[115] M. Guériau and I. Dusparic, “Quantifying the impact of connected and autonomous vehicles on traffic efficiency and safety in mixed traffic,” in *IEEE International Conference on Intelligent Transportation Systems*, Rhodes, Greece, 2020.

[116] E. R. Khansari, M. Tabibi, and F. M. Nejad, “A study on following behavior based on the time headway,” *J. Kejuruter.*, vol. 32, no. 2, pp. 187–195, 2020.

[117] H. Li, H. Li, Y. Hu, T. Xia, Q. Miao, and J. Chu, “Evaluation of fuel consumption and emissions benefits of connected and automated vehicles in mixed traffic flow,” *Front. Energy Res.*, vol. 11, art. 1207449, 2023.

[118] “World energy statistics and balances - Data product - IEA.” Available online: https://www.iea.org/data-and-statistics/data-product/world-energy-statistics-and-balances (accessed on 27 June 2024).

[119] B. Sun *et al.*, “Research on microscopic traffic flow modeling and energy characteristics in the energy-saving driving environment,” *Nonlinear Dyn.*, vol. 111, no. 15, pp. 14365–14378, 2023.

[120] “Energy efficiency 2021 – Analysis - IEA.” Avaialable online: https://www.iea.org/reports/energy-efficiency-2021 (accessed on 27 June 2024).

[121] Eia, “Global transportation energy consumption: Examination of scenarios to 2040 using ITEDD,” Available online: https://www.eia.gov/analysis/studies/transportation/scenarios/pdf/globaltransportation.pdf (accessed on 10

July 2024).

[122] “Energy use in Canada | Natural Resources Canada.” Available online: https://oee.nrcan.gc.ca/publications/statistics/trends/2017/transportation.cfm#L2 (accessed on 10 July 2024).

[123] B. Sun, Q. Zhang, N. Wei, Z. Jia, C. Li, and H. Mao, “The energy flow of moving vehicles for different traffic states in the intersection,” *Phys. A Stat. Mech. Its Appl.*, vol. 605, art. 128025, 2022.

[124] S. Bharadwaj, S. Ballare, Rohit, and M. K. Chandel, “Impact of congestion on greenhouse gas emissions for road transport in Mumbai metropolitan region,” *Transp. Res. Procedia*, vol. 25, pp. 3538–3551, 2017.

[125] Y. Li *et al.*, “Evaluating the energy consumption of electric vehicles based on car-following model under non-lane discipline,” *Nonlinear Dyn.*, vol. 82, pp. 629–641, 2015.

[126] J. Wang, I. Besselink, and H. Nijmeijer, “Electric vehicle energy consumption modelling and prediction based on road information,” *World Electr. Veh. J.*, vol. 7, no. 3, pp. 447–458, 2015.

[127] X. Xu, H. M. A. Aziz, H. Liu, M. O. Rodgers, and R. Guensler, “A scalable energy modeling framework for electric vehicles in regional transportation networks,” *Appl. Energy*, vol. 269, art. 115095, 2020.